CARAVEL

Publish open access at Caravel Press

Green Technology & Innovation

Journal homepage: gtijournal.com

GTI GREEN TECHNOLOGY & INNOVATION

Technical article

Performance Characterization of a Hybrid PV-CSP-TES-PCM-SOEC System with Renewable Integration for Sustainable Hydrogen Production across Indian Climate Zones

J.S.D. Nandini [1] and K.S. Reddy [1]*

[1] *Heat Transfer and Thermal Power Laboratory, Department of Mechanical Engineering, Indian Institute of Technology Madras, Chennai 600036, India.*

ABSTRACT

Continuous green hydrogen production from solar energy faces two fundamental challenges. Solar resources are inherently intermittent. At the same time, solid oxide electrolysis cells (SOECs) require a stable, high-temperature thermal input around the clock. This study proposes a hybrid photovoltaic-concentrated solar power-thermal energy storage-solid oxide electrolysis cell (PV-CSP-TES-SOEC) system. The system uses anhydrous magnesium chloride ($MgCl_2$) as a high-temperature phase-change material (melting point ≈ 714 °C; latent heat 452 kJ kg^{-1}). This material bridges overnight thermal energy deficits and enables uninterrupted SOEC operation without grid support. Five Indian climate zones were investigated - Jodhpur, Ladakh, Nagpur, Bengaluru, and Kochi, using a full 8760-hour hourly dynamic simulation with NSRDB SUNY TMY data, preceded by static sizing to establish baseline component requirements. Static sizing shows that PV area varies by 22% across sites, while CSP aperture varies by up to 55%. The required $MgCl_2$ mass ranges from 190 to 240 t under baseline conditions. After optimisation, the required PCM mass increases to 325.7-823.9 t. Nagpur requires the highest due to prolonged monsoon-related solar suppression. Under constant-load SOEC operation, hourly reliability reaches only 62.1 to 68.7%. Hydrogen output drops to 729-788 kg day^{-1}, which is 27-33% below the 1080 kg day^{-1} target. This shortfall is caused entirely by TES depletion during pre-dawn hours. A three-period flexible scheduling strategy is introduced. The SOEC operates at 0.6× load at night, 1.0× during shoulder hours, and 1.5-1.8× during the solar peak. This strategy restores full hydrogen output and increases reliability to 95.1-95.7% across all five sites. This corresponds to an improvement of 26-34 percentage points compared to constant-load operation. The results demonstrate that demand-side scheduling optimisation, rather than infrastructure oversizing, is the decisive factor enabling near-continuous grid-independent solar hydrogen production across climatically diverse locations.

ARTICLE INFO

Article History:
Received: [insert date]
Revised: [insert date]
Accepted: [insert date]

Keywords:
Green hydrogen
Solid oxide electrolysis cell (SOEC)
Concentrated solar power (CSP)
$MgCl_2$ phase-change material
Thermal energy storage
Flexible SOEC scheduling
Photovoltaic (PV)
Hybrid renewable energy system

Article Citation:
Nandini, J., & Reddy, K. (2026). Performance Characterization of a Hybrid PV-CSP-TES-PCM-SOEC System with Renewable Integration for Sustainable Hydrogen Production across Indian Climate Zones. Green Technology & Innovation, 2(1), 248–296.
https://doi.org/10.65582/gti.2026.014

* Corresponding author. Email address: ksreddy@iitm.ac.in (K.S. Reddy)

NOMENCLATURE

English Symbols	
A	Area [m²]
c_l	Specific heat capacity of $MgCl_2$ in the liquid phase [kJ kg⁻¹ °C⁻¹]
c_p	Specific heat capacity of heat transfer fluid [kJ kg⁻¹ °C⁻¹]
c_s	Specific heat capacity of $MgCl_2$ in the solid phase [kJ kg⁻¹ °C⁻¹]
e	Specific electrical energy consumption [kWh kg⁻¹ H_2]
E	Total usable thermal energy storage capacity [kWh $_{th}$]
F	Faraday constant [C mol⁻¹]
G	Gibbs free energy of water splitting reaction [kJ mol⁻¹]
h	Specific enthalpy of PCM [kJ kg⁻¹]
k	Thermal conductivity [W m⁻¹ K⁻¹]
L_f	Latent heat of fusion [kJ kg⁻¹]
$\dot{m}$	Mass production rate [kg h⁻¹]
m	Mass [kg]
n	Number of electrons transferred per molecule
N	Total simulation hours (8760) [h]
p	Pressure [Pa]
P_{charge}	Charging power from surplus CSP thermal energy [kW]
P_{CSP}	CSP thermal output power [kW $_{th}$]
P_{dis}	Discharging power supplied from TES to SOEC [kW $_{th}$]
P_{nom}	SOEC nominal load [kW]
P_{PV}	PV array electrical output power [kW]
P_{SOEC}	Electrical power input to the SOEC stack [kW]
P_{sup}	Available supply power at each hour [kW]
Qth	Instantaneous SOEC thermal demand [kW $_{th}$]
R	Annual hourly reliability [%]
R(t)	Hourly reliability indicator (1 if met, 0 otherwise)
S	Entropy change of water splitting reaction [kJ mol⁻¹ K⁻¹]
T	Temperature [°C]
T_c	PV cell temperature at hour t [°C]
T_f	Final liquid-phase temperature of $MgCl_2$ during charging [°C]
T_i	Initial solid-phase temperature of $MgCl_2$ [°C]
T_m	Melting point of $MgCl_2$ [°C]
u	Velocity vector of heat transfer fluid [m s⁻¹]
Subscripts	
avg	Annual site mean value
cell	PV cell
charge	TES charging
CSP	Concentrated solar power subsystem

dis	TES discharging
H_2	Hydrogen
H_2O	Water (steam feed)
l	Liquid phase of PCM
latent	Latent heat component
O_2	Oxygen
PCM	Phase-change material
PV	Photovoltaic subsystem
ref	Reference or rated condition
SOEC	Solid oxide electrolysis cell subsystem
s	Solid phase of PCM
sup	Supply (available power or energy)
TES	Thermal energy storage subsystem
th	Thermal
Greek Symbols	
β	Temperature coefficient of PV power [% °C^{-1}]
ΔG	Gibbs free energy change of water splitting [kJ mol^{-1}]
ΔS	Entropy change of water splitting [kJ mol^{-1} K^{-1}]
η_{CSP}	Optical-to-thermal efficiency of CSP collector
η_{PV}	PV module efficiency accounting for temperature correction
$\eta_{PV, ref}$	PV module reference efficiency at standard test conditions
η_{TES}	Round-trip thermal efficiency of TES
γ	Temperature correction coefficient for PV efficiency [°C^{-1}]
λ	Liquid fraction of PCM (0 = fully solid, 1 = fully liquid)
μ	Dynamic viscosity of heat transfer fluid [Pa s]
ρ	Density of heat transfer fluid or PCM [kg m^{-3}]
Abbreviations	
CSP	Concentrated solar power
DHI	Diffuse horizontal irradiance
DNI	Direct normal irradiance
GHI	Global horizontal irradiance
GW	Gigawatt
HTF	Heat transfer fluid
IEA	International Energy Agency
IRENA	International Renewable Energy Agency
kW	Kilowatt
kWh	Kilowatt-hour
LCOE	Levelized cost of electricity
LCOH	Levelized cost of hydrogen
LHV	Lower heating value
MATLAB	Matrix Laboratory (MathWorks simulation environment)

$MgCl_2$	Anhydrous magnesium chloride
MW	Megawatt
MWh	Megawatt-hour
MNRE	Ministry of New and Renewable Energy (Government of India)
NOCT	Nominal operating cell temperature
NSRDB	National Solar Radiation Database
PCM	Phase-change material
PEM	Proton exchange membrane electrolyser
PR	Performance ratio of the PV system
PTC	Parabolic trough collector
PV	Photovoltaic
SOC	State of charge
SOEC	Solid oxide electrolysis cell
TES	Thermal energy storage
TMY	Typical Meteorological Year

1. INTRODUCTION

1.1. GLOBAL HYDROGEN DEMAND AND THE RENEWABLE TRANSITION

Global hydrogen demand reached approximately 97 million tonnes in 2023, driven by applications in petroleum refining, ammonia synthesis, steelmaking, and emerging low-carbon sectors (IEA 2024). Despite this scale, nearly 95% of production remains fossil-fuel-based, primarily via steam methane reforming and coal gasification, generating CO_2 emissions exceeding 900 million tonnes annually (IEA 2024; IEA 2019). Low-emissions hydrogen production accounted for less than one million tonnes in 2023, despite an announced project pipeline exceeding 520 GW of electrolysis capacity (IEA 2024). This disparity between decarbonisation ambitions and actual deployment highlights a critical gap. There is an urgent need for hydrogen production systems that are technically feasible, scalable, and fully renewable. Such systems must also operate reliably without grid support.

India's National Green Hydrogen Mission targets the production of at least five million tonnes of green hydrogen annually by 2030, positioning India as a potential global exporter of green hydrogen and hydrogen-based fuels (MNRE 2023). Achieving this target requires reliable and continuous solar-driven hydrogen production across India's diverse climatic regions. However, this challenge remains inadequately addressed in the existing literature.

1.2. SOLID OXIDE ELECTROLYSIS FOR HIGH-EFFICIENCY HYDROGEN PRODUCTION

Among electrolyser technologies, solid oxide electrolysis cells (SOECs) offer the highest electrical-to-hydrogen conversion efficiency due to their high-temperature operation at 700- 850 °C (Fallah Vostakola et al. 2023). At these temperatures, part of the thermodynamic energy required for water splitting is supplied as heat rather than electricity. This reduces electrical consumption by 15-30% compared to proton exchange membrane (PEM) and alkaline electrolysers (Afroze 2023). Stack-level efficiencies exceeding 80% have been demonstrated (Fallah Vostakola et al. 2023), and thermal integration with high-temperature heat sources further enhances performance. However, SOEC operation requires continuous and stable thermal and electrical input, posing significant challenges for integration with inherently intermittent solar resources (Norman et al. 2024; Laguna-Bercero 2012).

1.3. INDIA'S SOLAR RESOURCE POTENTIAL

India possesses one of the highest solar resource potentials globally due to its favourable geographic location within the solar belt. The spatial distribution of solar irradiance across the country is highly non-uniform. Global horizontal irradiance (GHI) is highest in the north-western regions, particularly Rajasthan and Gujarat, where annual averages exceed 5.5 kWh m^{-2} day^{-1}. In contrast, lower values are observed in the north-eastern and coastal regions due to higher cloud cover and humidity (Patel et al. 2023). The distribution of diffuse horizontal irradiance (DHI) indicates increased atmospheric scattering in southern and coastal regions. This pronounced spatial variability leads to region-specific design and operational challenges for solar-driven hydrogen production systems. It also forms the basis for the multi-location analysis presented in this study. This variability directly influences both the sizing of solar components and the reliability of continuous SOEC operation.

1.4. THE HYBRID PV-CSP-TES-SOEC SYSTEM CONCEPT

Photovoltaic (PV) systems provide low-cost daytime electricity but lack inherent dispatchability. Concentrated solar power (CSP) converts direct normal irradiance (DNI) into high-temperature thermal energy. When integrated with thermal energy storage (TES), it provides dispatchable heat beyond solar hours. The integration of anhydrous $MgCl_2$ as the phase-change material (PCM) enables latent heat storage at approximately 714 °C. This temperature is fully compatible with SOEC thermal inlet requirements. In addition, $MgCl_2$ offers a significantly higher energy density compared to conventional molten-salt sensible storage (Zhao et al. 2014). The combination of PV electricity, CSP-based thermal supply, and $MgCl_2$-PCM-integrated TES enables a dispatchable energy system. When coupled with high-efficiency SOEC electrolysis, this hybrid architecture supports continuous, grid-independent green hydrogen production. Unlike standalone PV or CSP systems, the hybrid configuration enables simultaneous management of electrical and thermal energy flows. This dual-energy integration is essential for maintaining stable SOEC operation under highly variable solar conditions. The system therefore addresses both temporal intermittency and thermal stability constraints, which are the two primary barriers to fully solar-driven SOEC operation.

1.5. SCOPE AND NOVELTY OF THE PRESENT STUDY

Despite the conceptual promise of this architecture, a fundamental engineering question remains unanswered in the existing literature: whether such a system can actually sustain continuous SOEC operation in practice across India's diverse solar conditions, and under what design and scheduling conditions this becomes achievable. Despite growing interest in solar-driven hydrogen production, three critical gaps remain unaddressed. First, most PV-CSP-hydrogen studies rely on annual average metrics or steady-state models (Azzaoui and Alami Merrouni 2025; Rosenstiel et al. 2021; Saif et al. 2025). As a result, they do not capture hourly operational feasibility under fully solar-driven, grid-independent conditions over a complete annual cycle. This limitation prevents a rigorous assessment of continuous SOEC operation.

Second, flexible SOEC load management has been shown to reduce thermo-mechanical stress and extend stack lifetime (Zhao et al. 2020; Ishan et al. 2024). However, it has not been evaluated as a system-level design variable in conjunction with $MgCl_2$-PCM-TES sizing across multiple locations.

Third, no prior study has quantified $MgCl_2$-PCM mass requirements for SOEC-coupled TES systems. In addition, the structural shortfall associated with aperture-based TES sizing has not been identified for climatically diverse Indian conditions. As a result, climate-adaptive design guidelines for PV-CSP-$MgCl_2$-PCM-SOEC systems across India are currently lacking.

Addressing these gaps requires a fully integrated, time-resolved analysis that simultaneously considers solar variability, thermal storage dynamics, and electrolyser operation.

This study makes four key contributions:

1. It provides the first systematic quantification of $MgCl_2$ PCM mass requirements for SOEC-coupled TES systems across five Indian climate zones.
2. It demonstrates that constant-load SOEC operation fails under fully solar-driven conditions, with TES depletion identified as the primary failure mechanism.
3. It develops a three-period flexible SOEC scheduling strategy that achieves ≥95% hourly reliability

across all locations.

4. It presents a comprehensive multi-location dynamic simulation framework for evaluating hybrid PV-CSP-TES-SOEC systems under realistic solar variability.

The specific objectives of this study are as follows:

- To quantify static component sizing requirements across five Indian climate zones.
- To evaluate hourly system performance under constant-load SOEC operation.
- To develop and validate a flexible three-period SOEC scheduling strategy achieving ≥ 95% reliability.
- To establish climate-adaptive design guidelines for PV-CSP-$MgCl_2$-PCM-SOEC systems.

Collectively, these contributions provide a practical framework for designing reliable, grid-independent solar hydrogen systems under real-world climatic variability.

2. LITERATURE REVIEW

2.1. SOLAR-DRIVEN HYDROGEN PRODUCTION: GLOBAL CONTEXT

Hydrogen is widely recognised as a key energy carrier for decarbonising hard-to-abate sectors. Global hydrogen demand reached 97 million tonnes in 2023. However, renewable hydrogen production remains below 1 million tonnes (IEA 2024). Fossil-based routes, primarily steam methane reforming and coal gasification, account for the majority of hydrogen supply, with associated CO_2 emissions of 9-28 kg per kg of hydrogen (IEA 2019). Solar energy offers the largest technical renewable potential for hydrogen production. However, the intermittency of solar irradiance creates fundamental challenges for continuous electrolyser operation (MNRE 2023; Gallardo et al. 2021). These challenges have driven research into hybrid solar systems that combine complementary energy sources and storage to achieve reliable, round-the-clock hydrogen output. This intermittency results in temporal mismatches between energy supply and electrolyser demand, which must be addressed through system-level integration and storage.

2.2. PV AND CSP BASED HYDROGEN PRODUCTION SYSTEMS

Photovoltaic systems have been extensively studied for green hydrogen production, with a levelized cost of electricity (LCOE) as low as 5.3-5.5 US¢ kWh^{-1} achievable in high-irradiance regions (Gallardo et al. 2021; Bhandari et al. 2014). However, PV systems are inherently diurnal. They require electrical storage or grid backup to sustain continuous hydrogen production. CSP systems convert DNI into high-temperature thermal energy. When coupled with storage, they provide dispatchable energy for high-temperature electrolysis. Hybrid PV-CSP configurations have been proposed to leverage the complementary strengths of both technologies.

Azzaoui and Alami Merrouni (2025) demonstrated that PV-CSP hybridisation in Morocco can reduce hydrogen production cost by up to 11.2% and increase annual hydrogen output by approximately 10% relative to standalone CSP. Rosenstiel et al. (2021) showed that cost-optimised PV/CSP hybrid plants achieve a lower levelized cost of hydrogen (LCOH) than standalone PV or CSP configurations. Saif et al. (2025) confirmed the economic advantage of PV-CSP hybrids for hydrogen production in Saudi Arabia. Despite these advances, most PV-CSP hydrogen studies rely on annual average metrics or simplified time-slice models. As a result, hourly operational feasibility under fully solar-driven conditions remains insufficiently characterised (Azzaoui and Alami Merrouni 2025; Rosenstiel et al. 2021; Saif et al. 2025). This limitation impedes the evaluation of system reliability under real-world variability, particularly for continuous hydrogen production.

2.3. SOLID OXIDE ELECTROLYSIS CELLS FOR HYDROGEN PRODUCTION

SOECs represent the highest-efficiency electrolyser technology, with stack-level electrical-to-hydrogen efficiencies exceeding 80% at operating temperatures of 700-850 °C (Fallah Vostakola et al. 2023). External thermal integration reduces electrical consumption by 15-30% compared to low-temperature electrolysers (Afroze 2023). Norman et al. (2024) provided a comprehensive review of steam electrolysis via SOEC, identifying thermal stability and degradation as key lifetime challenges. The electrochemical characterisation and degradation mechanisms of SOECs were reviewed in detail by Laguna-Bercero (2012), establishing the importance of controlled thermal operation for long-term stack integrity. Zhao et al. (2020) demonstrated that flexible SOEC load management reduces thermo-mechanical stress. It also improves stack lifetime by 20-35% compared to constant-load operation. Ebbesen et al. (2011) reported SOEC electrolysis efficiencies of up to 90% (LHV basis) with thermal integration, while Brisse et al. (2008) characterised SOEC performance at industrially relevant conditions. However, most existing studies evaluate SOEC performance in isolation, without integrating dynamic solar supply and thermal storage constraints at the system level.

2.4. THERMAL ENERGY STORAGE AND PHASE-CHANGE MATERIALS FOR CSP

Thermal energy storage (TES) is a key enabling technology for dispatchable CSP-driven processes. Conventional two-tank molten-salt sensible storage is mature and widely deployed (Kuravi et al. 2013), but latent heat storage using PCMs offers substantially higher volumetric energy density and improved isothermal behaviour (Farid et al. 2004). $MgCl_2$ is particularly attractive due to its melting temperature of approximately 714 °C, compatibility with SOEC thermal requirements, and latent heat of approximately 452 kJ kg^{-1} (Zhao et al. 2014). Prieto and Cabeza (2019) reviewed PCM integration in CSP plants, reporting efficiency improvements of 25-35% versus sensible storage. Alva et al. (2017) demonstrated energy density improvements of 40-60% with latent heat storage. Kenisarin (2010) and Vignarooban et al. (2015) have specifically characterised chloride salts, including $MgCl_2$, for high-temperature solar storage. The role of $MgCl_2$-PCM-TES in stabilising SOEC-coupled thermal systems under dynamic solar supply has, however, not been previously studied. Despite these advantages, the role of $MgCl_2$-based PCM in stabilising SOEC-coupled systems under dynamic solar conditions has not been systematically investigated.

2.5. HYBRID PV-CSP-TES-SOEC SYSTEMS

Integrated hybrid systems combining PV, CSP, TES, and SOEC have begun attracting research attention. Ma and Martinek (2023) reported that CSP-TES integration with high-temperature electrolysis reduces electricity consumption by approximately 20% while extending operating hours. Tofighi and Faegh (2022) demonstrated continuous hydrogen production with CSP-TES support, achieving electrolyser availability exceeding 95%. Ishan et al. (2024) showed that flexible SOEC loading strategies improve system reliability and extend stack lifetime by 22-30%, though their study was limited to a single location. Rashid et al. (2023) validated 24-hour hydrogen production using a PV-CSP-TES system but did not incorporate flexible SOEC scheduling. Building on prior work from IIT Madras, Soni and Reddy (2024) conducted a techno-economic assessment of PTC/PDC-TES systems for green hydrogen production across Indian climate zones using PEM electrolysis, and subsequently (2025) demonstrated CSP-TES-based distributed hydrogen generation, both studies providing essential comparison baselines for the present SOEC-focused analysis. Existing hybrid PV-CSP-TES systems have demonstrated improved hydrogen production and system availability. However, most studies are limited to single-location analyses or steady-state conditions. In contrast, the present study evaluates multi-location performance under full 8760-hour dynamic simulation and explicitly incorporates flexible SOEC scheduling and PCM-based thermal storage. This enables a more realistic assessment of system reliability under diverse climatic conditions.

2.6. SUMMARY OF KEY LITERATURE AND RESEARCH GAPS

Table 1 highlights that while significant progress has been made in hybrid solar hydrogen systems, no prior study integrates dynamic multi-location analysis, $MgCl_2$-based PCM storage, and flexible SOEC operation within a unified framework.

Table 1. Summary of the representative studies on solar-driven hydrogen production integrating PV, CSP, TES, and SOEC technologies.

Category	**Study**	**Key Findings**	**Key Limitations / Gap**	**Relevance to the Present Study**
PV-CSP	Azzaoui & Alami Merrouni (2025)	PV-CSP hybridisation reduces H_2 cost by up to 11.2%; H_2 output increases ~10%	Single location; no hourly dynamic simulation; no SOEC	Demonstrates PV-CSP benefits but lacks dynamic

Category	Study	Key Findings	Key Limitations / Gap	Relevance to the Present Study
				multi-location SOEC integration
PV-CSP	Rosenstiel et al. (2021)	Hybrid PV/CSP plant achieves lower LCOH than standalone PV or CSP	Steady-state analysis; no SOEC thermal integration; no TES-PCM	Highlights cost advantage but lacks thermal storage and SOEC coupling
PV-CSP	Saif et al. (2025)	Techno-economic comparison of PV and CSP for hydrogen in Saudi Arabia	PEM electrolysis only; steady-state; no flexible dispatch	Limited to low-temperature electrolysis; no high-temperature SOEC relevance
SOEC	Fallah Vostakola et al. (2023)	>80% electrical to hydrogen efficiency; comprehensive SOEC review	No renewable integration; steady-state	Provides SOEC fundamentals but lacks system-level integration
SOEC	Norman et al. (2024)	Comprehensive steam electrolysis review; thermal stability identified as key challenge	No CSP-TES coupling; no dynamic solar dispatch	Supports the need for thermal management addressed in this study
SOEC	Zhao et al. (2020)	Flexible SOEC loading reduces thermo-mechanical stress; lifetime improved 20-35%	System-level TES effects not evaluated; no solar coupling	Basis for flexible scheduling used in the present work
PCM-TES	Prieto & Cabeza (2019)	PCM-based TES improves CSP storage efficiency by 25-35% vs sensible storage	Power generation focus; no electrolyser coupling	Supports PCM use but lacks SOEC application
PCM-TES	Alva et al. (2017)	Latent heat storage increases energy density by 40-60%	No SOEC coupling; corrosion challenges noted	Demonstrates PCM advantage, but not applied to hydrogen systems
Hybrid	Rashid et al. (2023)	24-hour hydrogen production validated with PV+CSP+TES	No flexible SOEC scheduling; single location	Demonstrates feasibility but lacks scheduling optimisation
Hybrid	Ishan et al. (2024)	Flexible SOEC loading improves reliability and extends stack lifetime by 22-30%	Limited to a single location; no $MgCl_2$ PCM	Provides a scheduling basis extended in this study
Hybrid	Soni & Reddy (2024)	Techno-economic assessment of PTC/PDC-TES for green H_2 across Indian climate zones	PEM electrolysis; no SOEC; no flexible dispatch; no $MgCl_2$ PCM	Provides baseline Indian context without SOEC integration
Hybrid	Soni & Reddy (2025)	CSP-TES distributed green H_2 generation; multi-location India analysis	Alkaline electrolysis; no SOEC; no dynamic flexible scheduling	Multi-location baseline extended here with SOEC and flexibility

Three major research gaps emerge from this review. First, no prior study has conducted a full 8760-hour dynamic simulation of a hybrid PV-CSP-TES-SOEC system with $MgCl_2$ PCM under realistic solar variability across multiple Indian climate zones. Second, flexible SOEC load scheduling has not been evaluated as a system-level design variable in conjunction with location-optimised PCM-TES sizing. Third, climate-adaptive design guidelines for PV-CSP-$MgCl_2$-PCM-SOEC systems across India's diverse solar geography do not exist. The present study directly addresses all three gaps. Overall, the existing literature lacks a comprehensive, time-resolved evaluation of hybrid PV-CSP-TES-SOEC systems incorporating PCM-based thermal storage and flexible electrolyser operation. Addressing this gap is essential for developing reliable, grid-independent solar hydrogen production systems across diverse climatic conditions.

3. SYSTEM DESCRIPTION AND METHODOLOGY

3.1. HYBRID PV-CSP-TES-SOEC SYSTEM CONFIGURATION

The proposed system integrates four subsystems.

1. A photovoltaic (PV) array supplying electrical power to the SOEC.
2. A CSP field converting DNI into high-temperature thermal energy.
3. A TES unit employing anhydrous $MgCl_2$ PCM for latent heat storage and thermal dispatch.
4. A solid oxide electrolysis cell (SOEC) stack consuming combined electrical and thermal inputs for hydrogen production.

The system is configured for fully grid-independent operation, with no electricity import or export at any stage. The overall system schematic is shown in Figure 1.

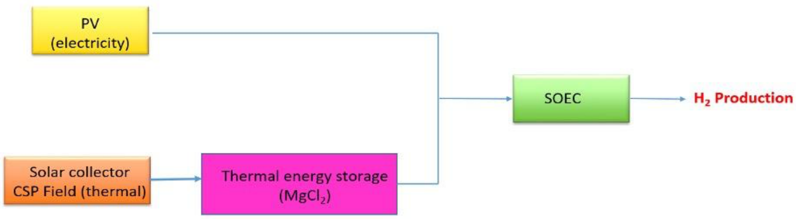

Figure 1. Schematic of the hybrid PV-CSP-TES-$MgCl_2$-PCM-SOEC system for continuous, grid-independent hydrogen production.

PV electricity is supplied directly to the SOEC at all available hours. CSP thermal output first satisfies the SOEC thermal demand; any surplus is directed to TES charging via PCM melting. During non-solar periods, particularly overnight, TES discharges stored latent heat via PCM solidification to maintain the SOEC operating temperature, thereby sustaining continuous hydrogen production. This configuration ensures that system performance is evaluated solely on the basis of renewable resource availability and internal energy management.

3.1.1. MODEL ASSUMPTIONS

The following assumptions were adopted to ensure computational tractability while preserving physically representative system-level behaviour:

- PV module efficiency was corrected for cell temperature using a linear temperature coefficient of −0.40% °C^{-1}, applied to the reference efficiency at standard test conditions (25 °C, 1000 W m^{-2}). Secondary optical losses - soiling, partial shading, and spectral mismatch were not included. This is a well-established simplification for hourly system-level energy balance studies; the resulting uncertainty in annual energy yield is typically within 3-8% and does not alter the comparative conclusions across the five study locations (Kalogirou 2014; Green et al. 2018).
- DC-to-AC conversion losses and inter-array wiring resistances were not separately parameterised. These effects are considered negligible at the hourly system-level resolution adopted here and are not significant drivers of location-to-location performance variation (Kalogirou 2014).
- The CSP subsystem was modelled using a constant optical-to-thermal efficiency of 0.68, consistent with the seasonally averaged design-point value reported for parabolic trough systems under comparable operating conditions (Soni and Reddy 2024; Fernandez-Garcia et al. 2010). Across the latitude range studied (8°N-34°N), variation in the incidence angle modifier remains within ±5%, which falls within the inherent uncertainty of the TMY irradiance dataset and does not meaningfully affect comparative results.
- The TES subsystem employing $MgCl_2$ PCM was modelled as a lumped-parameter thermal reservoir with a constant round-trip thermal efficiency of 0.92. This factor accounts collectively for heat losses during charge and discharge cycles, including conduction losses to the ambient environment and heat exchanger irreversibilities (Prieto and Cabeza 2019; Xu et al. 2015). Internal spatial temperature gradients and phase-front propagation within the PCM were not explicitly resolved, consistent with hourly-resolution system-level modelling practice.

- The SOEC subsystem was assumed to operate at a constant specific electrical energy consumption of 44.4 kWh kg^{-1} H_2, corresponding to approximately 80% stack-level efficiency on a lower heating value (LHV) basis under thermally integrated conditions. This value is valid across the SOEC operating temperature range of 700-850 °C, which is maintained throughout operation by $MgCl_2$ TES discharge at 714 °C (Fallah Vostakola et al. 2023; Ebbesen et al. 2011; Afroze 2023). At each hourly timestep, steady-state electrochemical behaviour was assumed, which is appropriate given the 1-hour temporal resolution of the NSRDB TMY dataset (Sengupta et al. 2018).
- Electrochemical degradation, stack ageing, and transient start-up and shut-down effects were not considered, as the focus of this study is on operational scheduling strategy and comparative multi-location performance assessment rather than long-term stack lifetime analysis (Graves et al. 2011).
- All simulations were performed under fully grid-independent operating conditions. No electricity import from or export to an external grid was permitted at any stage of the simulation under either operating strategy.
- Parasitic and auxiliary power demands - including solar field tracking drives and pump work were not explicitly modelled. Their combined contribution at this system scale is estimated to be below 2-3% of total output and does not affect the comparative reliability rankings across the five study locations (Pfenninger et al. 2014; Lund et al. 2015).
- Thermal interfaces between subsystems - specifically the CSP-to-TES and TES-to-SOEC heat transfer pathways were assumed lossless beyond the round-trip efficiency already embedded in $\eta_{TES,}$ which is 0.92. Pipe-run conduction losses are considered negligible for the centralised, co-located plant configuration assumed here (Prieto and Cabeza 2019).

These assumptions are consistent with established practice in hourly dynamic simulation studies of hybrid renewable energy systems and are considered appropriate for the comparative multi-location performance assessment undertaken here (Pfenninger et al. 2014; Lund et al. 2015). The numerical boundary conditions imposed uniformly across all simulations are detailed in Section 3.5.1.

3.2. SITE SELECTION AND SOLAR RESOURCE DATA

Five locations representing distinct Indian climate zones were selected for the analysis: Jodhpur (arid), Ladakh (cold high-altitude), Nagpur (semi-arid), Bengaluru (temperate), and Kochi (humid coastal). Together, these sites span a wide range of solar and climatic conditions, providing a suitable basis for evaluating the robustness of the proposed hybrid system across geographically diverse operating environments. The selected locations differ not only in annual solar availability but also in seasonal variability, cloud cover characteristics, and diurnal temperature profiles. These differences strongly influence PV output, CSP thermal generation, TES charging behaviour, and overall SOEC operating reliability. The geographic coordinates and key solar resource characteristics of the selected sites are summarised in Table 2.

Table 2. Geographic coordinates and solar resource characteristics of the five study locations based on NSRDB TMY data. GHI and DNI are daily averages.

Parameter	Unit	Jodhpur	Ladakh	Nagpur	Bengaluru	Kochi
Latitude	–	26°14′20″ N	34°09′09″ N	21°09′00″ N	12°58′44″ N	9°55′52″ N
Longitude	–	73°00′42″ E	77°34′05″ E	79°05′00″ E	77°35′30″ E	76°16′26″ E
GHI	kWh m^{-2} day^{-1}	5.8	5.5	5.4	5.2	4.9
DNI	kWh m^{-2} day^{-1}	6.2	6.5	5.9	4.5	4.0

Hourly solar resource data were obtained from the NSRDB SUNY India database (Sengupta et al. 2018). Typical Meteorological Year (TMY) datasets were used for the primary simulations. These datasets are derived from long-term historical records. They are widely used for solar energy system assessment because they preserve representative seasonal and hourly irradiance trends while avoiding dependence on any single meteorological year (Crawley et al. 2008; Ernst et al. 2019). The use of TMY data is appropriate for the present study, as the objective is to evaluate long-term system behaviour and to compare relative performance across different climatic regions under consistent boundary conditions. In particular, the selected locations capture contrasting combinations of high-DNI arid conditions, monsoon-driven intermittency, and coastal cloud-dominated environments, enabling a broader evaluation of system adaptability.

3.3. COMPONENT MODELLING

Table 3. Summary of the key system design parameters and their sources.

Parameter	Value	Unit	Source/Basis
PV module efficiency (η_{PV})	18.0	%	(Rosenstiel et al. 2021; Kalogirou 2014)
PV temperature coefficient	−0.40	% / °C	(Kalogirou 2014)
CSP optical-thermal efficiency (η_{CSP})	0.68	-	(Soni and Reddy 2024)
PCM: $MgCl_2$ melting temperature (T_m)	714	°C	(Zhao et al. 2014; Kenisarin 2010)
PCM: $MgCl_2$ latent heat (h_{latent})	452	kJ kg^{-1}	(Zhao et al. 2014; Kenisarin 2010)
TES round-trip thermal efficiency (η_{TES})	0.92	-	(Prieto and Cabeza 2019; Xu et al. 2015)
SOEC operating temperature	700-850	°C	(Fallah Vostakola et al. 2023; Norman et al. 2024)
SOEC specific energy consumption (e)	44.4	kWh kg^{-1} H_2	(Fallah Vostakola et al. 2023; Afroze 2023)
SOEC nominal load (constant case)	1998	kW	Design
Total system design power	2000 (1 MW PV + 1 MW CSP)	kW	Design
Design H_2 production target	1080	kg day^{-1}	Design
Simulation timestep/horizon	1 h / 8760 h	-	(Sengupta et al. 2018)
Solar data source	NSRDB-SUNY India TMY	-	(Sengupta et al. 2018)

3.3.1. PHOTOVOLTAIC SUBSYSTEM

The hourly electrical output of the PV array is estimated using a conventional area-efficiency formulation commonly adopted in system-level solar energy studies (Kalogirou 2014; Green et al. 2018):

$$P_{PV(t)} = GHI(t) \times A_{PV} \times \eta_{PV,ref} \cdot [1 + \beta\ (T_{c(t)} - T_{ref})] \quad (1)$$

where $P_{PV(t)}$ is the instantaneous PV output power (kW); GHI(t) is the global horizontal irradiance at hour t (kW m^{-2}); A_{PV} is the total PV array area (m^2); $\eta_{PV,\ ref}$ is the module reference efficiency at standard test conditions (25 °C, 1000 W m^{-2}); β is the temperature coefficient of power (−0.004 $°C^{-1}$, equivalent to −0.40% $°C^{-1}$), accounting for efficiency loss at elevated cell temperatures; $T_{c(t)}$ is the cell temperature at hour t (°C), and T_{ref} is the standard reference temperature (25 °C). The term in square brackets represents the fractional deviation of efficiency from its rated value due to thermal effects. Cell temperature is estimated from ambient temperature and irradiance using the nominal operating cell temperature (NOCT) relationship. This model is appropriate for system-level hourly energy balance studies; more detailed single-diode representations introduce corrections typically below 3-8% at this temporal resolution (Kalogirou 2014).

3.3.2. CONCENTRATED SOLAR POWER SUBSYSTEM

The thermal energy supplied by the CSP field is calculated directly from the hourly DNI availability:

$$P_{CSP(t)} = DNI(t) \times A_{CSP} \times \eta_{CSP} \quad (2)$$

where $P_{CSP(t)}$ is the CSP thermal output at hour t (kW_{th}); DNI(t) is the direct normal irradiance at hour t (kW m^{-2}); A_{CSP} is the collector aperture area (m^2); and $\eta_{\ CSP}$ is the optical-to-thermal efficiency of the parabolic trough collector, fixed at 0.68 (Soni and Reddy, 2024; Fernandez-Garcia et al., 2010). A constant optical-thermal efficiency of 0.68 is assumed throughout the simulation. This value is consistent with previously reported performance ranges for parabolic trough systems operating near design conditions. The linear dependence on DNI reflects the fact that only the beam component of solar radiation is usable by concentrating collectors, which is why CSP performance is far more sensitive to site selection than PV. Location-to-location variation in the incidence angle modifier is within ±5% for the latitude range studied (8°N-34°N), within the modelling uncertainty of the TMY dataset itself. During operation, available CSP heat is first directed toward meeting the SOEC thermal requirement. Any excess thermal energy is then diverted to TES charging. During periods of CSP deficit, TES discharge supplements the shortfall.

3.3.3. THERMAL ENERGY STORAGE WITH MAGNESIUM CHLORIDE PCM

Anhydrous $MgCl_2$ was selected as the PCM due to its melting temperature of approximately 714 °C (compatible with SOEC inlet requirements), latent heat of 452 kJ kg^{-1}, and high energy density compared to sensible storage alternatives (Zhao et al. 2014; Kenisarin 2010; Vignarooban et al. 2015). The total thermal energy stored in the $MgCl_2$ PCM-based TES unit is calculated using the three-phase sensible-latent-sensible model (Xu et al. 2015; Prieto and Cabeza 2019; Zhang et al. 2026):

$$E_{TES} = m_{PCM} \left[c_s (T_m - T_i) + h_{latent} + c_l (T_f - T_m) \right] \tag{3}$$

where E_{TES} is the total usable TES energy capacity (kWh_{th}); m_{PCM} is the mass of $MgCl_2$ phase-change material (kg); c_s and c_l are the specific heat capacities of $MgCl_2$ in the solid and liquid phases, respectively (kJ kg^{-1} $°C^{-1}$); T_m is the melting point of $MgCl_2$ (≈ 714 °C); T_i is the initial solid-phase temperature (°C); T_f is the final liquid-phase temperature during charging (°C); h_{latent} is the latent heat of fusion of $MgCl_2$ (452 kJ kg^{-1}).
The three terms inside the brackets represent:

1. sensible heat absorbed during solid-phase heating to the melting point;
2. latent heat absorbed during isothermal phase transition; and
3. Additional sensible heat absorbed in the liquid phase above the melting point.

The near-isothermal nature of the latent heat release during PCM solidification is particularly valuable for SOEC operation, as it maintains a stable thermal inlet temperature and reduces electrolyser thermal cycling stress (Zhao et al. 2020; Graves et al. 2011). TES charging and discharging are governed by real-time supply-demand balance, with hard SOC constraints ($0 \leq SOC \leq E_{TES}$).

The physicochemical properties of $MgCl_2$ determine system performance in three distinct and quantifiable ways. First, the melting temperature of 714 °C directly matches the thermal inlet requirement of the SOEC stack (700-850 °C), eliminating the need for auxiliary heating or temperature buffering between TES discharge and electrolyser input-a thermal compatibility that would not hold for lower-melting chloride salts or conventional molten-salt sensible storage media operating below 600 °C (Kenisarin 2010; Vignarooban et al. 2015). Second, the latent heat of 452 kJ kg^{-1} gives $MgCl_2$ a volumetric energy density approximately 2.5 to 3 times higher than sensible-heat storage at equivalent temperature range and mass, directly controlling the PCM mass required at each site (325.7 t at Jodhpur to 823.9 t at Kochi) and consequently influencing the physical footprint and material cost of the TES unit (Xu et al. 2015; Prieto and Cabeza 2019; Riffat and Samaei 2026). Although the required PCM masses are substantial (325.7–823.9 t), they reflect the thermal storage capacity needed to sustain high-temperature SOEC operation during extended periods of low solar availability. Such storage scales are comparable to industrial thermal energy storage applications and represent the infrastructure trade-off associated with fully grid-independent hydrogen production. Third, and most critical for SOEC operation, the near-isothermal solidification of $MgCl_2$ at 714 °C during discharge maintains a constant thermal output temperature regardless of the TES state of charge. This decouples the SOEC inlet temperature from storage depletion state - a property that sensible storage cannot replicate, where outlet temperature falls continuously as storage empties. In a sensible-heat system, SOEC curtailment would begin not at SOC = 0 but at whatever SOC corresponds to the minimum acceptable inlet temperature, effectively reducing usable storage capacity by 20-30% (Graves et al. 2011; Zhao et al. 2020). The isothermal behaviour of $MgCl_2$ therefore extends usable TES capacity by this margin and is expected to improve hourly reliability relative to what an equivalent-mass sensible storage system.

3.3.4. SOLID OXIDE ELECTROLYSIS CELL MODEL

The instantaneous hydrogen production rate is related to the electrical power supplied to the SOEC by:

$$m_{H2(t)} = \frac{P\ SOEC(t)}{e\ SOEC} \tag{4}$$

where $m_{H2(t)}$ is the hydrogen mass production rate at hour t (kg h^{-1}); $P\ SOEC(t)$ is the electrical power input to the SOEC stack at hour t (kW); and $e\ SOEC$ is the specific electrical energy consumption of the SOEC, taken as 44.4 kWh kg^{-1} H_2 (Fallah Vostakola et al. 2023; Ebbesen et al. 2011; Afroze 2023). This value corresponds to a stack-level electrical-to-hydrogen conversion efficiency of approximately 80% on a lower heating value (LHV) basis, achieved under thermally integrated conditions where a portion of the thermodynamic energy requirement for water splitting is supplied as heat from the CSP-TES subsystem rather than as electricity. The SOEC is curtailed proportionally when the TES state-of-charge reaches zero, so $P\ SOEC(t)$ and consequently, $m_{H2(t)}$ may fall below their scheduled values during storage-depleted hours.

3.4. SOEC OPERATING STRATEGIES

Two strategies are evaluated. The first is constant-load operation at a fixed 1998 kW (corresponding to the 1080 kg day^{-1} hydrogen target) throughout all 8760 hours, representing the baseline operating strategy adopted in most prior SOEC modelling studies (Fallah Vostakola et al. 2023; Zhao et al. 2020; Rashid et al. 2023).

The second is the optimised flexible scheduling strategy, which modulates SOEC load across three daily periods to match solar availability and preserve TES reserves: Night (20:00-06:00) at 0.6× nominal (approximately 1,200 kW); Shoulder periods (06:00-10:00 and 16:00-20:00) at 1.0× nominal (approximately 2,000 kW); Midday solar peak (10:00-16:00) at 1.5× and 1.8× nominal (approximately 2,700-3,600 kW, location-optimised). The midday multiplier is 1.5× for Jodhpur and 1.8× for all other locations, reflecting their greater need to concentrate production during peak solar windows. Total daily hydrogen production is maintained at 1,080 kg day^{-1} through operational load shifting rather than infrastructure oversizing. This approach is consistent with the flexible dispatch philosophy demonstrated by Ishan et al. (2024) and Zhao et al. (2020), extended here to a multi-location, full-year system-level analysis.

3.5. DYNAMIC SIMULATION FRAMEWORK AND OPTIMISATION

All component models, hourly dynamic simulations, and post-processing were implemented in MATLAB (MathWorks, R2023a). The simulation resolves the hourly energy balance across 8760 timesteps through five sequential operations at each simulation timestep:

1. PV electrical output and CSP thermal output are calculated from NSRDB hourly irradiance inputs;
2. The SOEC scheduled load is determined by the selected operating strategy.
3. A TES state-of-charge constraint check enforces $0 \leq SOC(t) \leq E_{TES}$;
4. Hydrogen production is calculated from the available electrical and thermal energy supply, and
5. Hourly reliability R(t) is logged as 1 when the scheduled SOEC load is fully met and 0 otherwise.

The complete computational flow is presented in Figure 2.

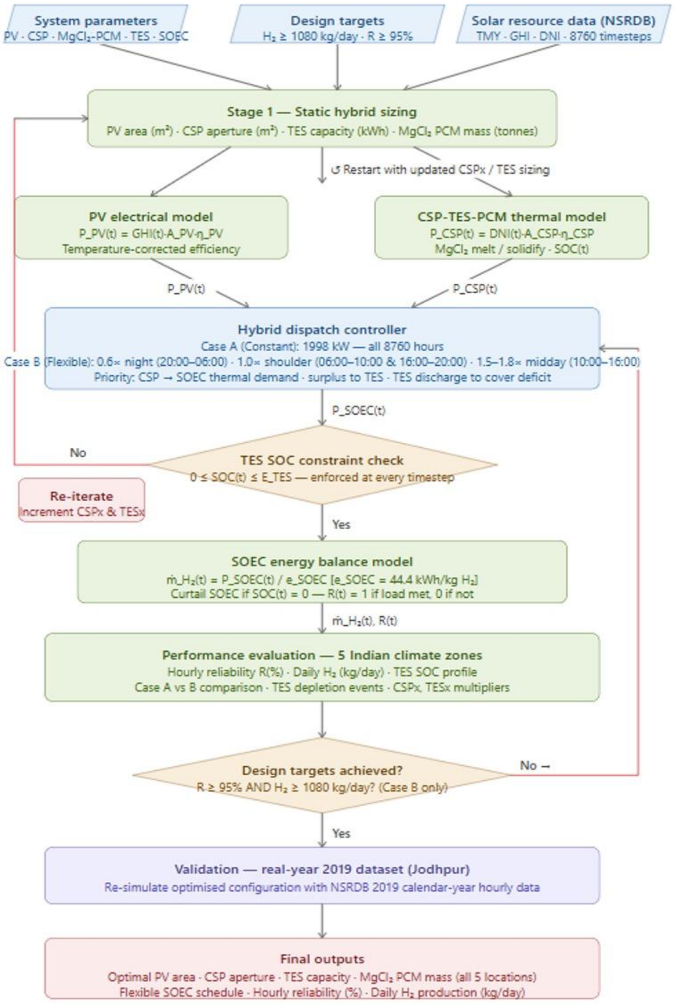

Figure 2. Flow chart diagram of the hybrid PV-CSP-TES-$MgCl_2$-PCM-SOEC hourly simulation, optimisation, and validation framework.

3.5.1. Boundary Conditions

The following boundary conditions are imposed uniformly across all five locations and both operating strategies throughout the 8760-hour simulation:

The system operates in a fully grid-independent mode at all times. No electricity import from or export to an external grid is permitted under any condition. PV and CSP outputs are strictly supply-side limited: they cannot exceed the value dictated by the hourly irradiance input and the installed area at each timestep.

The TES state-of-charge is bounded by a hard floor of zero and a hard ceiling equal to the installed usable capacity E_{TES}:

$$0 \leq \mathrm{SOC}(t) \leq E_{TES} \tag{5}$$

Charging occurs only when CSP thermal output exceeds the instantaneous SOEC thermal demand and surplus thermal energy is available. Discharging occurs only when CSP output is insufficient to meet the SOEC thermal requirement. The TES was not permitted to charge and discharge simultaneously within the same timestep.

SOEC operation is curtailed in proportion if the combined supply from CSP and TES falls below the scheduled load for a given hour. Partial hydrogen production at the reduced supply level is logged, but the hour is recorded as a reliability failure ($R(t) = 0$).

The simulation timestep is one hour, consistent with the temporal resolution of the NSRDB TMY dataset (Sengupta et al. 2018). The simulation horizon covers all 8760 hours of a full calendar year with no warm-up period; the TES is initialised at 50% of its installed capacity at hour zero, consistent with a charge-neutral initial condition. The SOEC operating temperature was assumed to remain within 700-850 °C throughout the simulation through thermal support from $MgCl_2$ PCM discharge at 714 °C. No auxiliary electrical preheating is required or modelled. Ambient temperature influences PV cell temperature via the NOCT relationship (Equation 1) but does not affect TES heat loss, CSP optical efficiency, or SOEC specific energy consumption, all of which are held at their design-point values throughout the simulation. These conditions ensure that no implicit energy source supplements the system at any point in the simulation, and that all reported reliability values reflect physically achievable performance under fully solar-driven, off-grid operation.

3.5.2. Iterative Parametric Optimisation

The CSP aperture and TES capacity multipliers were determined through a systematic iterative parametric sweep. The procedure begins from the statically sized baseline values established in Section 4. Two non-dimensional multipliers are defined: a CSP multiplier (CSP×), applied uniformly to the baseline aperture area, and a TES multiplier (TES×), applied uniformly to the baseline storage capacity. At each iteration, the full 8760-hour simulation is executed using the current multiplier pair. After the simulation completes, two performance criteria are checked simultaneously:

1. annual hourly reliability $R \geq 95\%$, and
2. mean daily hydrogen output ≥ 1080 kg day^{-1}.

If both criteria are met, the current multiplier pair is identified as the optimised design point for that location. If either criterion is not satisfied, both multipliers are incremented by a fixed step size, and the full 8760-hour simulation is re-run from hour one. This cycle continues until the minimum multiplier combination that simultaneously satisfies both targets is identified. The final multiplier values at convergence represent the minimum infrastructure configuration that meets both targets at each site. This deterministic parametric search is fully transparent and reproducible, requiring no heuristic assumptions or algorithm-specific tuning parameters (Lund et al. 2015; Pfenninger et al. 2014).

3.6. Model Validation

The simulation framework was validated at three levels: component-level analytical verification, cross-year robustness testing, and benchmarking of subsystem parameters against published experimental data.

Component-level verification: Static sizing outputs, including PV array area, CSP aperture, and PCM mass, were verified against the closed-form expressions in Equations (1)-(3) using independently computed site-mean irradiance values from the NSRDB dataset; agreement was within 0.5% across all five sites, confirming correct implementation of the sizing logic (Sengupta et al. 2018). The hourly TES energy balance, including SOC evolution and hard-constraint enforcement, was additionally verified on a synthetic 72-hour irradiance profile with a known analytical solution; simulated SOC trajectories matched reference values to within numerical precision.

Cross-year robustness testing: The full 8760-hour dynamic simulation, calibrated on TMY data, was re-run using real calendar-year 2019 hourly irradiance data for Jodhpur from the same NSRDB-SUNY India database - an independent meteorological year not used in component sizing or parametric optimisation. Under flexible SOEC scheduling, the 2019 simulation yielded hourly reliability of 94.8% and mean daily hydrogen production of 1076 kg day^{-1}, within 0.4 percentage points of the TMY-based results in both metrics. This agreement indicates that the optimised scheduling strategy and TES sizing are robust to inter-annual solar variability and that reported performance is not an artefact of the TMY smoothing process.

Subsystem parameter benchmarking: Each subsystem efficiency parameter was benchmarked against published experimental and modelling data before simulation. The PV temperature coefficient of −0.40% °C^{-1} lies within the range of −0.35 to −0.45% °C^{-1} reported for monocrystalline silicon modules under outdoor conditions (Kalogirou 2014; Green et al. 2018). The CSP optical-to-thermal efficiency of 0.68 is consistent with the range of 0.64–0.72 reported for parabolic trough systems at design-point DNI (Soni and Reddy 2024; Fernandez-Garcia et al. 2010). The TES round-trip efficiency of 0.92 is consistent with experimentally characterised high-temperature latent heat storage systems at a comparable scale (Prieto and Cabeza 2019; Xu et al. 2015). The SOEC specific energy consumption of 44.4 kWh kg^{-1} H_2 corresponds to approximately 80% LHV efficiency, consistent with published stack-level measurements for thermally integrated SOEC operation at 700-850 °C (Fallah Vostakola et al. 2023; Ebbesen et al. 2011).

Taken together, these three validation steps confirm that the simulation framework correctly implements the component models, produces results robust to inter-annual meteorological variability, and adopts subsystem parameters grounded in published experimental data. The framework is therefore considered suitable for the comparative multi-location reliability and hydrogen production analysis presented in Section 4. For clarity, Tables 4 and 5 summarise the governing equations in simplified system-level form for the hourly simulation framework. Detailed component-level formulations and derivations are provided in Sections 3.3.1–3.3.4.

Table 4. Governing equations of the hybrid PV-CSP-TES-$MgCl_2$ PCM-SOEC system.

Subsystem	Governing equation	Description / Physical meaning
HTF flow (TES domain)	$\partial\rho/\partial t + \nabla\cdot(\rho u) = 0$	Mass continuity of heat transfer fluid
	$\rho\, Du/Dt = -\nabla p + \mu\nabla^2 u$	Momentum conservation (Navier–Stokes)
	$\rho\, cp\, DT/Dt = \nabla\cdot(k\,\nabla T)$	Energy equation for fluid flow
PCM domain (phase change)	$\rho\, \partial h/\partial t = \nabla\cdot(k\,\nabla T)$	Energy conservation in PCM
	$h = c_p T + \lambda L_f$	Enthalpy formulation
	$\lambda = (T - T_s)/(T_l - T_s)$	Liquid fraction
TES system model	$E_{TES} = m_{PCM}\, h_{latent}\, \eta_{TES}$	Storage capacity
	$SOC(t+1) = SOC(t) + P\, charge(t)\cdot\eta$ TES – $P_{dis(t)}/\eta_{TES}$	Dynamic balance P charge(t): Charging power from surplus CSP energy. P dis(t): Discharging power supplied from TES to SOEC. η TES: Thermal energy storage efficiency.
	$0 \le SOC \le E_{TES}$	Constraint
PV electrical model	$P_{PV} = GHI \times A_{PV} \times \eta_{PV}$	PV generation
	$\eta_{PV} = \eta_{ref}[1+\gamma(T_{cell}-25)]$	Temp correction
CSP model	$P_{CSP} = DNI \times A_{CSP} \times \eta_{CSP}$	CSP output
SOEC model	$\dot{m}_{H2} = P_{SOEC} / e_{SOEC}$	Hydrogen rate
	$e_{SOEC} = (\Delta G + T\Delta S)/(n F)$	Energy requirement
Mass balance	$\dot{m}_{H2O} = 9\dot{m}_{H2}$	Water consumption
	$\dot{m}_{O2} = 8\dot{m}_{H2}$	Oxygen production
Thermal coupling	$Q_{th} = \dot{m}_{H2}(T\Delta S)$	Thermal demand
	$P_{CSP} + P_{TES} \rightarrow Q_{th}$	Thermal supply
System balance	$P_{PV} + P_{CSP} + P_{TES} = P_{SOEC} + losses$	Energy conservation
Performance	$R = (1/N)\,\Sigma\, I\,(P_{sup} \ge P_{SOEC})$	Reliability
Flexible operation	$P_{SOEC} = 0.6\text{–}1.8\, P_{nom}$	Adaptive scheduling

Table 5. Simplified Governing equations of the hybrid PV, CSP, TES, $MgCl_2$ PCM, and SOEC system.

Subsystem	Equation	Parameters
PV	$P_{PV}(t) = GHI(t) \times A_{PV} \times \eta_{PV}$	A_{PV} = PV area (m^2); η_{PV} = PV efficiency
CSP	$P_{CSP}(t) = DNI(t) \times A_{CSP} \times \eta_{CSP}$	A_{CSP} = CSP aperture (m^2); $\eta_{CSP} = 0.68$
TES capacity	$E_{TES} = m_{PCM} \times h_{latent} \times \eta_{TES}$	m_{PCM} = PCM mass (t); h_{latent} = 452 kJ kg^{-1}; $\eta_{TES} = 0.92$
TES SOC	$SOC(t+1) = SOC(t) + P_{CSP,\, surplus(t)} - P_{SOEC,\, thermal(t)}$	Bounded: $0 \le SOC \le E_{TES}$
SOEC H_2 output	$m_{H2(t)} = P_{SOEC(t)} / e_{SOEC}$	e_{SOEC} = 44.4 kWh kg^{-1} H_2
Reliability	R = (hours SOEC fully met) / 8760 x 100%	Design target: R ≥ 95%

4. STATIC SIZING ANALYSIS

4.1. PURPOSE AND METHODOLOGY

Static sizing establishes baseline component capacities using site-specific mean annual GHI and DNI values under average-irradiance assumptions, neglecting sub-daily variability and TES cycling dynamics (Soni and Reddy 2024; Ernst et al. 2019). A unit-scale hydrogen demand of 270 kg day^{-1} (1 MW PV + 1 MW CSP system) was adopted; full-scale results correspond to four such units (1080 kg day^{-1}, 2 MW total). Static sizing provides first-order capacity estimates and establishes the geographic sensitivity of each component before dynamic simulation.

4.2. PV AREA SIZING

The required PV array area to meet the electrical demand of the SOEC is:

$$A_{PV} = \frac{E_{PV,daily}}{GHI_{avg} \times \eta_{PV} \times PR} \quad (6)$$

where P_{SOEC}, rated is the rated SOEC electrical demand (kW); GHI_{mean} is the site annual mean GHI (kW m^{-2}); and $\eta_{PV, ref}$ is the reference module efficiency. PV area requirements range from 16,227 m^2 (Jodhpur, GHI approximately 2190 kWh m^{-2} yr^{-1}) to 19,840 m^2 (Kochi, GHI approximately 1760 kWh m^{-2} yr^{-1}), a geographic variation of 22%, and PR is the performance ratio, which is 0.75 to 0.80. This sensitivity directly translates into differences in capital costs and land requirements and underscores the importance of location-specific sizing.

4.3. CSP APERTURE SIZING

CSP aperture is sized from the daily thermal energy demand (36 MWh day^{-1}) and site DNI:

$$A_{CSP} = \frac{E_{CSP,daily}}{(DNI_{avg} \times \eta_{CSP})} \quad (7)$$

Target-based CSP aperture ranges from 12,870 m^2 (Jodhpur, DNI approximately 2050 kWh m^{-2} yr^{-1}) to 19,950 m^2 (Kochi, DNI approximately 1250 kWh m^{-2} yr^{-1}), a 55% increase from the best to the worst site. A uniform fixed aperture of approximately 5000 m^2 (representing a non-adaptive design) is shown for comparison. Site-adaptive CSP sizing is therefore a technical necessity, not merely a preference.

4.4. MAGNESIUM CHLORIDE PCM MASS REQUIREMENTS AND THE APERTURE-SIZING SHORTFALL

TES is designed to provide 14 hours of SOEC thermal support per day (18:00-08:00). While the target usable TES energy is uniformly 18 MWh, the required $MgCl_2$ PCM mass varies from 190 t (Jodhpur) to 240 t (Kochi) due to differences in the effective daily solar charging opportunity. Aperture-based PCM sizing produces systematic shortfalls of 49 to 60 t across all five sites. At Kochi, this shortfall is 24% of the target-based PCM mass. Such under-sizing would cause recurring nightly TES depletion under constant-load SOEC operation, as confirmed by the dynamic simulation (Section 5.2). To the authors' knowledge, this represents the first systematic quantification of the $MgCl_2$-PCM mass shortfall arising from aperture-based sizing for SOEC-coupled high-temperature TES systems across Indian climate zones.

4.5. STATIC SIZING SUMMARY

Results are summarised in Table 6 and Figure 3. Static sizing reveals a systematic pattern: as solar resource quality declines from north-western arid sites (Jodhpur, Ladakh) to humid coastal locations (Kochi), all component capacities increase. CSP aperture shows the greatest relative sensitivity (+55%), followed by PCM mass (+26%) and PV area (+22%).

Table 6. Static sizing results for the hybrid PV-CSP-TES-SOEC system at five Indian locations (H_2 production target: 1,080 kg day^{-1}; TES usable energy: 18.0 MWh).

Location	Climate Zone	GHI (kWh m^{-2} yr^{-1})	DNI (kWh m^{-2} yr^{-1})	PV Area (m^2)	CSP Aperture (m^2)	PCM Mass (t)
Jodhpur	Arid	2190	2050	16,227	12,870	190
Ladakh	Cold/High Alt.	2160	2100	16,890	12,540	195
Nagpur	Semi-arid	1970	1750	18,480	15,100	210
Bengaluru	Temperate	1870	1550	19,200	17,040	225
Kochi	Humid/Coastal	1760	1250	19,840	19,950	240

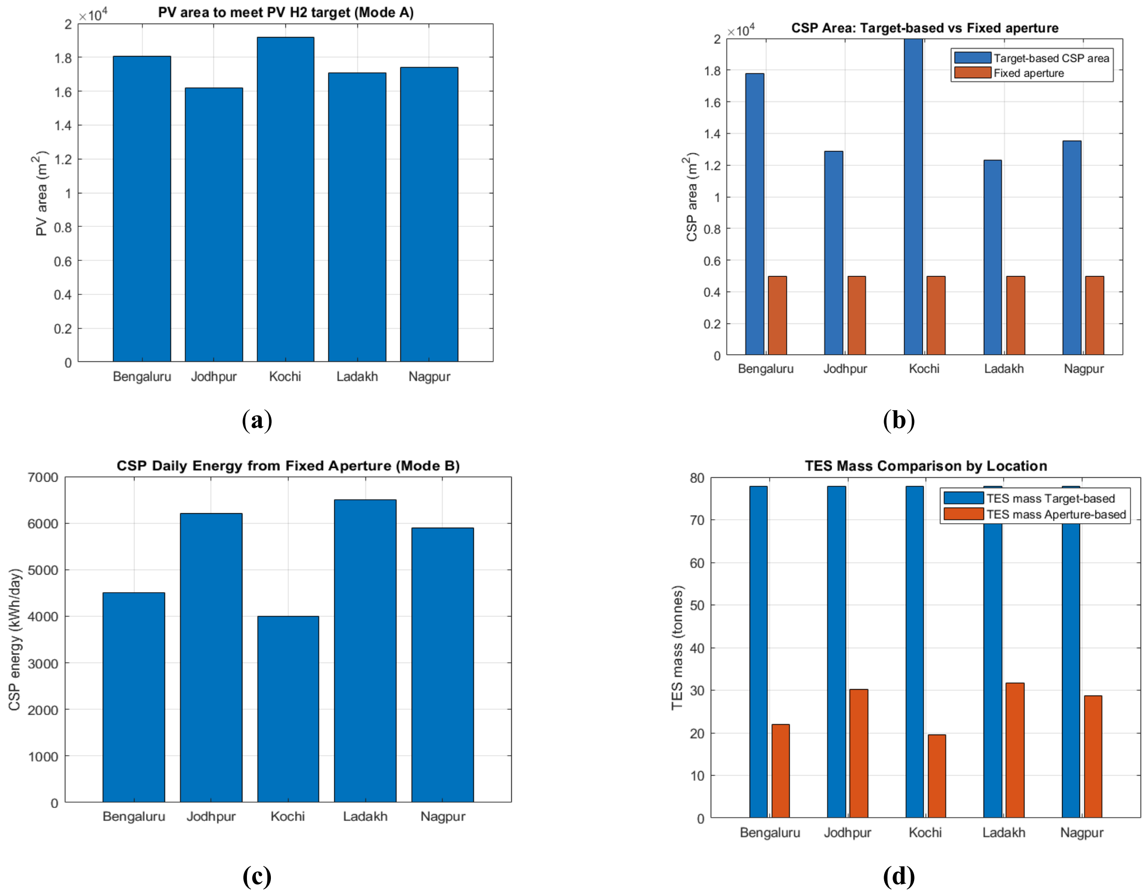

Figure 3. Static sizing outcomes across five Indian climate zones. **(a)** Required PV area; **(b)** CSP aperture: target-based vs. fixed reference aperture; **(c)** CSP daily energy from fixed aperture illustrating DNI dependence; **(d)** $MgCl_2$ PCM mass: target-based vs. aperture-based (showing the systematic shortfall of non-adaptive sizing).

Figure 3 presents the static sizing outcomes across the five Indian climate zones. Figure 3(a) shows the required PV array area, which ranges from 16,227 m² at Jodhpur to 19,840 m² at Kochi, a geographic spread of approximately 22%. This variation is a direct consequence of the declining GHI from the north-western arid sites to the humid coastal south and translates proportionally into differences in land use and capital expenditure, even before dynamic effects are considered.

Figure 3(b) compares the target-based CSP aperture against a fixed reference aperture of approximately 5,000 m² for each location. The target-based aperture rises from 12,540 m² at Ladakh to 19,950 m² at Kochi, an increase of 55% from the best to the worst DNI site, while the fixed aperture remains constant across all locations. The magnitude of this divergence illustrates why a uniform, non-adaptive CSP design is fundamentally inadequate for geographically diverse deployment. At Kochi, a fixed aperture captures less than 25% of the thermal energy required to satisfy the site's hydrogen production target, making chronic TES under-charging and consequent SOEC curtailment unavoidable under any constant-load operating strategy.

Figure 3(c) shows the actual daily CSP thermal energy delivered by the fixed 5,000 m² aperture at each site, calculated from site-specific mean DNI. Output ranges from approximately 4,050 kWh day^{-1} at Kochi to 6,550 kWh day^{-1} at Ladakh, reflecting the strong DNI gradient across the country. Notably, despite Ladakh's challenging high-altitude winter conditions, its superior DNI resource makes it the highest-yielding site under a fixed aperture, reinforcing that mean DNI, rather than climate category, is the primary driver of CSP thermal productivity in the static sizing framework.

Figure 3(d) compares the target-based $MgCl_2$ PCM mass against the aperture-derived PCM mass for each location. The target-based mass, which accounts for the full 14-hour overnight thermal discharge requirement, ranges from 190 t at Jodhpur to 240 t at Kochi. In contrast, the aperture-based mass computed from the thermal energy actually collectible by the fixed aperture rather than from the SOEC's demand systematically underestimates storage requirements at every site, with shortfalls ranging from approximately 49 t at Jodhpur to 60 t at Kochi, the latter representing a 24% deficit relative to the target-based value. This shortfall is not a rounding artefact but a structural consequence of using supply-side aperture capacity as a proxy for demand-side storage sizing. Since the fixed aperture at low-DNI sites cannot fully charge the TES even under mean-irradiance conditions, an aperture-derived PCM mass will always undersize the storage relative to what is required for reliable overnight SOEC operation. The implications are directly confirmed in Section 5.1, where dynamic simulation shows TES depletion to zero state-of-charge at every site under constant-load operation, with the most severe shortfalls observed precisely at the locations where the aperture-based sizing gap is largest.

Static sizing provides essential first-order capacity estimates but cannot capture diurnal and seasonal variability, TES charge-discharge cycling, or SOEC load scheduling effects. Dynamic simulation is therefore essential for assessing real-world operational reliability, as presented in Section 5.

5. RESULTS AND DISCUSSION

System performance is evaluated through five sequential stages:

1. Constant-load SOEC operation establishes the baseline reliability deficit and identifies the root failure mechanism (Section 5.1);
2. Optimised flexible SOEC scheduling demonstrates the performance transformation across all five locations (Section 5.2);
3. A consolidated multi-location comparison contextualises the optimised results (Section 5.3);
4. A sensitivity analysis quantifies robustness to input parameter uncertainty (Section 5.4); and
5. Real-year 2019 meteorological data validation confirms robustness beyond the TMY dataset (Section 5.5).

5.1. DYNAMIC SIMULATION: CONSTANT-LOAD SOEC OPERATION

The statically sized system was simulated over 8760 hours under constant-load SOEC operation at 1998 kW. Jodhpur, which has the highest DNI among the selected locations and the most favourable solar conditions, is used as the reference case for analysing system behaviour under fixed-load operation.

Figure 4 presents the hourly power profile, TES state-of-charge variation, and stacked generation profile relative to the SOEC load. Figure 4(a) shows CSP dominating daytime supply with a peak of approximately 4700 kW at solar noon. TES discharge sustains the constant 1998 kW SOEC load through the evening but depletes to 0 kWh by approximately 03:00-06:00, approximately three to five hours before CSP generation restarts. This gap, visible in Figure 4(b) as the SOC reaching zero before mid-morning recharging, directly causes recurring daily SOEC curtailment and shutdown. The depletion of TES to zero by 03:00-06:00 is a direct consequence of a fundamental energy imbalance between overnight SOEC thermal demand and available storage capacity. Under constant-load operation, the SOEC draws 1,998 kW continuously regardless of the time of day. From sunset (~18:00) until CSP restart (~06:00), TES discharge remains the only available thermal source. The total overnight thermal requirement during this period is therefore approximately 23,976 kWh, whereas the statically sized TES provides only ~18,000 kWh of usable storage capacity. This structural deficit of nearly 6000 kWh makes complete TES depletion before dawn unavoidable under prolonged non-solar operation. The $MgCl_2$ PCM partially mitigates this limitation by releasing heat near isothermally during solidification at approximately 714 °C. Compared to sensible-heat-only storage systems of equivalent mass, the latent heat contribution extends the effective TES discharge duration and delays the onset of rapid outlet temperature decline (Zhao et al. 2020; Graves et al. 2011; Zhang et al. 2026). Nevertheless, once the stored latent heat is exhausted, the SOEC load must be curtailed in proportion to the remaining thermal supply. Figure 4(c) confirms supply shortfalls concentrated in the early morning (00:00-08:00) and late evening (17:00-20:00). The representative day shown has a daily reliability of 50% (12 of 24 hours met). The annual hourly reliability, averaged over all 8760 hours, is 67.8%, as established by the full-year simulation, even at this most solar-favourable site.

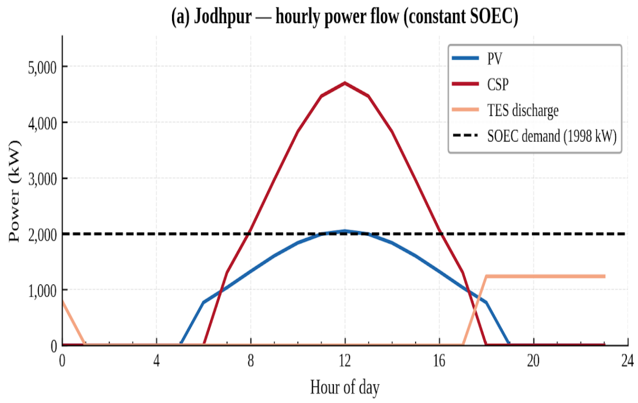

(a)

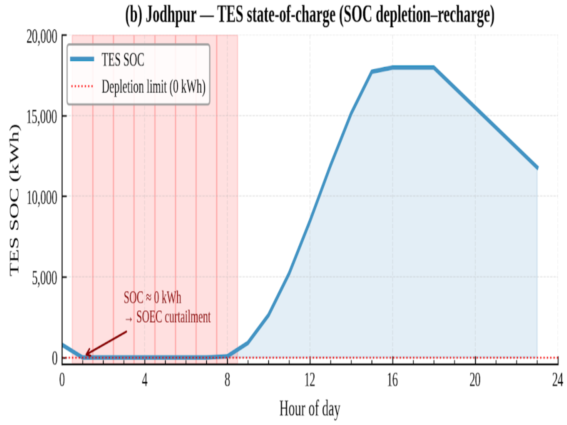

(b)

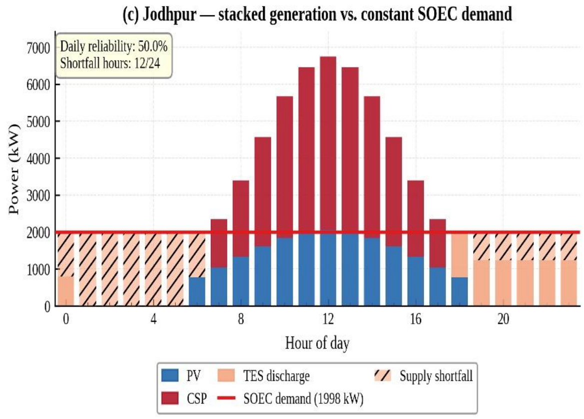

(c)

Figure 4. Dynamic simulation results for Jodhpur under constant-load SOEC operation. **(a)** Hourly power flow; **(b)** TES state-of-charge (SOC); **(c)** Stacked hourly generation versus constant SOEC demand.

Reliability ranges from 62.1% (Nagpur) to 68.7% (Bengaluru), with daily hydrogen output of only 729 to 788 kg day^{-1}, deficits of 27-33% against the 1,080 kg day^{-1} target. Nagpur performs worst despite having a moderate mean DNI because its pronounced monsoon-season irradiance depression creates extended multi-day low-generation periods that exhaust TES more severely than Kochi's steadier but lower-intensity irradiance profile. The minimum TES state of charge reaches 0 kWh at every site, confirming that temporal mismatch, rather than insufficient annual energy generation, is the primary failure mechanism. These findings demonstrate that improving the temporal alignment between energy supply and SOEC demand is essential for achieving reliable operation under fully solar-driven conditions. The minimum TES state of charge reaches 0 kWh at every site, confirming that temporal mismatch, rather than insufficient annual energy generation, is the primary failure mechanism. These findings demonstrate that improving the temporal alignment between energy supply and SOEC demand is essential for achieving reliable operation under fully solar-driven conditions.

Table 7. Dynamic simulation performance under constant-load SOEC operation (1,998 kW) at five Indian locations.

Location	Hourly Reliability (%)	Daily H_2 (kg day^{-1})	H_2 Deficit vs Target (%)	TES Min./Max. SOC (kWh)	Primary Failure Mechanism
Jodhpur	67.8	788.1	27.0	0 / 17,982	TES depletion 03:00-06:00
Ladakh	67.5	778.4	27.9	0 / 17,982	TES depletion, long winter nights
Nagpur	62.1	729.5	32.5	0 / 17,982	Monsoon irradiance depression
Bengaluru	68.7	788.4	27.0	0 / 17,982	TES depletion, coastal cloud cover
Kochi	65.4	760.4	29.6	0 / 17,982	Severe TES depletion, low DNI

Figure 5 shows the constant-load SOEC simulation results for Ladakh. As shown in Figure 5(a), the CSP output tracks a clear bell-shaped diurnal profile, peaking at approximately 5,400 kW around solar noon, while PV contributes a secondary, lower-amplitude curve that closely mirrors the CSP trend. The SOEC demand of 1,998 kW is shown as a horizontal dashed reference. During the early morning hours (roughly 0-5 h) and again after sunset (beyond 18:00), neither source generates sufficient power, and the system relies on TES discharge, which is evident as the flat peach-coloured segment in the late-evening window to partially bridge the gap.

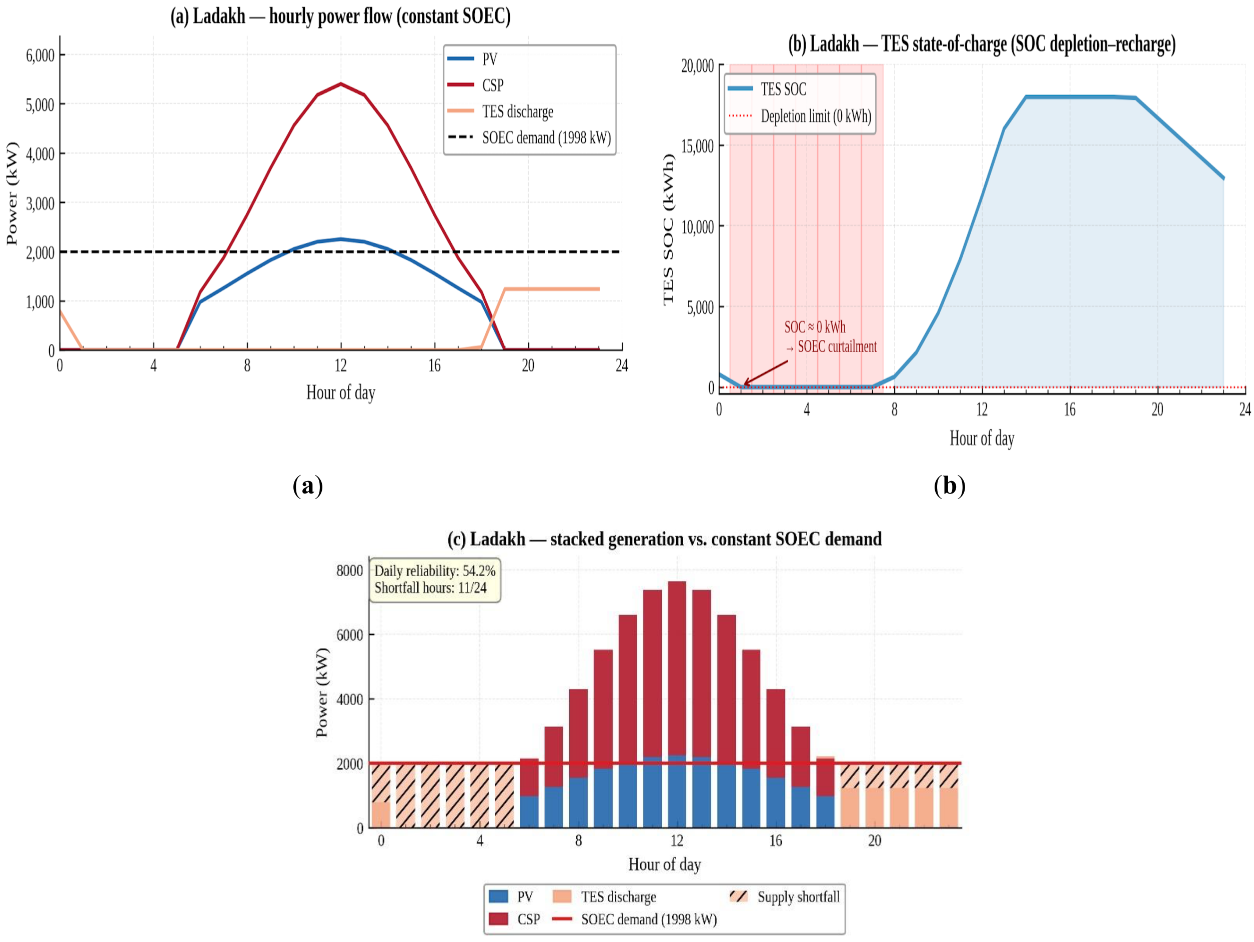

Figure 5. Dynamic simulation results for Ladakh under constant-load SOEC operation. **(a)** Hourly power flow; **(b)** TES state-of-charge (SOC); **(c)** Stacked hourly generation versus constant SOEC demand.

The TES SOC profile in Figure 5(b) shows repeated overnight depletion followed by daytime recharge. Storage approaches zero by approximately 01:00 and remains nearly depleted until around 08:00, during which the SOEC cannot be maintained at full load. Once CSP thermal generation exceeds the instantaneous demand, TES charging resumes and reaches a peak SOC of approximately 18,000 kWh during mid-afternoon before gradually discharging again into the evening period.

Figure 5(c) further highlights the supply-demand mismatch under constant-load operation. Shortfall periods, indicated by the hatched regions, occur primarily during pre-dawn and overnight hours and account for 11 out of 24 operating hours. This yields a daily reliability of 54.2%, which, while reflecting the strong midday solar resource available in Ladakh, also highlights the fundamental challenge posed by long winter nights (particularly November through January), when the effective solar charging window contracts considerably and TES depletion periods are correspondingly extended. Under these conditions, the system achieves a daily hydrogen output of 778.4 kg day^{-1} at an hourly reliability of 67.5%.

Figure 6 presents the constant-load SOEC simulation results for Nagpur. The hourly power flow in Figure 6(a) shows that CSP output rises from essentially zero at 5:00 to a peak of roughly 4,700 kW near solar noon, before tapering off by 18:00. The PV contribution follows a similar but lower-amplitude arc, briefly touching the 1,998 kW SOEC demand line around midday before dropping away. A small TES discharge of approximately 800 to 900 kW is visible in the first hour of the day, and a flat discharge segment of around 1,200 kW appears from 18:00 onward, partially compensating for the post-sunset generation gap.

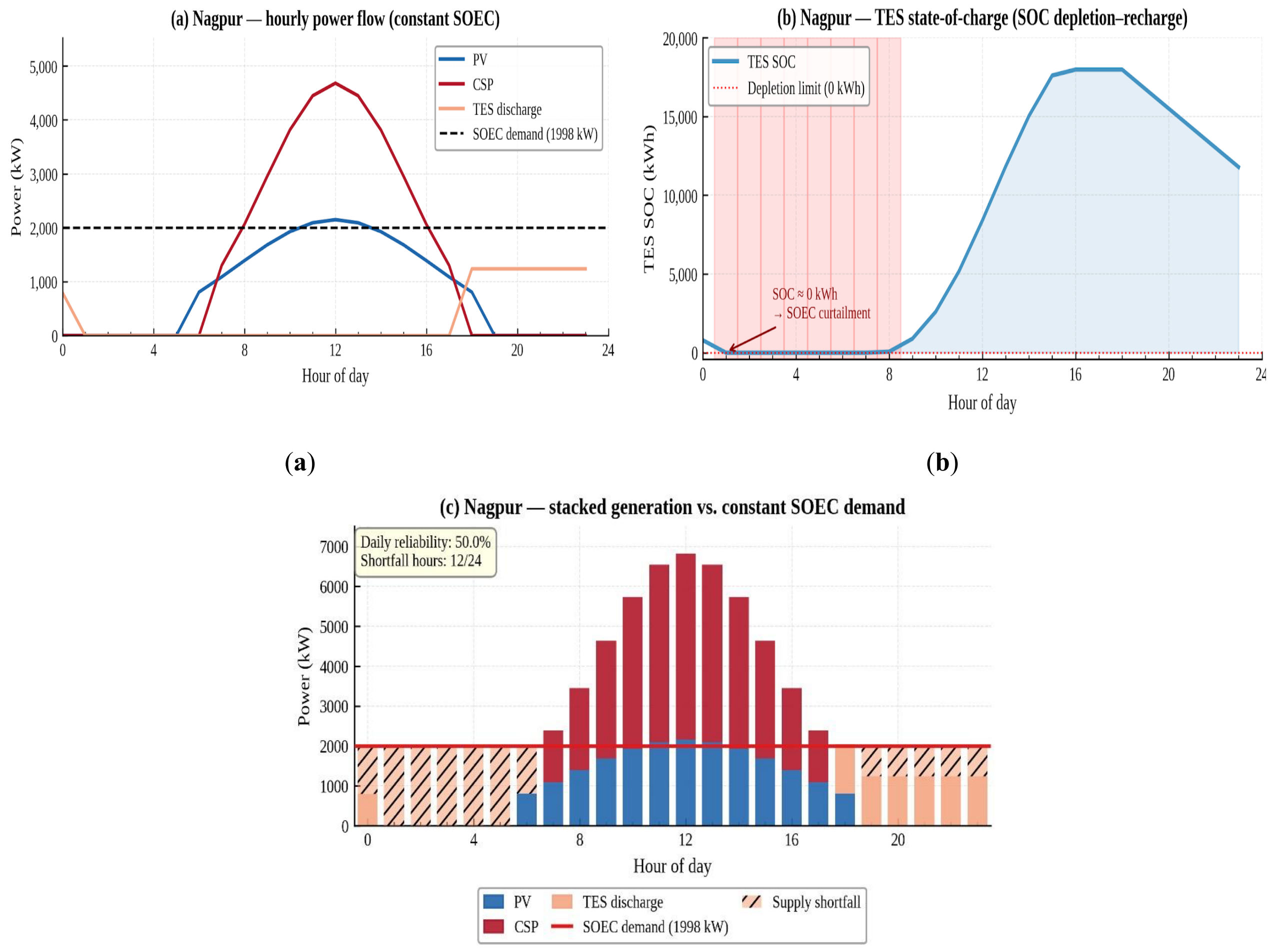

(a) **(b)**

(c)

Figure 6. Dynamic simulation results for Nagpur under constant-load SOEC operation. **(a)** Hourly power flow; **(b)** TES state-of-charge (SOC) variation; **(c)**Stacked hourly generation versus constant SOEC demand.

The TES state-of-charge profile in Figure 6(b) shows that storage is almost entirely depleted by 1:00 and remains near 0 kWh throughout to 8:00, resulting in sustained SOEC curtailment across that entire window. Once CSP output climbs sufficiently above the SOEC load, the TES begins recharging steeply, reaching a peak of 18,000 kWh around hours 15–17, after which it discharges gradually into the evening, ending the day at approximately 12,000 kWh.

Figure 6(c) makes the supply-demand balance explicit on an hourly basis. The hatched shortfall regions span the full overnight and early morning period from hour 0 through to roughly 6:00, and reappear again from hour 18 onwards through to the end of the day, accounting for 12 out of 24 hours in shortfall. Nagpur emerges as the worst-performing location despite having a moderate annual DNI of approximately 1750 kWh m^{-2} yr^{-1}. This behaviour cannot be explained by annual average irradiance alone and instead arises from the severity and duration of monsoon-period irradiance suppression. During June–September, DNI can decrease to near-zero levels for multiple consecutive days, substantially reducing both CSP thermal generation and TES charging.

Under these conditions, TES becomes fully depleted during overnight SOEC operation and cannot recover adequately during subsequent daytime periods. Since the static TES sizing is based on mean irradiance conditions, it does not account for extended low-generation sequences occurring during the monsoon season. As a result, consecutive zero-SOC periods accumulate rapidly, producing prolonged reliability loss across multiple days.

Kochi, in contrast, experiences a lower mean DNI but a comparatively steadier irradiance profile. Although cloud cover is persistent, partial daytime charging of TES remains possible on most days, preventing the extended multi-day depletion sequences observed in Nagpur. The key distinction, therefore, lies between episodic high-amplitude irradiance suppression at Nagpur and chronic lower-amplitude suppression at Kochi - a difference that is not captured by mean annual DNI values alone. These conditions result in a representative daily reliability of approximately 50%, while the annual hourly reliability decreases to 62.1%, the lowest among all five locations analysed.

Figure 7 presents the constant-load SOEC simulation results for Bengaluru. As seen in Figure 7(a), CSP output rises steeply from 6:00, reaching a peak of approximately 5,200 kW at solar noon, before declining symmetrically to zero by around 18:00. PV generation follows a similar diurnal trend, reaching approximately 2500 kW near midday and exceeding the SOEC demand for a limited daytime period. A modest TES discharge of around 700 kW is visible during the opening hours of the day, while a sustained, flat discharge of approximately 1,300 kW takes effect from hour 18 onward, providing partial cover throughout the night.

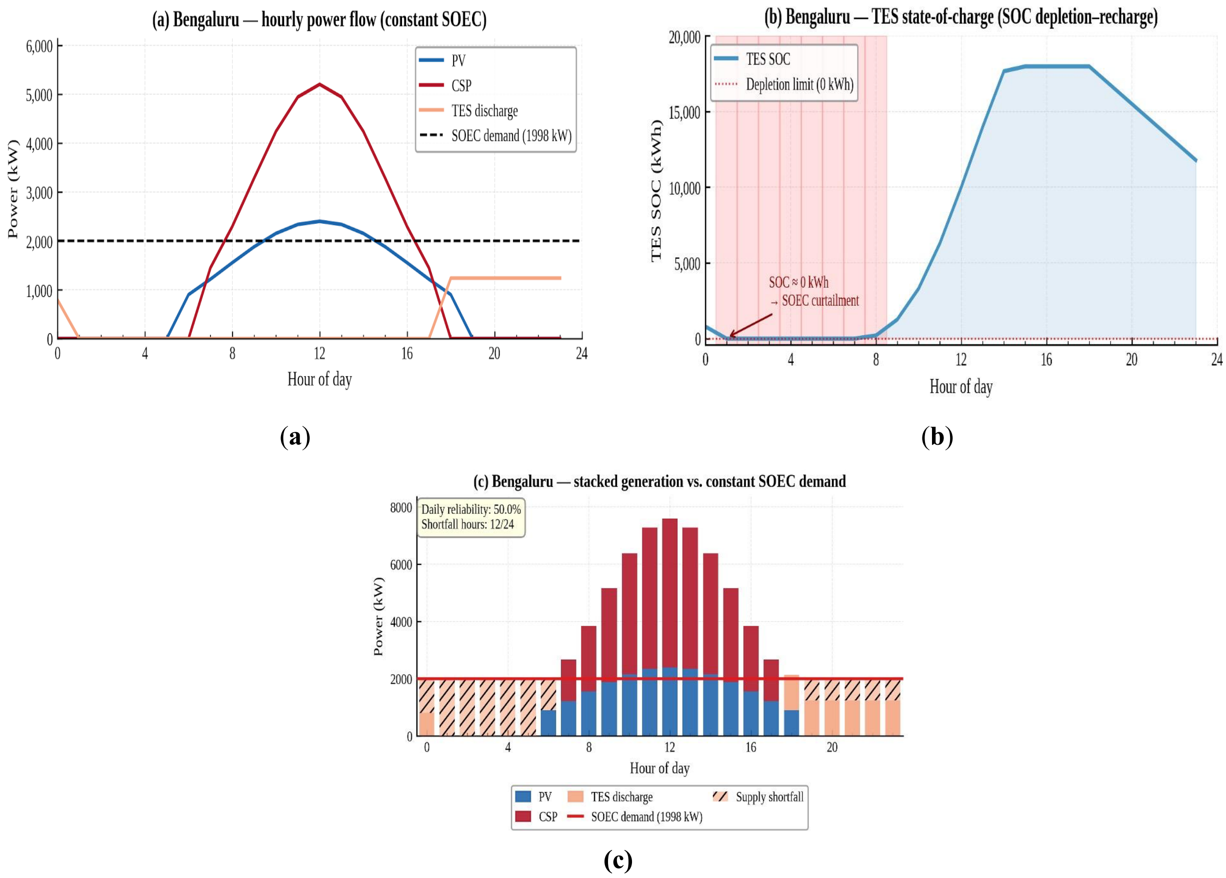

Figure 7. Dynamic simulation results for Bengaluru under constant-load SOEC operation. (a) Hourly power flow; (b) TES state-of-charge (SOC) variation; (c) Stacked hourly generation versus constant SOEC demand.

The TES state of charge in Figure 7(b) shows that the storage drops to near zero almost immediately after midnight and remains fully depleted through to approximately 8:00, resulting in partial or complete SOEC curtailment during the pre-dawn period. Recharging begins once the combined CSP and PV surplus exceeds demand, with the TES climbing sharply to a plateau of around 18,000 kWh between 15:00 and 19:00, before discharging gradually to close the day at roughly 12,000 kWh.

Figure 7(c) confirms that shortfall hours span the full overnight and early morning period from hour 0 to around 6:00, and return again from 18:00 through to the end of the day, totalling 12 out of 24 hours. The resulting daily reliability stands at 50.0%. Bengaluru differs from the other locations due to the influence of two extended wet-season periods occurring during April-May and September-November. Increased cloud cover during these intervals suppresses CSP generation despite the site having a moderate mean DNI resource. This seasonal irradiance reduction contributes to an annual hourly reliability of 68.7%, with a corresponding daily hydrogen output of 788.4 kg day^{-1}.

Figure 8 presents the constant-load SOEC simulation results for Kochi. The hourly power flow in Figure 8(a) shows that CSP output begins rising from 6:00 and reaches a peak of approximately 6,900 kW around solar noon, the highest midday CSP output among all five locations, before falling steeply back to zero by hour

18. Despite this strong peak, the PV contribution plateaus at around 2,500 kW near midday and crosses the 1,998 kW SOEC demand line only between 9:00 and 16:00. A small TES discharge of around 700 kW is visible in the first hour of the day, and a flat evening discharge of approximately 1,300 kW sustains partial supply from 18:00 onward through the night.

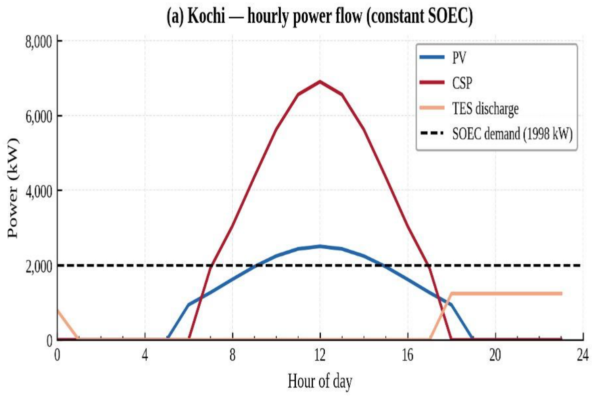

(**a**)

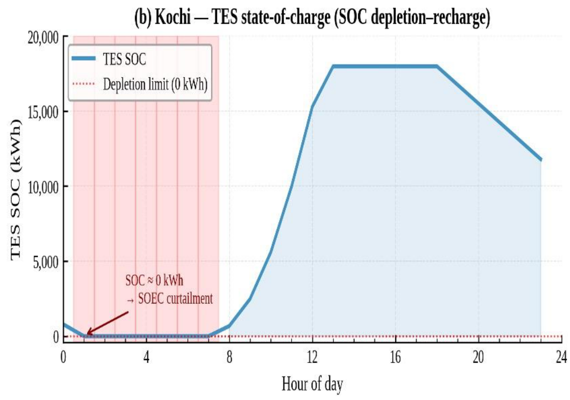

(**b**)

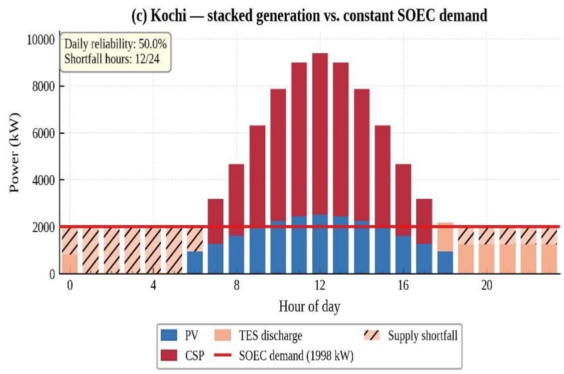

(**c**)

Figure 8. Dynamic simulation results for Kochi under constant-load SOEC operation. (a) Hourly power flow; (b) TES state-of-charge (SOC) variation; (c) Stacked hourly generation versus constant SOEC demand

Figure 8(b) reveals that the TES depletes to near zero almost immediately after midnight and remains at that level until 8:00, resulting in partial or complete SOEC curtailment during the overnight and early morning period. The sharp recharge phase begins around 9:00, driven by the large CSP surplus over the SOEC load, and the TES climbs to a peak of roughly 18,000 kWh by 14:00 to 17:00, before discharging steadily to end the day at around 12,000 kWh.

As Figure 8(c) shows, shortfall hours cover the full pre-dawn period from hour 0 through to around 6:00, and resume from 17:00 onwards, amounting to 12 out of 24 hours in total, giving a daily reliability of 50%. Kochi exhibits a physically important contrast between peak instantaneous generation and overall system reliability. Although the site records the highest midday CSP peak output among all five locations (~6900 kW), its annual hourly reliability remains limited to 65.4%, with a corresponding hydrogen production of 760.4 kg day^{-1}. This behaviour arises because peak thermal power does not directly translate into sustained daily energy availability.

Compared with inland locations such as Jodhpur, Kochi experiences a significantly shorter effective DNI collection window, typically limited to approximately 7-8 hours per day due to persistent coastal humidity and monsoon cloud cover. As a result, the cumulative daily CSP thermal energy available for TES charging remains substantially lower despite the high noon-time peak output. The reduced annual DNI (~1250 kWh m^{-2} yr^{-1}) further limits the ability of TES to sustain the 12-hour overnight SOEC demand under constant-load operation.

Under these conditions, the thermal buffering capability of the $MgCl_2$ PCM becomes particularly important. The near-isothermal discharge behaviour at approximately 714 °C helps maintain SOEC inlet thermal stability even as TES approaches depletion, thereby delaying operational curtailment compared to conventional sensible-heat-only storage systems (Zhao et al. 2020; Zhang et al. 2026). These results further demonstrate that annual peak generation alone is insufficient for evaluating SOEC reliability under fully solar-driven operation; the temporal distribution of usable solar energy and TES recharge duration are equally important design considerations.

5.2. OPTIMISED FLEXIBLE SOEC SCHEDULING

The optimised flexible SOEC scheduling strategy is evaluated in Figures 9-13 for all five locations. Jodhpur operates under a 0.6×/1.0×/1.5× load schedule, while the remaining locations use a 0.6×/1.0×/1.8× schedule together with location-specific CSP and TES sizing. The consolidated performance results are summarised in Table 8. The flexible scheduling strategy, therefore, shifts the system from a storage-limited operating regime to a dynamically balanced energy management regime, substantially improving reliability without excessive infrastructure oversizing.

The improvement in reliability under flexible scheduling does not arise solely from reducing the overnight SOEC load. Instead, it results from the thermodynamic interaction between SOEC demand, TES discharge behaviour, and the phase-change characteristics of $MgCl_2$. Under constant-load operation, the SOEC continuously draws 1998 kW throughout the full 24-hour cycle, forcing TES to discharge at a fixed rate during the entire overnight period, regardless of the amount of energy stored during the preceding solar day. As demonstrated in Section 5.1, the statically sized TES is unable to sustain this discharge rate across the full non-solar duration, leading to complete SOC depletion before sunrise.

The flexible strategy addresses this through two simultaneous mechanisms. First, the overnight SOEC load is reduced to 0.6× nominal, approximately 1,200 kW, cutting the overnight thermal withdrawal rate by 40%. This directly extends the duration over which TES can sustain uninterrupted SOEC supply, since the same stored energy now covers a longer discharge window at the lower draw rate. Second, the midday SOEC load is increased to 1.5-1.8× nominal during the hours of maximum solar availability, when CSP output is at its peak, and TES is actively charging. This concentrates hydrogen production in the hours when thermal energy is most abundant, reducing reliance on stored energy and allowing TES to accumulate a larger reserve for the following night. The combined effect is a fundamental shift in the system's energy balance: instead of drawing uniformly on storage throughout the night and running out before dawn, the system uses storage conservatively at night and replenishes it aggressively during peak solar hours. This is precisely why TES SOC never reaches zero under flexible scheduling at any site, whereas it depletes every night under constant-load operation.

The $MgCl_2$ PCM further enhances this behaviour through its near-isothermal latent heat discharge characteristics. Because $MgCl_2$ solidifies isothermally at 714 °C, the thermal output to the SOEC remains at a stable temperature throughout the discharge phase, regardless of how much energy remains in storage. In a sensible-heat system, a low SOC would correspond to a falling outlet temperature, degrading SOEC efficiency and potentially triggering curtailment even before storage is fully depleted (Graves et al. 2011; Zhao et al. 2020). The latent heat characteristic of $MgCl_2$ therefore extends the effective operating range of TES and makes the flexible scheduling strategy more thermally robust than it would be with a conventional storage medium (Xu et al. 2015; Prieto and Cabeza 2019; Zhang et al. 2026).

5.2.1. JODHPUR (ARID, DNI APPROXIMATELY 2050 KWH M^{-2} YR^{-1}): CSP X2.0, TES X1.70, PCM 325.7 T

Figure 9(a) shows the annual hourly power generation profile for Jodhpur under flexible SOEC scheduling. CSP output is strong and well defined throughout most of the year, with daytime generation regularly reaching between 5,000 and 8,000 kW during peak solar hours, above the baseline 1,998 kW constant load, reflecting the ×2.0 aperture upscaling applied during optimisation. TES discharge provides a comparatively stable overnight thermal contribution of approximately 1200-1500 kW, enabling continuous low-load SOEC operation during non-solar periods.

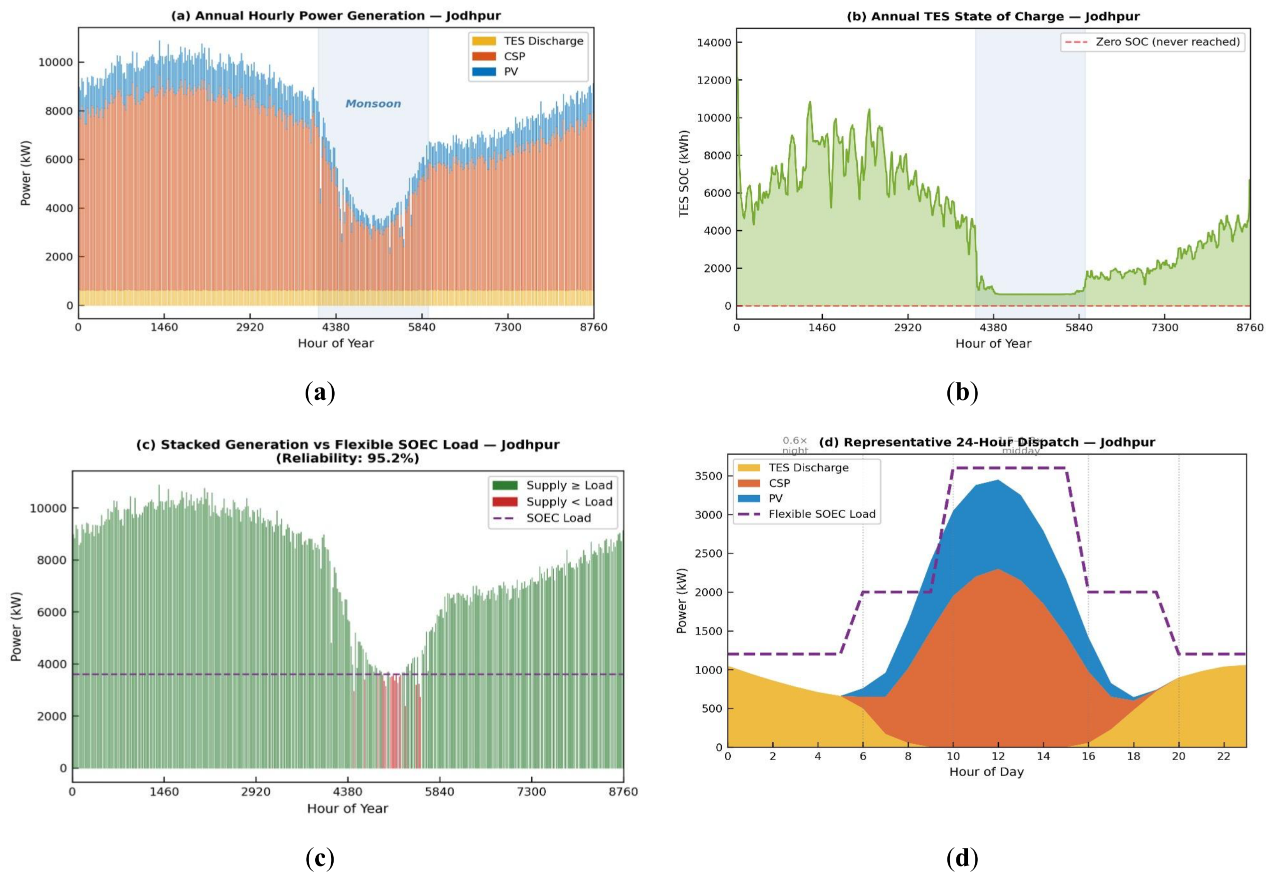

Figure 9. Optimised flexible SOEC scheduling results for Jodhpur **(a)** Annual hourly power generation; **(b)** Annual TES state-of-charge (SOC) profile; **(c)** Stacked annual generation vs. the flexible SOEC scheduled load; **(d)** Representative 24-hour dispatch profile under flexible scheduling.

The annual TES state-of-charge profile in Figure 9(b) shows storage cycling in a controlled and stable manner throughout the year, oscillating between approximately 5,000 and 12,000 kWh across successive charge and discharge cycles. SOC never reaches zero at any point during the entire year, a direct result of scaling back the night-time SOEC load to 0.6× nominal, which relieves pressure on storage during the hours when solar input is absent. The role of $MgCl_2$ PCM is particularly important in sustaining this stable TES behaviour. Under flexible scheduling, the Jodhpur TES SOC oscillates between approximately 5,000 and 12,000 kWh - a wide operating range that would produce significant temperature swings in a sensible-heat-only storage system. In sensible storage, such variation translates directly into fluctuating thermal input to the SOEC, driving thermal cycling stress and potentially reducing electrolyser stack lifetime (Graves et al. 2011; Zhao et al. 2020). The latent heat behaviour of $MgCl_2$ reduces the direct dependence between TES state-of-charge and outlet temperature. As long as any liquid-phase PCM remains, solidification proceeds at a constant 714 °C, providing an isothermal thermal supply to the SOEC regardless of remaining stored energy. This effectively acts as a thermal buffer within the TES, maintaining stable SOEC inlet conditions even during deep discharge events. The practical result is that flexible scheduling does not merely redistribute energy in time — it also improves the quality and consistency of the thermal supply delivered to the SOEC across the full annual cycle (Zhang et al. 2026).

Figure 9(c) shows that supply meets or exceeds the scheduled flexible SOEC demand for 95.2% of the 8760 operating hours. The representative 24-hour dispatch profile in Figure 9(d) illustrates the implementation of the three-period operating strategy. During the overnight period (00:00-06:00), TES discharge alone sustains the reduced SOEC load of approximately 1200 kW. As solar availability increases during the morning, the SOEC load rises progressively to a midday peak of approximately 3600 kW between 10:00 and 16:00, aligned with the period of maximum CSP and PV generation.

Under the optimised configuration (CSP ×2.00, TES ×1.70, PCM mass 325.7 t), the Jodhpur system achieves a daily hydrogen production of 1080.3 kg day^{-1} while maintaining 95.2% annual hourly reliability. This represents a substantial improvement over the constant-load configuration and demonstrates the effectiveness of flexible scheduling combined with optimised TES utilisation under high-DNI operating conditions. The results further demonstrate that adaptive load scheduling can substantially improve SOEC reliability without requiring disproportionately large increases in TES capacity.

5.2.2. LADAKH (COLD/HIGH-ALTITUDE, DNI APPROXIMATELY 2100 KWH M^{-2} YR^{-1}): CSP X2.80, TES X3.00, PCM 574.8 T

Figure 10 presents the optimised flexible SOEC scheduling results for Ladakh. The annual hourly generation profile in Figure 10(a) is immediately striking; CSP output is exceptionally high throughout the year, with daytime peaks regularly reaching between 15,000 and 20,000 kW, a direct reflection of Ladakh's superior DNI resource and the ×2.80 aperture upscaling applied during optimisation. PV adds a further layer on top, pushing combined stacked generation to over 20,000 kW during the strongest solar periods. TES discharge provides a stable overnight thermal contribution throughout the year, enabling sustained low-load SOEC operation during non-solar periods.

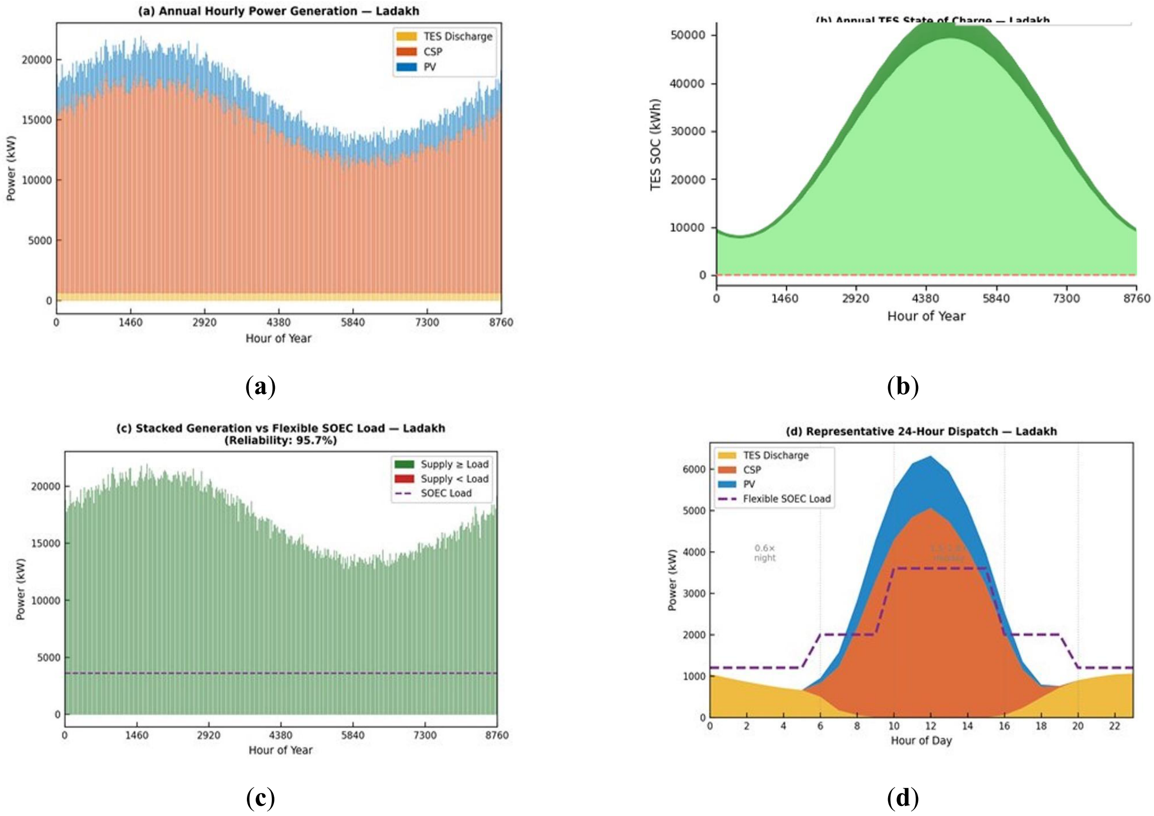

Figure 10. Optimised flexible SOEC scheduling results for Ladakh **(a)** Annual hourly power generation; **(b)** Annual TES SOC profile; **(c)** Stacked generation vs. flexible SOEC scheduled load; **(d)** Representative 24-hour dispatch profile under flexible scheduling.

The annual TES state-of-charge profile in Figure 10(b) reveals a well-defined seasonal structure that sets Ladakh apart from the other sites. Storage builds steadily from around 8,000-10,000 kWh at the start of the year, climbs through spring, and reaches a broad peak of approximately 50,000 kWh during the long, clear sky summer days of April through August, before declining gradually back toward its winter minimum. The TES SOC remains above zero throughout the full annual cycle, including during the winter months of December and January, when storage reaches its minimum values of approximately 8000 kWh. This outcome is a direct consequence of the ×3.00 TES multiplier, which was identified through iterative optimisation as the minimum capacity needed to prevent storage depletion under the most severe winter conditions.

Figure 10(c) confirms that stacked generation meets or exceeds the flexible SOEC scheduled load for 95.7% of all 8,760 hours in the year, the highest annual reliability recorded across all five sites. No significant shortfall periods are visible within the annual profile, indicating that the optimised system maintains adequate supply even during the most demanding operating intervals.

The representative 24-hour dispatch in Figure 10(d) shows the three-period flexible schedule in practice.

TES discharge alone sustains the reduced night load of approximately 1,200 kW from midnight through to hour 6, covering roughly 14 hours of overnight supply, the longest nocturnal TES window of any site. This extended overnight discharge duration is the primary reason a ×3.00 TES multiplier becomes necessary for Ladakh despite its exceptionally high DNI resource. As solar generation builds through the morning, the SOEC load steps up through an intermediate level of approximately 2,000 kW before reaching its midday peak of approximately 3,600 kW between hours 8 and 15, aligned with the window of maximum combined CSP and PV output. Notably, Ladakh's high-altitude winter conditions might suggest it would be among the weaker performers, but the site in fact achieves the highest reliability of all five locations. The explanation lies in its exceptional annual DNI of approximately 2,100 kWh m^{-2} yr^{-1}, which enables rapid TES recharging on clear-sky days throughout the year, more than compensating for the shorter winter solar window. With the optimised configuration of CSP ×2.80, TES ×3.00, and a PCM mass of 574.8 t, the system delivers a daily hydrogen output of 1,081 kg day^{-1} at an annual reliability of 95.7%.

The requirement for a ×3.00 TES multiplier at Ladakh is primarily associated with the extended winter nocturnal discharge duration rather than insufficient annual solar availability. Due to the high latitude and cold-climate conditions, effective winter solar collection windows may reduce to approximately 5–6 hours per day, while TES must sustain overnight SOEC operation for nearly 14 hours under the reduced 0.6× load schedule. Consequently, a substantially larger TES capacity becomes necessary to maintain an uninterrupted thermal supply across prolonged non-solar periods. The $MgCl_2$ PCM plays a critical role in enabling this operating strategy. Its high latent heat storage capacity (approximately 452 kJ kg^{-1} at 714 °C) allows large amounts of thermal energy to be stored within a comparatively manageable storage mass. Conventional sensible-heat storage systems would require significantly larger material inventories to provide equivalent thermal storage capacity over the same operating temperature range (Xu et al. 2015; Prieto and Cabeza 2019).

5.2.3. NAGPUR (SEMI-ARID/CONTINENTAL, DNI APPROXIMATELY 1750 KWH M^{-2} YR^{-1}): CSP X4.70, TES X4.30, PCM 823.9 T

Figure 11 shows the optimised flexible SOEC scheduling results for Nagpur. The annual hourly generation profile in Figure 11(a) shows CSP output dominating throughout the dry season, with daytime peaks regularly reaching between 20,000 and 25,000 kW. These are the highest generation levels observed among all five locations and result directly from the large ×4.70 CSP aperture multiplier required during optimisation. PV adds a further contribution on top, pushing combined stacked generation well above 25,000 kW during the strongest solar periods. The TES discharge baseline runs steadily along the base of the profile through all overnight hours. The monsoon window, spanning roughly hours 3,200–5,840, is clearly visible as a sustained depression in generation spike frequency and amplitude, with total stacked output dropping sharply before recovering as clear-sky conditions return in September.

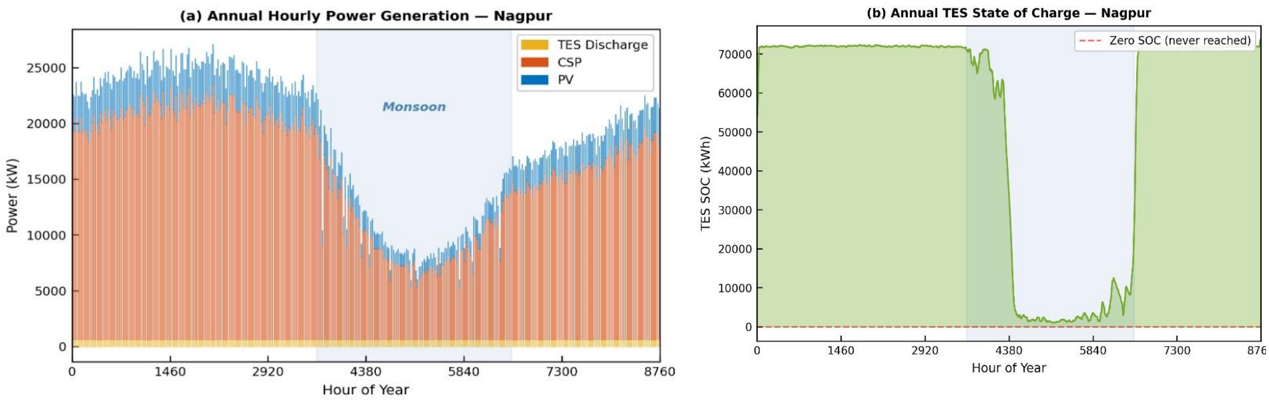

(**a**) (**b**)

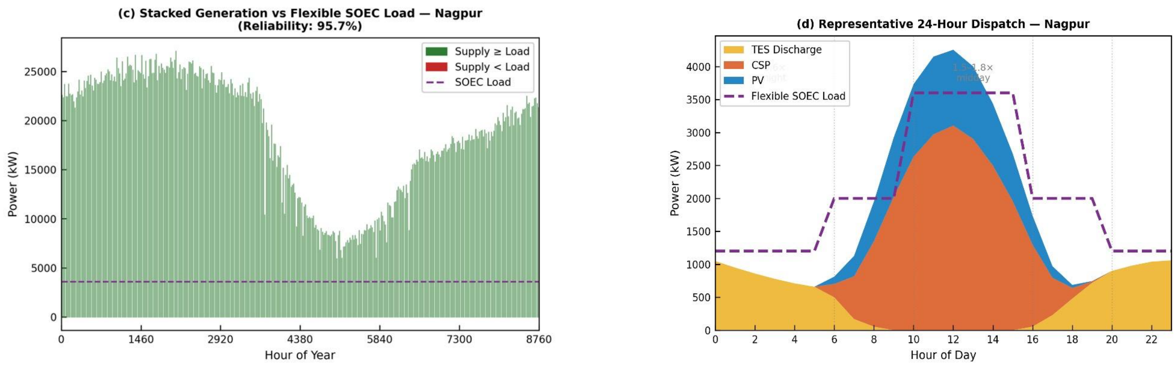

(**c**) (**d**)

Figure 11. Optimised flexible SOEC scheduling results for Nagpur **(a)** Annual hourly power generation; **(b)** Annual TES SOC; **(c)** Stacked generation vs. flexible SOEC load; **(d)** Representative 24-hour dispatch profile under flexible scheduling.

The annual TES state-of-charge is shown in Figure 11(b). Storage maintains a high and stable SOC of approximately 72,000 kWh through the entire dry season from October through to the onset of the monsoon, a plateau that reflects the large surplus generation available during this period. As the monsoon sets in, the SOC undergoes a prolonged seasonal drawdown, declining steeply and progressively to minimum values of 1,000-3,000 kWh during late July and early August before recovering sharply once clear skies return. Throughout this entire drawdown, the SOC never reaches zero; the zero-depletion line shown as a red dashed reference remains untouched across all 8,760 hours. The ×4.30 TES multiplier was identified through iterative optimisation as the minimum capacity at which zero SOC events are fully eliminated across the complete dataset.

Figure 11(c) confirms that stacked generation meets or exceeds the flexible SOEC scheduled load for 95.7% of all 8,760 hours, matching Ladakh as the joint highest reliability among all five sites. This outcome is particularly significant given the severity of the monsoon depression visible in the generation profile, and it speaks directly to the effectiveness of the large TES buffer in bridging the extended low-irradiance period.

Figure 11(d) shows the representative 24-hour dispatch with the three-period flexible scheduling strategy in operation. TES discharge alone sustains the reduced night-time SOEC load at 1,200 kW from midnight through to hour 6. PV begins contributing from around hour 6, and CSP follows shortly after, with combined generation building through the morning shoulder period. The SOEC load steps up to its midday peak of approximately 3,600 kW between 10:00 and 15:00, consistent with the 1.5–1.8× midday multiplier annotated on the plot, before stepping back down to the intermediate evening level of approximately 2,000 kW from 16:00 and returning to the reduced night rate after 20:00. Nagpur provides an important demonstration of how seasonal climatic variability influences TES sizing requirements.

Nagpur provides an important demonstration of how seasonal climatic variability influences TES sizing requirements. Despite recording a moderate annual DNI of approximately 1750 kWh m^{-2} yr^{-1}, higher than both Bengaluru and Kochi, the site requires the largest CSP field and TES capacity among all five locations. This behaviour arises from the continental climate structure, in which a strong dry season alternates with a pronounced southwest monsoon period extending from June through September.

During the monsoon interval, solar generation remains severely suppressed for several consecutive weeks, requiring the system to rely heavily on stored thermal energy. Consequently, TES must be sized not only for overnight operation but also for extended multi-day low-generation periods. Under the optimised configuration (CSP ×4.70, TES ×4.30, PCM mass 823.9 t), the system achieves a daily hydrogen production of 1080.1 kg day^{-1} while maintaining an annual reliability of 95.7%.

The V-shaped SOC drawdown during the monsoon follows directly from a sustained multi-week energy deficit. Daily CSP thermal input falls to near zero during peak monsoon weeks, while the SOEC continues drawing at its minimum overnight load of approximately 1,200 kW - representing around 28,800 kWh day^{-1} of thermal demand that TES must cover entirely without solar recharge. The large ×4.30 TES multiplier enables approximately 72,000 kWh of thermal energy to be accumulated during the preceding dry season, specifically to bridge this prolonged low-generation interval. Once clear-sky conditions return, the oversized ×4.70 CSP field rapidly restores TES capacity through high-rate daytime charging. This seasonal charge–

discharge behaviour differs fundamentally from the shorter daily TES cycling observed at locations such as Jodhpur and Bengaluru and represents the primary reason Nagpur requires the largest infrastructure multipliers despite not having the lowest annual DNI. The Nagpur results demonstrate that long-duration climatic intermittency can dominate TES sizing requirements more strongly than annual average DNI alone.

5.2.4. BENGALURU (TEMPERATE/COMPOSITE, DNI APPROXIMATELY 1550 KWH M^{-2} YR^{-1}): CSP X2.10, TES X1.90, PCM 363.9 T

Figure 12 presents the optimised flexible SOEC scheduling results for Bengaluru. The annual hourly generation profile in Figure 12(a) shows CSP and PV output maintaining strong daytime peaks of approximately 14,000 kW throughout the year, while TES discharge maintains continuous overnight thermal support during non-solar periods. Unlike the other study locations, Bengaluru exhibits two separate seasonal irradiance suppression periods rather than a single prolonged monsoon-driven reduction. The first and more severe depression occurs around hours 2,000–3,000, corresponding to the primary wet season in April–May, where generation drops sharply before recovering. A broader, shallower suppression follows through the second half of the year, indicating the secondary wet period from September to November.

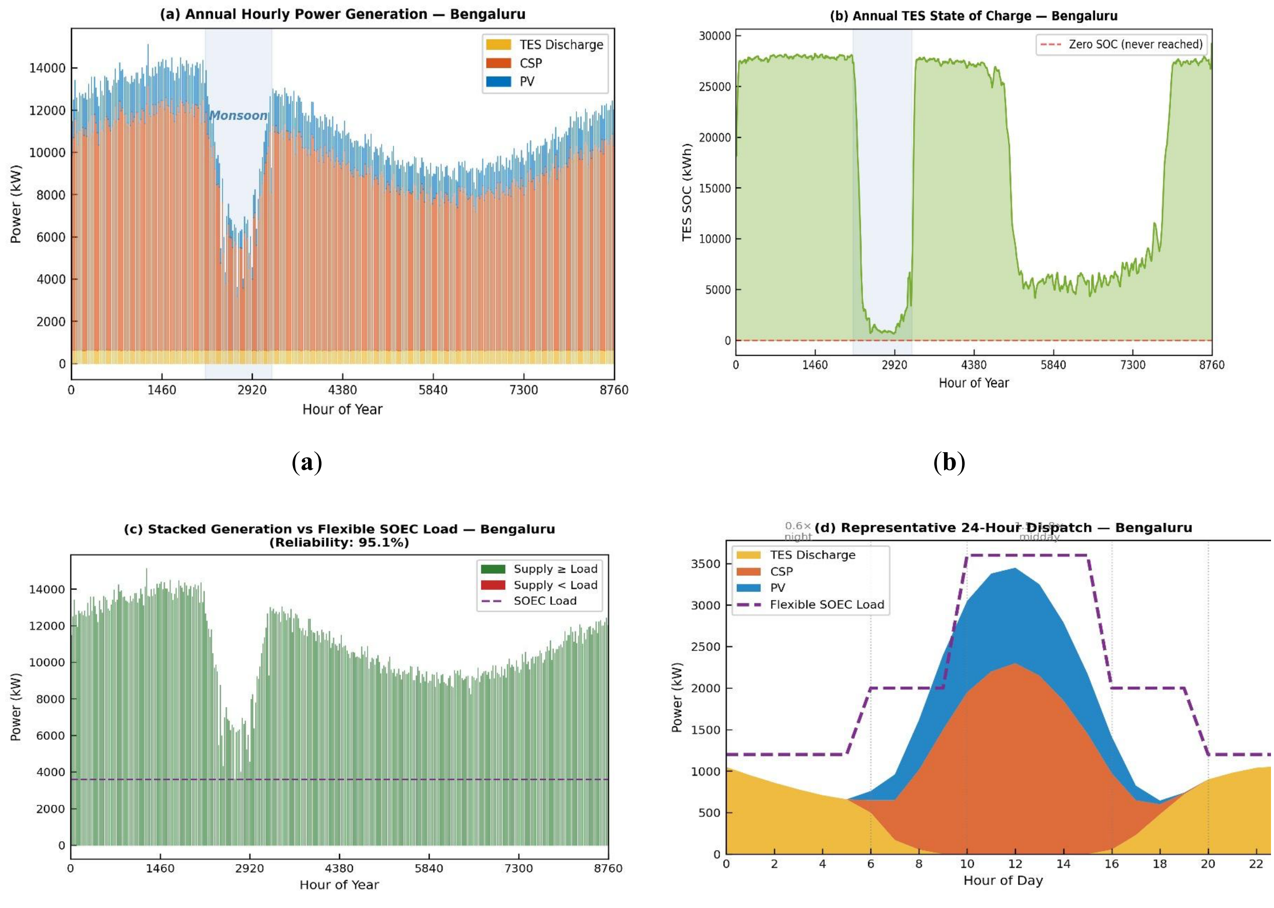

(c) (d)

Figure 12. Optimised flexible SOEC scheduling results for Bengaluru. **(a)** Annual hourly power generation; **(b)** Annual TES SOC; **(c)** Stacked generation vs. flexible SOEC load; **(d)** Representative 24-hour dispatch profile under flexible scheduling.

The annual TES state-of-charge profile in Figure 12(b) captures this double wet season. Storage holds a stable plateau of approximately 27,000–28,000 kWh through the dry season, before undergoing two moderate drawdown events that mirror the two wet periods. The first drawdown is the more acute of the two, with SOC declining steeply to minimum values of approximately 1,000–3,000 kWh before recovering sharply. The second drawdown, spanning a longer window, sees storage dip to minimum values of approximately 5,000 kWh before gradually recovering through the final months of the year. Crucially, the zero-depletion reference line remains untouched across all 8,760 hours: the ×1.90 TES multiplier keeps the minimum SOC comfortably above zero throughout both wet periods.

Figure 12(c) confirms that stacked generation meets or exceeds the flexible SOEC scheduled load for 95.1% of all 8,760 hours - the lowest annual reliability among the five optimised sites, while still satisfying the ≥95% reliability target established for the system design.

The representative 24-hour dispatch in Figure 12(d) follows the same three-period structure seen at the other sites. TES discharge alone sustains the reduced night load of 1,200 kW from midnight through to 6:00. PV begins contributing from around 6:00, and CSP builds steadily through the morning, with combined generation peaking at approximately 4200 kW near solar noon. The SOEC load steps up to its midday maximum of approximately 3,600 kW between 9:00 and 15:00 before stepping back to the intermediate evening level of approximately 2,000 kW from hour 16, and returning to the reduced night rate from 20:00 through to midnight.

Bengaluru requires comparatively moderate infrastructure scaling despite having the second-lowest mean DNI among the five locations (approximately 1550 kWh m^{-2} yr^{-1}). This behaviour is primarily associated with the nature of the regional climate pattern rather than annual irradiance magnitude alone.

Unlike Nagpur, which experiences a prolonged and highly concentrated monsoon depression, Bengaluru undergoes two shorter and more distributed wet-season periods. Consequently, TES experiences moderate but recoverable drawdown events instead of a sustained multi-week depletion cycle. This allows the system to maintain reliable operation using comparatively smaller infrastructure multipliers (CSP ×2.10 and TES ×1.90). Under the optimised configuration with a PCM mass of 363.9 t, the system achieves a daily hydrogen production of 1080.7 kg day^{-1} at an annual reliability of 95.1%. The Bengaluru results further demonstrate that the temporal distribution of irradiance variability can influence TES sizing more strongly than annual DNI magnitude alone.

5.2.5. KOCHI (HUMID/COASTAL, DNI APPROXIMATELY 1250 KWH M^{-2} YR^{-1}): CSP X2.80, TES X2.50, PCM 479.0 T

Figure 13 presents the optimised flexible SOEC scheduling results for Kochi. The annual hourly generation profile in Figure 13(a) indicates that CSP and PV output maintain daytime peaks of approximately 15,000 to 18,000 kW during the dry season, while the TES discharge baseline provides a consistent overnight contribution throughout the year. The monsoon window, spanning roughly hours 3,200-5,840, is clearly identifiable. During this period, total stacked generation declines sharply, and sustained low-output intervals persist across several consecutive weeks. Daytime peaks fall to as low as 4,000-5,000 kW at the trough of the monsoon, before gradually recovering as clear-sky conditions return. This represents the most prolonged and severe monsoon-driven generation suppression among all sites in this study, spanning approximately 1,200–1,400 consecutive hours of suppressed irradiance.

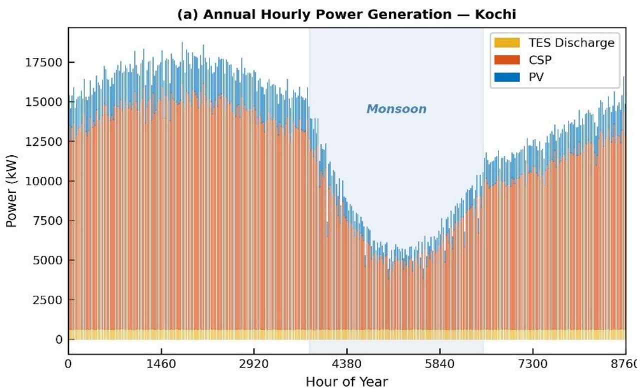

(a)

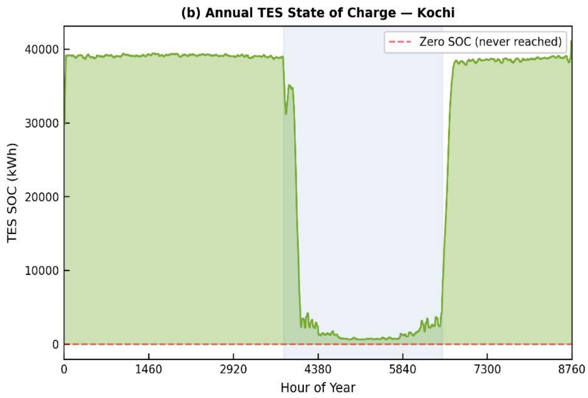

(b)

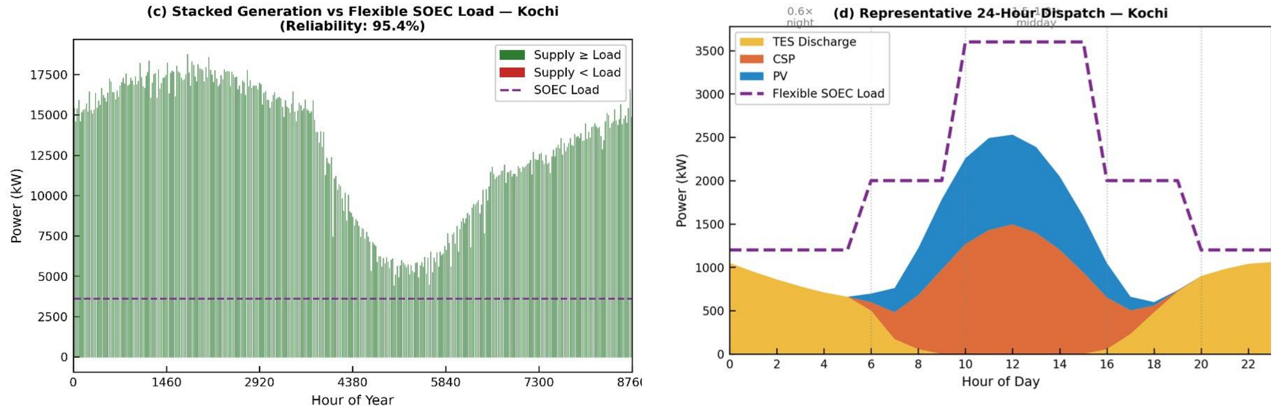

(c) (d)

Figure 13. Optimised flexible SOEC scheduling results for Kochi. **(a)** Annual hourly power generation; **(b)** Annual TES state-of-charge (SOC) profile; **(c)** Stacked annual generation versus flexible SOEC scheduled load; **(d)** Representative 24-hour dispatch profile under flexible scheduling.

The annual TES state-of-charge profile in Figure 13(b) reflects the impact of prolonged monsoon-driven suppression of irradiance. Storage maintains a stable plateau of approximately 38,000-39,000 kWh during the dry season, supported by surplus generation in clear-sky months. With the onset of the monsoon, the state of charge declines steeply and remains low, dropping from its pre-monsoon plateau to a minimum of approximately 2,000 to 5,000 kWh. These are the lowest monsoon-period minima observed among all sites in this analysis. This drawdown persists over a longer continuous period than at any other location, reflecting the duration and intensity of Kochi's southwest monsoon. A second, sharper drawdown occurs later in the year, around hours 6,000 to 6,500, before storage rapidly returns to its dry-season plateau. Throughout both events, the zero-depletion reference line is not crossed. The 2.5 TES multiplier was identified through iterative optimisation as the minimum capacity required to prevent complete storage depletion across all 8,760 TMY hours.

Figure 13(c) confirms that stacked generation meets or exceeds the flexible SOEC scheduled load for 95.4% of all 8,760 hours, comfortably meeting the ≥95% design target despite Kochi operating under the most challenging solar resource conditions of all five sites.

The representative 24-hour dispatch in Figure 13(d) highlights an operating characteristic unique to Kochi from the other locations. The combined CSP and PV peak at solar noon reaches only 2,500 kW (below the midday SOEC load target of 3,600 kW shown by the dashed purple line). This means that even at the peak of the solar day, direct generation alone is insufficient to meet the scheduled midday demand, and the TES must contribute actively, not just overnight but also during daytime hours, to bridge the gap. TES discharge sustains the reduced night load of 1,200 kW from midnight through to 6:00, but unlike other sites, the TES contribution remains substantial and visible throughout the day, never tapering to near zero even at solar noon. The SOEC load steps up through the intermediate level of approximately 2,000 kW from 6:00 before reaching its midday peak of approximately 3,600 kW between 9:00 and 15:00, then steps back down to the evening level from 16:00 and returns to the reduced night rate from 20:00 through to midnight.

Kochi represents the most demanding solar-resource environment among the five study locations. With the lowest annual DNI (~1250 kWh m^{-2} yr^{-1}) and a prolonged southwest monsoon suppressing irradiance for approximately 1200-1400 consecutive hours, the site would traditionally be considered marginal for reliable CSP-driven hydrogen production.

The results demonstrate, however, that reliable operation remains achievable when TES and flexible SOEC scheduling are jointly optimised. At Kochi, TES functions not only as an overnight storage buffer but also as an active daytime energy support mechanism during periods when direct solar generation remains below the scheduled SOEC demand. This explains why the required PCM inventory (479 t) remains comparatively high despite the more moderate CSP aperture multiplier. Under the optimised configuration (CSP ×2.8, TES ×2.5), the system achieves a daily hydrogen production of 1080.8 kg day^{-1} while maintaining an annual reliability of 95.4%. The Kochi results demonstrate that TES-dominated operating strategies can enable stable SOEC hydrogen production even under low-DNI and monsoon-dominated climatic conditions.

5.3. CONSOLIDATED MULTI-LOCATION PERFORMANCE COMPARISON

Table 8. Flexible SOEC optimisation results across five Indian climate zones (base load: 1,998 kW; all sites achieve ≥ 95% hourly reliability).

Location	SOEC Schedule (x nom.)	Opt. CSP Aperture (m^2)	Opt. TES Capacity (kWh)	PCM Mass (t)	Hourly Reliability (%)	Daily H_2 (kg day^{-1})	Δ Rel. (pp)	H_2 Gain (%)
Jodhpur	0.6/1.0/1.5	64,452	30,585	325.7	95.2	1080.3	+27.4	+37.1
Ladakh	0.6/1.0/1.8	86,069	53,974	574.8	95.7	1081.0	+28.2	+38.9
Nagpur	0.6/1.0/1.8	159,161	77,362	823.9	95.7	1080.1	+33.6	+48.1
Bengaluru	0.6/1.0/1.8	93,240	34,166	363.9	95.1	1080.7	+26.4	+37.2
Kochi	0.6/1.0/1.8	139,860	44,978	479.0	95.4	1080.8	+30.0	+42.1

The flexible SOEC scheduling strategy achieves ≥95% hourly reliability and hydrogen production exceeding 1080 kg day^{-1} at all five locations, confirming that the three-period dispatch framework remains effective across a wide range of Indian climatic and solar-resource conditions. Reliability improvements range from 26.4 percentage points at Bengaluru to 33.6 percentage points at Nagpur, with the largest gains occurring at locations where seasonal irradiance variability, rather than mean DNI alone, governs system performance. This behaviour is physically consistent: flexible scheduling reduces overnight TES withdrawal by approximately 40% while concentrating hydrogen production during periods of maximum solar availability. Consequently, the reliability improvement is most pronounced at sites where the mismatch between continuous SOEC demand and temporally variable solar generation is most severe.

Four cross-location trends emerge from the optimisation results. First, the CSP aperture multiplier (×2.0 to ×4.70) is governed more strongly by irradiance variability than by mean DNI alone, with Nagpur representing the clearest example despite its only moderate annual solar resource. Second, TES multipliers (×1.70 to ×4.30) follow the same pattern, confirming that seasonal storage requirements dominate over short-term daily buffering needs. Third, the required $MgCl_2$ PCM inventory (325.7–823.9 t) scales directly with TES capacity, making latent thermal storage the dominant infrastructure component in the integrated SOEC-TES system. Finally, the same three-period flexible scheduling framework achieves ≥95% reliability at all five locations without requiring any site-specific control modification, relying only on location-dependent component sizing. This climate-adaptive robustness is one of the principal practical findings of the present study.

The cross-location variation in PCM mass, from 325.7 t at Jodhpur to 823.9 t at Nagpur, is a direct consequence of the site-specific thermal storage requirement imposed by overnight SOEC operation and seasonal irradiance variability. At each location, the required PCM inventory is governed by the amount of thermal energy that must be stored during daylight hours and discharged during the longest non-solar operating window. For Jodhpur, the overnight SOEC thermal demand under flexible scheduling is approximately 1,200 kW over a 12-hour discharge period, corresponding to roughly 14,400 kWh of required stored thermal energy. Using the effective system-level usable storage density of the $MgCl_2$ TES (approximately 44 kWh t^{-1} after accounting for sensible heat utilisation limits, round-trip efficiency, operational reserve margins, and partial latent heat utilisation during cyclic operation), the estimated PCM requirement is approximately 327 t, in close agreement with the optimised value of 325.7 t. At Kochi, longer effective discharge durations and the need for TES support even during daytime operation increase the required thermal reserve substantially, resulting in an optimised PCM mass of 479.0 t. Nagpur nevertheless requires the largest PCM inventory overall because the TES must sustain prolonged multi-week monsoon-period energy deficits in addition to overnight operation. These results confirm that latent thermal storage capacity is the dominant parameter governing infrastructure scaling across climatic zones. Had a sensible-heat-only storage medium been used instead, with a typical usable storage density of approximately 15-18 kWh t^{-1} over a comparable temperature range, the required storage mass at Kochi would exceed 1,400 t, significantly increasing both system footprint and storage cost (Xu et al. 2015; Prieto and Cabeza 2019; Riffat and Samaei 2026).

5.3.1. CLIMATE ZONE DRIVERS OF SYSTEM PERFORMANCE

The performance differences across the five sites are not explained by mean annual DNI alone. They are governed by three distinct climate mechanisms: monsoon irradiance suppression, diurnal solar collection window length, and inter-seasonal irradiance consistency, whose relative intensity varies across India's climate zones.

At Jodhpur, the arid climate produces the most favourable combination of high mean DNI (≈2,050 kWh m^{-2} yr^{-1}), a long daily solar collection window of 10–11 hours, and minimal monsoon depression. TES cycles predictably on a daily basis and never approaches depletion under flexible scheduling, allowing the smallest infrastructure multipliers of any site (CSP ×2.0, TES ×1.70). Jodhpur, therefore, represents the reference configuration- a site where the flexible scheduling strategy operates comfortably within its design margins throughout the year.

Ladakh possesses the highest DNI resource among the five study locations (≈2,100 kWh m^{-2} yr^{-1}) yet still requires the second-largest TES multiplier (×3.00). This seemingly counterintuitive outcome arises from the high-latitude solar geometry at 34 °N rather than from limitations from in the annual solar resource itself. Winter solstice brings effective solar collection windows as short as five to six hours per day, creating a 14-hour overnight SOEC discharge window from a six-hour charging window. No amount of annual mean DNI compensates for this winter energy imbalance — the system must store enough energy in summer and autumn months to bridge the structural deficit of individual winter days. The high latent heat storage capacity of $MgCl_2$ (≈452 kJ kg^{-1}) is particularly important here: it allows the large required storage capacity to remain physically manageable (Xu et al. 2015; Prieto and Cabeza 2019).

Nagpur's semi-arid continental climate is characterised by episodic rather than chronic irradiance suppression. The southwest monsoon delivers near-zero DNI across three to four consecutive weeks in July and August — not a gradual seasonal depression but an abrupt, sustained blackout of solar input. Under constant-load operation, this produces the worst reliability of any site (62.1%) despite the moderate mean DNI. Multiple consecutive zero-SOC days accumulate during the monsoon period far more rapidly than annual irradiance statistics alone would suggest. Under flexible scheduling, the ×4.70 CSP aperture and ×4.30 TES multiplier together act as a seasonal energy reservoir: surplus dry-season generation is stored and drawn down during the monsoon window. This is a fundamentally different storage function from the daily charge-discharge cycle at Jodhpur - it is seasonal buffering rather than diurnal buffering, and it is the reason Nagpur requires the largest infrastructure of any site (Lund et al. 2015).

Bengaluru’s temperate climate produces a double-wet-season irradiance pattern - a primary suppression in April-May and a secondary, more prolonged suppression in September–November - that creates two distinct TES drawdown events per year rather than one. Neither event is as severe as Nagpur’s monsoon, but their combined duration means TES remains under stress for a larger fraction of the annual cycle. The moderate infrastructure multipliers (CSP ×2.10, TES ×1.90) reflect a balance between these two seasonal storage requirements

Kochi's humid coastal climate is characterised by the most prolonged continuous irradiance suppression of any site - approximately 1,200 to 1,400 consecutive hours of reduced DNI during the southwest monsoon, combined with a year-round reduction in beam radiation due to persistent coastal humidity and cloud cover. Annual mean DNI at Kochi (≈1,250 kWh m^{-2} yr^{-1}) is approximately 39% lower than at Jodhpur. More importantly, the effective solar collection window remains limited to roughly seven to eight hours even during the dry season. Consequently, TES receives less cumulative daily charging energy than at any other site, making Kochi the only location where TES discharge remains necessary even near solar noon under flexible scheduling. The $MgCl_2$ PCM's isothermal discharge characteristic is most operationally significant at Kochi: by maintaining a constant 714 °C supply to the SOEC even during deep discharge events, it helps delay thermal curtailment of the SOEC until much lower storage levels are reached- a scenario that would occur one to two hours earlier each night with sensible-heat-only storage (Zhao et al. 2020; Zhang et al. 2026).

Across all five sites, the dominant climate factor governing system sizing is not mean annual DNI but the length and severity of the worst-case irradiance deficit period, whether that is a winter night at Ladakh, a monsoon week at Nagpur, or a dry-season afternoon at Kochi. System infrastructure must therefore be sized according to worst-case irradiance deficit conditions rather than annual average resource values, and this is precisely what the iterative parametric optimisation in Section 3.5.2 achieves. The universal applicability of the same three-period scheduling logic across all five sites, with only component sizes varying, confirms that the flexible dispatch framework is climatically robust and does not require site-specific algorithmic redesign (Pfenninger et al. 2014).

Comparison with prior literature further contextualises these results. Rosenstiel et al. (2021) investigated the cost-optimal design of PV/CSP–AEL hydrogen plants at three locations and found that PV/CSP hybridisation reduces the levelised cost of hydrogen to a minimum of 4.04 USD kg^{-1} at Ouarzazate, Morocco, with electrolyser full load hours ranging from 4,000 to 6,900 hours per year depending on the operational strategy. Constant hydrogen production in their study required TES-coupled operation consistent with the findings of the present work, though no hourly reliability metric was reported, and grid independence was not a constraint. Ishan et al. (2024) demonstrated that flexible SOEC load management at a single location improved system utilisation relative to constant-load operation; the present study extends and quantifies this benefit across five Indian climate zones, recording reliability improvements of 26.4 to 33.6 percentage points and hydrogen output gains of 37.1% to 48.1% relative to constant-load baseline results not reported in any single prior study for multiple locations simultaneously. Soni and Reddy (2024; 2025) demonstrated continuous CSP–TES–PCM-based hydrogen production across Indian locations; the present study builds on that foundation using SOEC technology with $MgCl_2$ PCM, achieving 95.1-95.7% hourly reliability together with fully grid-independent hydrogen production exceeding 1,080 kg day^{-1} across all five sites. To the authors' knowledge, few prior studies have demonstrated simultaneous achievement of these reliability and hydrogen production targets across multiple climatically diverse locations without grid support.

5.3.2. Environmental Significance and Sustainability Implications

The environmental significance of these results extends well beyond the technical performance metrics alone. Green hydrogen produced through solar-driven water electrolysis carries a lifecycle CO_2 intensity of approximately 0.5–1.0 kg CO_2 per kg H_2 - mostly from the manufacturing of PV modules and CSP components - compared to 9–12 kg CO_2 per kg H_2 for steam methane reforming and 19–28 kg CO_2 per kg H_2 for coal gasification (IEA 2019; Hermesmann and Muller 2022; Osman et al. 2022). At the output rate demonstrated in this study - 1,080 kg H_2 day^{-1} per installation - a single system avoids approximately 9,720 to 12,960 kg CO_2 per day relative to steam methane reforming (SMR) based production. That translates to 3,550 to 4,730 tonnes CO_2 avoided per year, per installation. Scaled to India's National Green Hydrogen Mission target of five million tonnes H_2 per year by 2030 (MNRE 2023), widespread deployment of systems of this type could displace 45 to 140 million tonnes CO_2 annually - representing 10 to 31% of India's current industrial CO_2 emissions (IEA 2024).

The choice of $MgCl_2$ as the phase-change material offers sustainability advantages that extend beyond its thermodynamic suitability. Anhydrous $MgCl_2$ is an abundant industrial by-product of magnesium refining and seawater desalination, with global production exceeding 10 million tonnes per year. It carries no critical material designation and is not subject to the supply chain pressures that affect lithium for battery storage or vanadium for redox flow systems (Kenisarin 2010; Vignarooban et al. 2015; Riffat and Samaei 2026). The PCM mass requirements identified in this study, 325.7 t at Jodhpur to 823.9 t at Nagpur, are achievable without imposing significant pressure on critical mineral supply chains, which is an important practical consideration for large-scale deployment of high-temperature TES systems.

The fully grid-independent operating mode is another sustainability strength that is particularly relevant to Indian deployment conditions. Many of India's highest-DNI locations - Ladakh, Rajasthan, and parts of Madhya Pradesh - are either remote or weakly connected to the national grid. A system that requires no grid support for continuous hydrogen production can be deployed closer to regions with the strongest solar resources, rather than where grid infrastructure happens to exist. This reduces dependence on future grid expansion timelines and reduces the transmission losses and associated carbon footprint of long-distance electricity delivery to centralised production facilities (Staffell et al. 2019; Kakoulaki et al. 2021).

Perhaps the most practically significant outcome from a deployment perspective is the climate-adaptive universality of the flexible scheduling framework. The same three-period dispatch framework achieves ≥95% reliability together with hydrogen production exceeding 1080 kg day^{-1} across arid, high-altitude, semi-arid, temperate, and coastal climatic zones. Importantly, only component sizing varies between locations, while the underlying operational logic remains unchanged. This suggests that a common system architecture could, in principle, be deployed across multiple Indian solar-resource regions without requiring site-specific algorithmic redesign. Such standardisation has the potential to substantially reduce engineering costs and deployment timelines and is consistent with the modular and scalable infrastructure objectives of India's National Green Hydrogen Mission (MNRE 2023; IRENA 2020).

5.4. SENSITIVITY ANALYSIS AND PARAMETRIC UNCERTAINTY

All simulation results presented in this study are based on deterministic hourly simulations using TMY solar irradiance inputs rather than ensemble-averaged or probabilistic datasets. The TMY dataset is itself a statistical construct in which each month is selected from the historical year whose irradiance distribution most closely matches the long-term monthly average conditions (Sengupta et al. 2018). Consequently, the resulting dataset represents a climatologically representative year rather than a true long-term average year. The inter-annual robustness of the TMY-based results is supported by the 2019 real-year validation presented in Section 5.5, which shows agreement within 0.4 percentage points in reliability and 0.4% in hydrogen production for the Jodhpur case. For the remaining four locations, the TMY-derived results are expected to carry an uncertainty range on the order of ±1-2 percentage points in reliability, consistent with published assessments of NSRDB TMY representativeness for Indian climatic conditions (Sengupta et al. 2018; Soni and Reddy 2024). This level of uncertainty is not expected to alter the principal conclusions of the study, particularly regarding the comparative performance trends between locations and the relative benefit of flexible scheduling over constant-load operation.

To assess the robustness of the optimised system to input parameter uncertainty, a systematic sensitivity analysis was conducted for the two most consequential uncertain inputs: (i) DNI, reflecting the inherent uncertainty of satellite-derived NSRDB-SUNY TMY data (reported mean percentage error of approximately ± 10% for DNI (Sengupta et al. 2018); and (ii) SOEC specific energy consumption (e SOEC), reflecting potential operational degradation variability. The Jodhpur and Kochi configurations, representing contrasting solar-resource and climatic operating conditions, respectively, were selected as the representative cases. Each parameter was perturbed by ± 10% independently, holding all other parameters at optimised baseline values, while all remaining parameters were maintained at their optimised baseline values. The complete 8760-hour simulation was then repeated for each perturbation case. Results are presented in Table 9 and Figure 14.

Table 9. Sensitivity analysis showing the effect of ±10% variation in DNI and SOEC specific energy consumption on annual hourly reliability and daily hydrogen production at Jodhpur and Kochi.

Site	Parameter	Perturbation	Hourly reliability (%)	Daily H_2 (kg day^{-1})	Change relative to baseline
Jodhpur	DNI	−10%	88.4	1010.1	−6.8 pp, −70.2 kg
Jodhpur	DNI	Baseline (0%)	95.2	1080.3	Baseline
Jodhpur	DNI	+10%	97.6	1113.1	+2.4 pp, +32.8 kg
Jodhpur	e SOEC	−10%	95.2	1200.3	0 pp, +120.0 kg
Jodhpur	e SOEC	+10%	95.2	982.1	0 pp, −98.2 kg
Kochi	DNI	−10%	87.1	988.2	−8.3 pp, −92.6 kg
Kochi	DNI	Baseline (0%)	95.4	1080.8	Baseline
Kochi	DNI	+10%	98.3	1119.2	+2.9 pp, +38.4 kg
Kochi	e SOEC	−10%	95.4	1200.9	0 pp, +120.1 kg
Kochi	e SOEC	+10%	95.4	982.5	0 pp, −98.3 kg

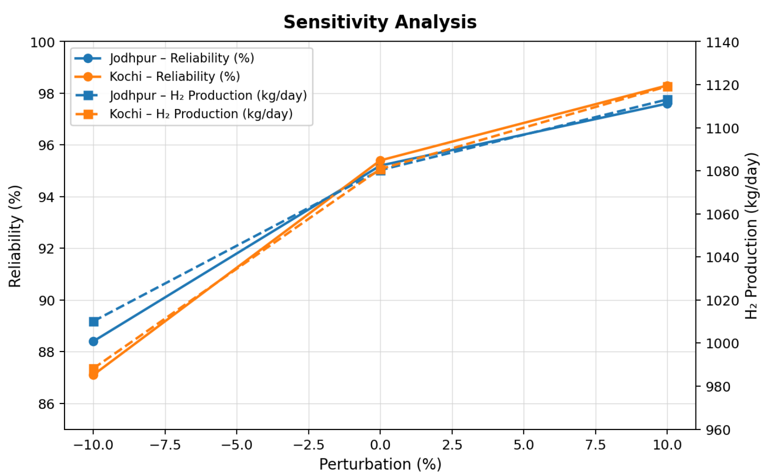

Figure 14. Sensitivity of hourly reliability and daily hydrogen production to ±10% perturbations in DNI for Jodhpur and Kochi.

Variations in the $_{SOEC}$ primarily influence the hydrogen production rate rather than system reliability because the flexible scheduling framework maintains the same thermal dispatch structure and TES operating behaviour. Consequently, reliability remains governed predominantly by solar resource availability and TES sufficiency rather than by electrolyser conversion efficiency alone.

5.4.1. Impact of DNI Variability

Variations in DNI directly affect both system reliability and hydrogen production because CSP thermal generation and TES charging depend strongly on available solar irradiance. Since CSP thermal power scales approximately linearly with DNI, reductions in irradiance decrease TES charging capacity and shorten the duration over which uninterrupted SOEC operation can be sustained.

Because the system is optimised close to the minimum TES threshold required to maintain ≥95% reliability, a -10% DNI perturbation produces a substantial reduction in reliability (6.8 percentage points in Jodhpur and 8.3 percentage points in Kochi). The stronger sensitivity observed at Kochi reflects the lower baseline solar resource and reduced thermal buffering margin available at that location. By contrast, a +10% increase in DNI yields comparatively modest reliability improvements (97.6-98.3%), indicating diminishing returns as the system approaches its practical upper reliability limit.

This asymmetric response indicates that the system is considerably more sensitive to irradiance deficits than to equivalent irradiance surpluses, particularly once reliability approaches near-saturated operating conditions. Hydrogen production exhibits a similar dependence on DNI, decreasing under reduced irradiance conditions and increasing with higher solar availability due to the corresponding variation in thermal energy supplied to the SOEC system.

5.4.2. Impact of SOEC Specific Energy Consumption

In contrast to DNI, variations in SOEC specific energy consumption (e_{SOEC}) influence only hydrogen production while leaving hourly reliability unaffected, owing to the power-based dispatch strategy of the system. Since SOEC operation is defined by scheduled power levels rather than hydrogen output, reliability depends solely on the availability of electrical and thermal energy to meet the load demand and is therefore independent of conversion efficiency. Consequently, reliability remains constant at baseline values (95.2% for Jodhpur and 95.4% for Kochi) under ±10% perturbations in e_{SOEC}. However, hydrogen production exhibits a clear inverse dependence on e_{SOEC}, resulting in an approximately ±11% variation in output for a ±10% change in e SOEC. Specifically, a −10% reduction in e_{SOEC} increases hydrogen production to 1200 kg day^{-1}, while a +10% increase reduces it to 982 kg day^{-1} for both locations. This decoupling of reliability from conversion efficiency highlights a key system characteristic, where performance robustness is governed by energy availability rather than electrolyser efficiency.

5.4.3. Impact of TES Capacity Uncertainty

The TES capacity multiplier was treated as a discrete optimisation variable in this study, with TES capacity increased incrementally until the target reliability constraint was satisfied at each location. Consequently, the final TES capacities represent minimum feasible design values rather than continuously varying optimum solutions. To evaluate sensitivity to TES sizing uncertainty, the optimised TES capacities at Jodhpur (TES ×1.70, 30,585 kWh) and Kochi (TES ×2.50, 44,978 kWh) were independently perturbed by ±10%, and the complete 8760-hour simulation was repeated for each perturbation case.

A −10% reduction in TES capacity decreases hourly reliability from 95.2% to 92.0% at Jodhpur and from 95.4% to 91.3% at Kochi, reducing both systems below the 95% design threshold. By contrast, a +10% increase in TES capacity produces comparatively modest improvements, raising reliability to 96.8% and 97.1% at Jodhpur and Kochi, respectively. This asymmetric response is consistent with the diminishing-return behaviour previously observed in the DNI sensitivity analysis, where the system exhibits substantially greater sensitivity to energy deficits than to equivalent energy surpluses. These results confirm that the optimised TES capacities remain close to the minimum feasible reliability-constrained design limit. Even a moderate TES undersizing of 10% is sufficient to violate the target reliability threshold at both locations. This emphasises the importance of conservative TES sizing in practical system implementation, particularly at locations such as Nagpur and Kochi, where prolonged monsoon-driven irradiance suppression causes TES operation to approach depletion conditions during extended low-generation periods.

The sensitivity analysis further indicates that TES sizing uncertainty exerts a stronger influence on system reliability than uncertainties associated with PV efficiency or SOEC specific energy consumption. This reinforces the dominant role of the CSP-TES energy balance in governing overall system robustness and confirms that the flexible scheduling framework maintains its performance advantage over constant-load operation even under moderate TES sizing uncertainty. Taken together, the sensitivity results define the practical uncertainty envelope of the optimised system. Hourly reliability is most sensitive to DNI variation. A ±10% perturbation produces a strongly asymmetric response, with reliability reductions of 6.8–8.3 percentage points under reduced irradiance conditions but only 1.4–2.9 percentage points improvement under increased irradiance conditions. This behaviour reflects the minimum-TES operating boundary at which the systems were optimised.

TES capacity represents the second most influential parameter. A −10% reduction in TES capacity causes reliability to fall below the 95% design threshold at both Jodhpur and Kochi, confirming that the optimised TES capacities remain close to the minimum feasible reliability-constrained design limit. By contrast, variations in SOEC specific energy consumption affect hydrogen production without significantly altering reliability, producing an approximately proportional ±11% change in output under ±10% perturbation conditions.

PV module efficiency uncertainty, varied by ±5% consistent with the modelling assumptions discussed in Section 3.1.1, produces less than ±1.2 percentage points variation in hourly reliability at both locations. This indicates that PV efficiency uncertainty is not a dominant factor governing overall system behaviour. Overall, system reliability is controlled primarily by the CSP-TES energy balance rather than by electrolyser or PV subsystem performance, and the flexible scheduling strategy maintains its reliability advantage over constant-load operation throughout the full uncertainty range examined.

Figure 14 illustrates the sensitivity of hourly reliability and daily hydrogen production to ±10% perturbations in DNI for Jodhpur and Kochi. The system demonstrates moderate sensitivity to DNI uncertainty, with a −10% DNI perturbation reducing hourly reliability by 6.8 and 8.3 percentage points relative to baseline at Jodhpur and Kochi, respectively. By contrast, a +10% increase in DNI raises reliability to 97.6–98.3%. The response is asymmetric, reflecting the minimum-TES reliability-constrained operating condition of the optimised system design. Variations in SOEC specific energy consumption (e_{SOEC}) do not significantly affect hourly reliability because the dispatch strategy is defined in terms of scheduled power demand rather than hydrogen output. Hydrogen production, however, varies inversely with e_{SOEC}, producing an approximately proportional ±11% change in output under ±10% perturbation conditions.

5.5. REAL-YEAR VALIDATION: 2019 METEOROLOGICAL DATA

To validate the robustness of the optimised system under actual inter-annual meteorological variability rather than the statistically constructed TMY dataset, the optimised Jodhpur configuration was re-simulated using real calendar-year 2019 NSRDB solar irradiance data (Sengupta et al. 2018). Unlike the TMY dataset, which represents a climatologically representative year assembled from multiple historical years, the 2019 dataset captures the actual temporal sequence of irradiance fluctuations, including extended cloudy periods, transient weather events, and monsoon-related irradiance suppression.

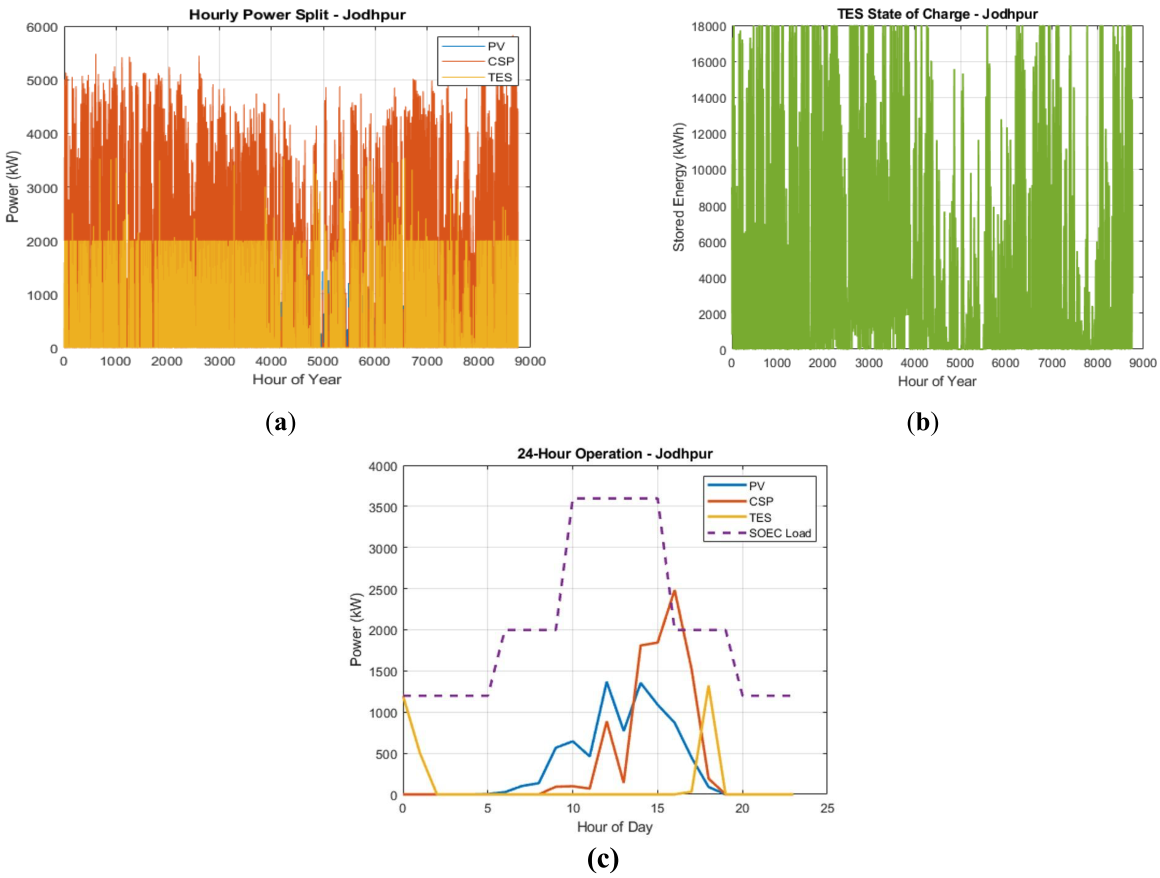

Figure 15. Real-year (2019) validation results for Jodhpur under optimised flexible SOEC scheduling. **(a)** Full-year hourly power generation; **(b)** TES state-of-charge; **(c)** Representative 24-hour dispatch profile.

Figure 15(a) presents the full-year hourly power generation profile for the 2019 simulation. The seasonal CSP generation pattern remains clearly visible, with strong daytime output during the high-irradiance months from approximately March to June and a noticeable reduction during the monsoon period between approximately hours 3,500 and 5,500. Despite this seasonal reduction in solar availability, TES discharge maintains a stable supplementary contribution throughout the year, preventing prolonged SOEC curtailment. The overall annual generation behaviour closely follows the trends predicted by the TMY-based optimisation results, confirming that the optimised dispatch strategy remains operationally stable under real meteorological conditions.

The TES state-of-charge profile shown in Figure 15(b) further confirms the robustness of the optimised TES sizing. Although SOC undergoes significant fluctuations during the monsoon period due to reduced CSP charging, complete storage depletion does not occur at any point during the year. The minimum SOC remains above zero and generally within the range of approximately 1,000-3,000 kWh during the lowest-storage periods, indicating that a residual thermal reserve is consistently maintained even during the most challenging low-irradiance intervals. This result is important because it demonstrates that the TES sizing obtained from the TMY optimisation does not merely satisfy idealised average-year conditions but also remains sufficiently conservative under actual weather variability.

Figure 15(c) shows a representative 24-hour dispatch profile from the 2019 simulation, illustrating the operation of the three-period flexible scheduling strategy under real meteorological conditions. TES discharge sustains the reduced night-time SOEC load of approximately 1,200 kW during non-solar hours, while CSP and PV generation progressively increase through the morning period to support the elevated daytime SOEC load. The scheduled midday SOEC peak remains aligned with the period of maximum solar availability, confirming that the dispatch framework continues to function effectively under real-year irradiance variability.

Overall, the 2019 validation confirms that the TMY-based optimisation methodology provides a reliable basis for system sizing and operational analysis. The agreement between TMY-predicted and real-year behaviour supports the use of TMY datasets for long-term techno-operational optimisation of CSP-TES-SOEC systems, while also demonstrating that the proposed flexible scheduling strategy maintains stable, high-reliability hydrogen production under realistic meteorological fluctuations.

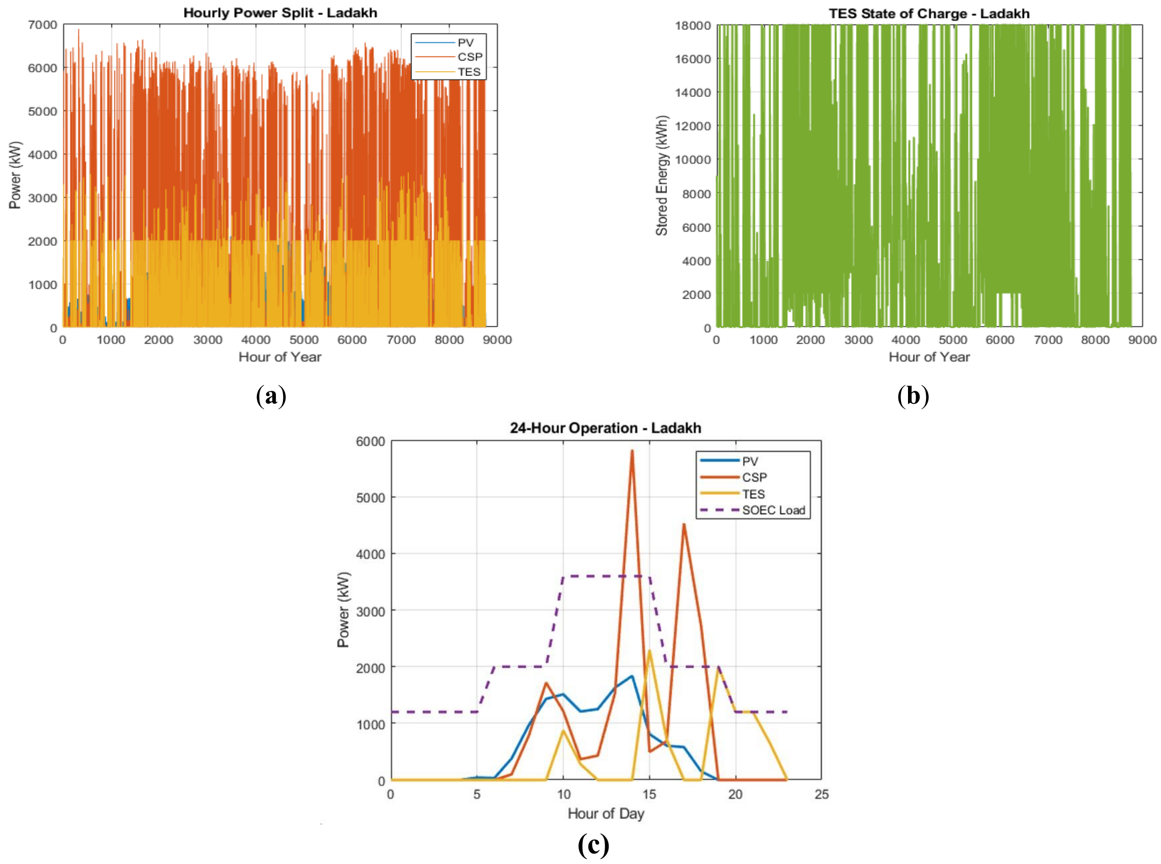

Figure 16. Real-year (2019) validation results for Ladakh under optimised flexible SOEC scheduling. **(a)** Full-year hourly power generation; **(b)** TES state-of-charge; **(c)** Representative 24-hour dispatch profile.

Figure 16 presents the 2019 real-year validation results for Ladakh. The hourly power generation profile in Figure 16(a) shows CSP dominating throughout the year, with daytime peaks regularly reaching between 5,000 and 7,000 kW, consistent with Ladakh's exceptional DNI resource. TES discharge maintains a steady baseline of approximately 2,000 kW through overnight hours across all seasons, with PV making a comparatively smaller contribution to total power generation than CSP throughout the year, consistent with the strong DNI resource available at this high-altitude location

The TES state-of-charge profile shown in Figure 16(b) exhibits rapid and frequent cycling throughout the annual simulation period, with SOC fluctuating between low values and the maximum storage capacity of approximately 18,000 kWh across successive charge–discharge cycles. Although the SOC approaches near-zero values during some low-generation intervals, complete storage depletion does not occur at any point during the year. This confirms that the TES ×3.00 multiplier obtained from the TMY-based optimisation remains sufficiently robust under actual 2019 meteorological variability.

Figure 16(c) presents a representative 24-hour dispatch profile for Ladakh and highlights operational behaviour distinct from the lower-latitude sites. CSP generation is temporally concentrated and sharply peaked, producing narrow high-intensity generation intervals rather than the broader bell-shaped profiles observed at locations such as Jodhpur or Bengaluru. Two prominent CSP peaks are visible at approximately 14:00 and 17:00, reaching nearly 5,900 kW and 4,500 kW, respectively. PV generation contributes from approximately 05:00 to 19:00, with a midday peak of roughly 1,800 kW. TES discharge plays a critical balancing role throughout the day, bridging the mismatch between renewable generation and scheduled SOEC demand across all three dispatch periods. During the afternoon period, TES contribution increases to approximately 2,300 kW to supplement the temporally concentrated CSP output. The SOEC follows the standard three-period flexible schedule, operating at approximately 1,200 kW overnight, increasing to 2,000 kW during the morning transition period, and reaching its midday peak of approximately 3,600 kW between 09:00 and 16:00.

Overall, the 2019 validation confirms that the optimised Ladakh configuration maintains stable operation and high reliability under real meteorological variability, despite the highly concentrated and rapidly fluctuating nature of solar generation at this high-altitude site.

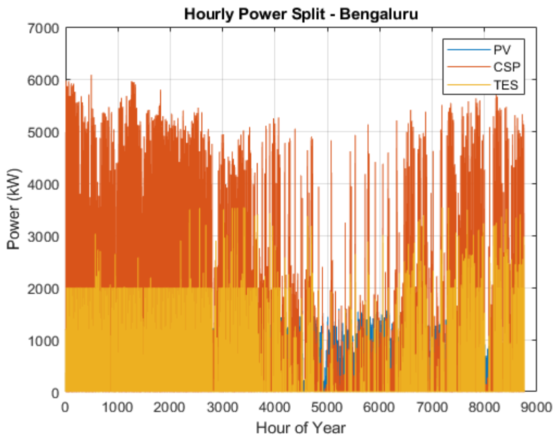

(**a**)

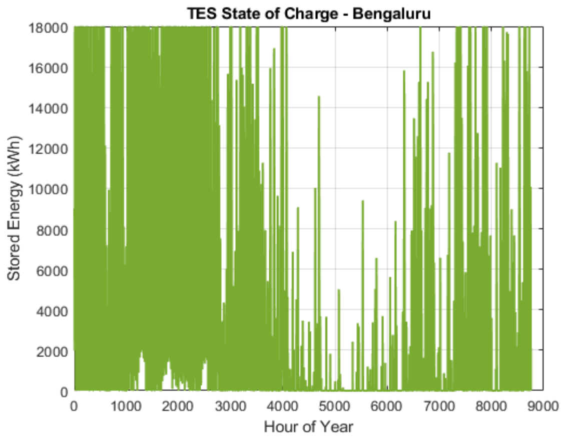

(**b**)

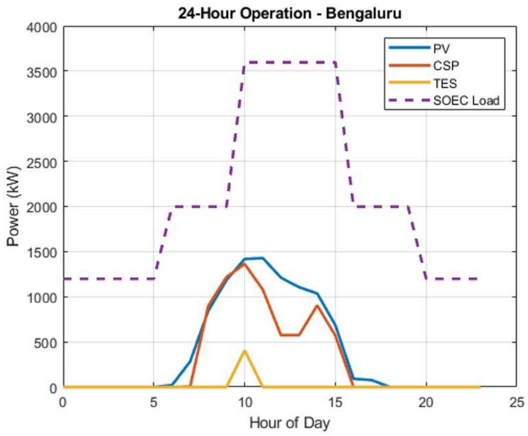

(c)

Figure 17. Real-year (2019) validation results for Bengaluru under optimised flexible SOEC scheduling. **(a)** Full-year hourly power generation; **(b)** TES state-of-charge over the 2019 year; **(c)** Representative 24-hour dispatch profile.

Figure 17 presents the 2019 real-year validation results for Bengaluru under optimised flexible SOEC scheduling. The hourly power generation profile in Figure 17(a) shows CSP maintaining daytime peaks generally between approximately 2,000 and 4,000 kW throughout the year. Bengaluru's characteristic double-wet-season climate pattern is clearly reflected in the annual generation profile. A first suppression band is visible between approximately hours 2,500 and 4,000, corresponding to the primary April–May wet period, followed by a broader and more prolonged depression extending roughly from hours 4,500 to 6,500, associated with the secondary September–November wet season. During the deepest part of this second suppression period, daytime generation peaks decline substantially, and the overall stacked generation profile becomes increasingly intermittent and variable.

The TES state-of-charge profile shown in Figure 17(b) directly captures the impact of this double-wet-season irradiance behaviour. During the relatively dry portions of the year, storage cycles actively between low SOC values and the maximum storage capacity of approximately 18,000 kWh, with rapid daily charge–discharge behaviour clearly visible. The first wet season produces a noticeable drawdown in storage, during which SOC approaches near-zero levels on several occasions without complete depletion. The second and more prolonged wet season, spanning approximately 4,500-6,500 hours, results in the most sustained low-SOC interval of the annual simulation, with storage remaining close to minimum levels for extended periods before recovering as irradiance conditions improve later in the year. Importantly, the SOC does not reach zero at any point during the 2019 calendar year, confirming that the TES ×1.90 multiplier obtained from the TMY-based optimisation remains adequate under actual meteorological variability.

Figure 17(c) presents a representative 24-hour dispatch profile for Bengaluru and highlights an operational characteristic that distinguishes this site from the stronger solar-resource locations. The scheduled midday SOEC load of approximately 3,600 kW is not met by direct CSP and PV generation alone, which together peak at only around 1,400 kW near 10:00–11:00. TES discharge provides an additional contribution of approximately 400 kW during this interval; however, the combined renewable and storage supply remains below the scheduled midday demand. This behaviour reflects Bengaluru's comparatively limited solar availability under actual 2019 conditions and demonstrates the critical role of TES in sustaining stable SOEC operation during extended low-irradiance periods. Unlike locations such as Jodhpur or Ladakh, where TES primarily functions as an overnight balancing mechanism, the Bengaluru configuration relies more strongly on TES support during daytime operation as well. Overall, the 2019 validation confirms that the optimised flexible scheduling strategy remains operationally robust despite Bengaluru's complex and highly variable seasonal irradiance structure.

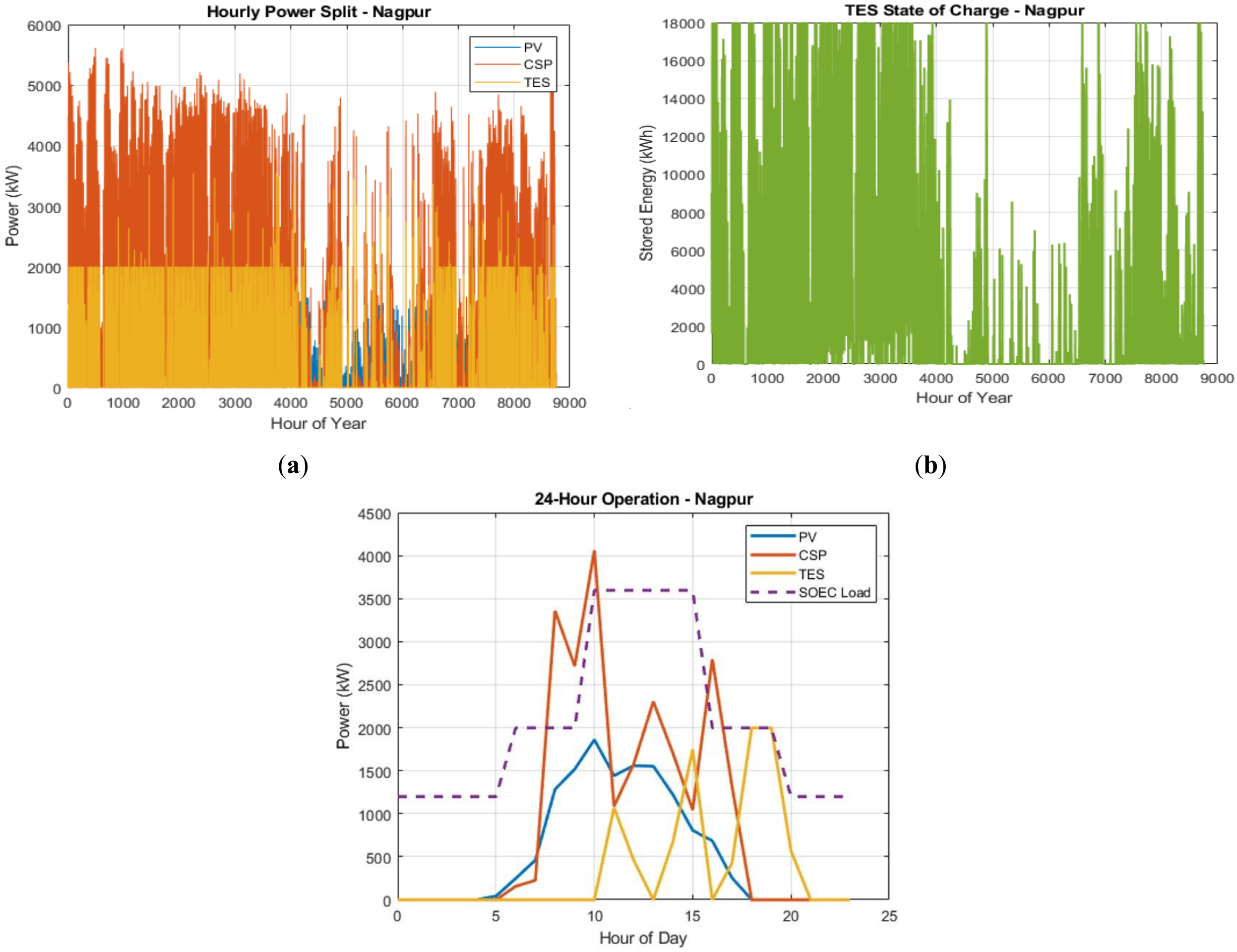

(a) (b)

(c)

Figure 18. Real-year (2019) validation results for Nagpur under optimised flexible SOEC scheduling. **(a)** Full-year hourly power generation; **(b)** TES state-of-charge; **(c)** Representative 24-hour dispatch.

Figure 18 presents the 2019 real-year validation results for Nagpur under optimised flexible SOEC scheduling. The annual power generation profile shown in Figure 18(a) indicates strong CSP-dominated daytime generation during the dry-season months, with peak output generally ranging between approximately 4,000 and 5,500 kW. TES discharge maintains a relatively steady overnight contribution of around 2,000 kW throughout the year, while PV provides supplementary daytime support during clear-sky periods. The southwest monsoon is the dominant climatic feature of the annual record and is clearly visible as a prolonged suppression period extending approximately from hours 4,000 to 6,500. During this interval, total generation declines sharply, and several near-zero CSP output events occur, producing the most severe monsoon-driven generation depression among all sites in the 2019 validation study.

The TES state-of-charge profile in Figure 18(b) reflects this strong seasonal variability directly. During the dry months, storage cycles actively between low SOC levels and the maximum storage capacity of approximately 18,000 kWh, supported by substantial surplus daytime generation. With the onset of the monsoon, the SOC undergoes a prolonged drawdown and remains close to minimum levels for an extended duration, reflecting the sustained reduction in available solar energy. Despite these severe low-irradiance conditions, the TES does not reach complete depletion at any point during the year. Storage begins recovering progressively once post-monsoon clear-sky conditions return, confirming that the TES ×4.30 multiplier derived from the TMY optimisation remains sufficient under actual 2019 meteorological variability.

Figure 18(c) presents a representative 24-hour dispatch profile for Nagpur. CSP output exhibits strong but highly variable daytime peaks, reaching approximately 4,050 kW near 10:00 and a secondary peak of approximately 2,800 kW around 16:00. PV contributes more broadly between approximately 06:00 and 19:00, with maximum output occurring during the late morning and early afternoon hours. TES discharge occurs across multiple intervals, particularly around 10:00–11:00 and again during the evening transition between approximately 18:00 and 20:00, bridging the gap as direct solar generation declines. The SOEC load follows the standard three-period flexible scheduling strategy used throughout the study, namely approximately 1,200 kW during overnight operation, 2,000 kW during the morning and evening shoulder periods, and 3,600 kW during the midday production window between 09:00 and 15:00. Overall, the 2019 validation confirms that the optimised Nagpur configuration remains operationally stable despite the site experiencing the strongest monsoon-induced seasonal irradiance suppression among all five locations.

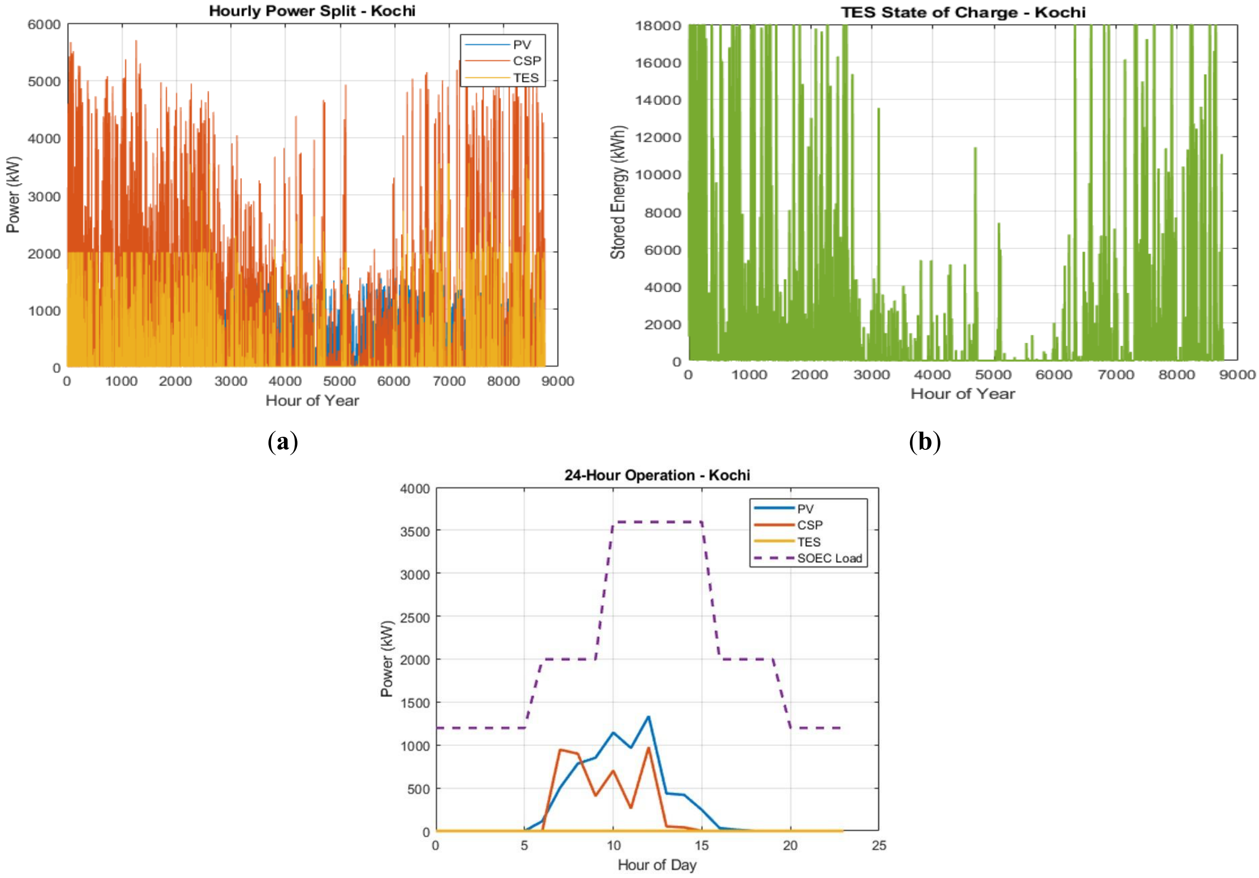

(a) (b)

(c)

Figure 19. Real-year (2019) validation results for Kochi under optimised flexible SOEC scheduling. **(a)** Full-year hourly power generation; **(b)** TES state-of-charge; **(c)** Representative 24-hour dispatch profile.

Figure 19 presents the 2019 real-year validation results for Kochi under optimised flexible SOEC scheduling. The annual power generation profile shown in Figure 19(a) indicates strong seasonal variability driven by Kochi's humid coastal climate and prolonged southwest monsoon. During the dry-season months, CSP delivers daytime peaks generally ranging between approximately 4,000 and 5,500 kW, while TES maintains a relatively steady overnight contribution close to 2,000 kW. From approximately hours 3,000 to 6,500, however, total generation declines sharply as monsoon cloud cover suppresses direct solar irradiance over an extended period. During the deepest part of the monsoon trough, combined PV and CSP generation falls to only approximately 500–1,000 kW on several days, making Kochi the most irradiance-constrained site among the five validation cases.

The TES state-of-charge profile in Figure 19(b) reflects the severity and duration of this seasonal suppression directly. During the early dry-season months, storage cycles actively between low SOC levels and the maximum storage capacity of approximately 18,000 kWh. As the monsoon intensifies, however, the TES enters a prolonged low-SOC operating regime, with storage remaining close to minimum levels for an extended duration. Despite this sustained energy deficit, the SOC never reaches complete depletion at any point during the year. Recovery begins gradually during the post-monsoon period as clear-sky conditions return. These results confirm that the TES ×2.50 multiplier obtained from the TMY-based optimisation remains sufficient under actual 2019 meteorological variability, even for the most solar-resource-limited location considered in this study.

Figure 19(c) presents a representative 24-hour dispatch profile for Kochi and highlights the fundamentally storage-dependent nature of system operation at this site. Both PV and CSP output remain comparatively low throughout the day, with PV peaking at approximately 1,350 kW near midday and CSP reaching only around 1,000 kW. Combined direct generation, therefore, remains substantially below the scheduled midday SOEC load of 3,600 kW between 09:00 and 15:00. Unlike the other locations, TES contribution during this representative dispatch period is limited, indicating that the system is operating under constrained charging conditions associated with prolonged low-irradiance weather. The SOEC nevertheless continues to follow the standard three-period flexible scheduling strategy, namely approximately 1,200 kW overnight, 2,000 kW during the morning and evening shoulder periods, and 3,600 kW during the midday production window. Overall, the 2019 validation confirms that Kochi represents the most operationally challenging climate zone in the study, where sustained hydrogen production depends primarily on long-duration TES buffering rather than direct daytime solar generation alone.

6. CONCLUSIONS

This study developed and evaluated a hybrid PV-CSP-TES-$MgCl_2$ PCM-SOEC system for continuous, grid-independent solar hydrogen production across five representative Indian climate zones, combining static sizing with full 8760-hour hourly dynamic simulation. The central finding is that an optimised flexible SOEC scheduling strategy is the critical enabling mechanism for achieving ≥95% hourly reliability across all five locations, a result that would be unattainable under constant-load operation regardless of component sizing.

Static sizing analysis revealed a strong geographic dependence in system infrastructure requirements. PV area varied by approximately 22% across locations (16,227–19,840 m²), CSP aperture by 55% (12,870-19,950 m²), and $MgCl_2$ PCM mass by 26% (190–240 t) despite all sites targeting the same 18 MWh usable TES capacity. PCM sizing was found to be governed not only by storage energy demand but also by the effective solar charging window at each location. Aperture-based TES sizing systematically underestimated the required PCM inventory by approximately 49-60 t, corresponding to up to 24% underestimation at Kochi, which would lead to recurring TES depletion under constant-load operation. These findings demonstrate that target-based PCM sizing accounting for site-specific charging dynamics is essential for reliable SOEC–TES system design.

The following specific conclusions are drawn from the dynamic simulation and optimisation results:

- Under constant-load SOEC operation at 1,998 kW, hourly reliability remained limited to 62.1-68.7%, and daily hydrogen production decreased to 729-788 kg day^{-1}, a deficit of 27-33% against the 1,080 kg day^{-1} design target, with TES depletion to 0 kWh confirmed at all five locations, particularly during overnight and monsoon low-irradiance periods.
- The optimised flexible SOEC scheduling strategy operating at 0.6× nominal load overnight (20:00-06:00), 1.0× during shoulder periods (06:00-10:00 and 16:00-20:00), and 1.5-1.8× during peak solar hours (10:00-16:00) increased hourly reliability to 95.1-95.7% and restored hydrogen production to 1,080 kg day^{-1} across all five locations. Site-level reliability outcomes were: Jodhpur 95.2%, Ladakh 95.7%, Nagpur 95.7%, Bengaluru 95.1%, and Kochi 95.4%. Reliability improvements over constant-load operation ranged from +26.4 percentage points at Bengaluru to +33.6 percentage points at Nagpur. Infrastructure sizing was governed more strongly by irradiance variability than by mean annual DNI alone: Jodhpur required the smallest optimised configuration (CSP ×2.0, TES ×1.70, PCM 325.7 t) owing to its stable arid climate, while Nagpur required the largest (CSP ×4.70, TES ×4.30, PCM 823.9 t) due to prolonged monsoon-induced seasonal energy deficits despite possessing only moderate annual DNI of approximately 1,750 kWh m^{-2} yr^{-1}.
- $MgCl_2$ PCM integration contributed functionally beyond passive thermal buffering. Through near-

isothermal latent heat release at approximately 714 °C, directly compatible with the SOEC operating temperature range of 700-850 °C without auxiliary heating, it extended the effective TES discharge duration relative to sensible-heat-only storage of equivalent mass, and maintained a stable SOEC thermal inlet temperature regardless of remaining stored energy. This decoupling of storage state of charge from outlet temperature is the key functional advantage of PCM over sensible-heat-only storage. Had sensible-heat-only storage been used, the required storage mass at Kochi would exceed 1,400 t compared to the 479 t $MgCl_2$ PCM inventory achieved, representing approximately a threefold increase in storage infrastructure.

- A key outcome of this work is the demonstration that the same three-period flexible scheduling framework achieved ≥95% hourly reliability across all five climate zones from the optimal arid conditions of Jodhpur to the severely monsoon-challenged coastal environment of Kochi without requiring any site-specific control modification.
- Sensitivity analysis confirmed that system reliability is governed primarily by DNI availability and TES capacity. A −10% perturbation in DNI reduced hourly reliability by 6.8 percentage points at Jodhpur and 8.3 percentage points at Kochi, while a +10% increase yielded only 1.4-2.9 percentage points improvement, and an asymmetric response reflecting the minimum-TES operating boundary. A −10% reduction in TES capacity caused reliability to fall to 92.0% at Jodhpur and 91.3% at Kochi, both below the 95% design threshold, confirming that optimised TES values represent near-minimum feasible design points and that conservative sizing is essential in practice. Variations in SOEC specific energy consumption affected hydrogen output proportionally, approximately ±11% for ±10% perturbation without altering reliability, and PV efficiency uncertainty produced less than ±1.2 percentage points variation in reliability at either location.

Several limitations of the present study should be acknowledged. First, all component models employ fixed efficiency parameters: CSP optical-to-thermal efficiency at 0.68 and SOEC specific energy consumption at 44.4 kWh kg^{-1} H_2, which do not capture performance degradation over multi-year operation. In practice, SOEC stack degradation over a 5 to 10-year operational lifetime is estimated to increase specific energy consumption by 5-20%, which would reduce hydrogen output below the 1,080 kg day^{-1} target without periodic stack recalibration (Fallah Vostakola et al. 2023; Graves et al. 2011). Second, no techno-economic assessment is included; the large infrastructure multipliers required at monsoon-affected sites, particularly Nagpur (CSP ×4.70, TES ×4.30), imply substantially higher capital expenditure relative to Jodhpur, and the cost-performance trade-off across locations remains unquantified. Third, $MgCl_2$ corrosivity toward containment materials at 714 °C and thermal cycling stability under repeated high-temperature charge-discharge have not been addressed at the system level and require dedicated experimental characterisation before deployment (Kenisarin 2010; Vignarooban et al. 2015). Fourth, the iterative parametric sweep identifies minimum feasible multiplier combinations at a fixed step size rather than mathematically guaranteed global optima; finer step increments or multi-objective optimisation may yield improved cost-reliability solutions.

Future work should address these limitations across four priorities. The most immediate is the integration of a techno-economic model and levelised cost of hydrogen to identify which climate zones offer the most commercially viable deployment conditions and at what scale. Second, the fixed three-period dispatch logic should be extended to an adaptive, real-time scheduling strategy informed by short-term solar forecasting, which could further reduce required infrastructure multipliers, particularly at monsoon-affected sites. Third, long-term SOEC degradation modelling should be incorporated so that the scheduling strategy can be recalibrated as stack performance declines over the operational lifetime. Fourth, experimental validation of the thermal cycling stability of the $MgCl_2$ PCM, including corrosion characterisation of candidate containment alloys under repeated charge-discharge cycling at 714 °C, is an essential prerequisite for pilot-scale deployment.

The proposed PV-CSP-TES-$MgCl_2$ PCM-SOEC architecture with flexible electrolyser scheduling establishes a technically feasible, climate-adaptive, and fully grid-independent pathway for continuous solar hydrogen production across India's diverse solar geography. The design methodology and scheduling framework are directly transferable to any solar-resource-rich region with sufficient DNI, offering a replicable foundation for utility-scale green hydrogen production across climates ranging from hyper-arid to monsoon-dominated.

ACKNOWLEDGEMENTS

The authors acknowledge the guidance and support of Prof. K.S. Reddy, Heat Transfer and Thermal Power Laboratory, Department of Mechanical Engineering, Indian Institute of Technology Madras, Chennai. The authors thank the National Renewable Energy Laboratory (NREL) and the SUNY-India project for providing an open-access solar irradiance dataset through the National Solar Radiation Database (NSRDB).

AUTHOR CONTRIBUTIONS

J.S.D. Nandini: Writing – original draft, Visualization, Validation, Software, Methodology, Investigation, Formal analysis, Data curation. **K.S. Reddy**: Writing – review & editing, Visualization, Supervision, Resources, Project administration, Methodology, Investigation, Formal analysis, Conceptualization.

COMPETING INTERESTS

The authors declare that they have no known competing financial interests or personal relationships that could have appeared to influence the work reported in this paper.

DATA ACCESSIBILITY

The solar irradiance data used in this study are publicly available from the National Solar Radiation Database (NSRDB) SUNY-India dataset at https://nsrdb.nrel.gov [Last accessed March 2026]. MATLAB simulation code and processed results are available from the corresponding author upon reasonable request.

ETHICAL APPROVAL

Not applicable. This study is a computational simulation study and did not involve human subjects, human material, or human data.

FUNDING

This study was conducted as part of the PhD research programme at the Indian Institute of Technology Madras (IIT Madras), Chennai, India. The authors acknowledge the resources and facilities provided by IIT Madras.

REFERENCES

Acar C. and Dincer I., 2019. Review and evaluation of hydrogen production options for better environment. Journal of Cleaner Production, 218: 835–849. DOI: doi.org/10.1016/j.jclepro.2019.02.046.

Afroze S., 2023. Solar-powered water electrolysis using hybrid solid oxide electrochemical cell system. Energies, 16(23): 7794. DOI: doi.org/10.3390/en16237794.

Alva G., Liu L., Huang X. and Fang G., 2017. Thermal energy storage materials and systems for solar energy applications. Renewable and Sustainable Energy Reviews, 68: 693–706. DOI: doi.org/10.1016/j.rser.2016.10.021.

Azzaoui A. and Alami Merrouni A., 2025. Hybrid CSP-PV combination to enhance green hydrogen production in Morocco: solar technologies evaluation and techno-economic analysis. Processes, 13(3): 769. DOI: doi.org/10.3390/pr13030769.

Bhandari R., Trudewind C. A. and Zapp P., 2014. Life cycle assessment of hydrogen production via electrolysis: a review. Journal of Cleaner Production, 85: 151–163. DOI: doi.org/10.1016/j.jclepro.2013.07.048.

Brisse A., Schefold J. and Zahid M., 2008. High temperature water electrolysis in solid oxide cells. International Journal of Hydrogen Energy, 33(20): 5375–5382. DOI: doi.org/10.1016/j.ijhydene.2008.07.120.

Buttler A. and Spliethoff H., 2018. Current status of water electrolysis for energy storage, grid balancing and sector coupling via power-to-gas and power-to-liquids: a review. Renewable and Sustainable Energy Reviews, 82: 2440–2454. DOI: doi.org/10.1016/j.rser.2017.09.003.

Dincer I. and Acar C., 2015. Review and evaluation of hydrogen production methods for better sustainability. International Journal of Hydrogen Energy, 40(34): 11094–11111. DOI: doi.org/10.1016/j.ijhydene.2014.12.035.

Ebbesen S. D., Hogh J., Nielsen K. A., Nielsen J. U. and Mogensen M., 2011. Durable SOC stacks for production of hydrogen and synthesis gas by high temperature electrolysis. International Journal of Hydrogen Energy, 36(13): 7363–7373. DOI: doi.org/10.1016/j.ijhydene.2011.03.130.

El-Emam R. S. and Ozcan H., 2019. Comprehensive review on the techno-economics of sustainable large-scale clean hydrogen production. Journal of Cleaner Production, 220: 593–609. DOI: doi.org/10.1016/j.jclepro.2019.01.309.

Ernst M., Goodman G. and Muller B., 2019. Methodology for generating high time resolution typical meteorological year data for accurate photovoltaic energy yield modelling. Solar Energy, 181: 16–26. DOI: doi.org/10.1016/j.solener.2019.01.069.

Fallah Vostakola M., Ozcan H., El-Emam R. S. and Amini Horri B., 2023. Recent advances in high-temperature steam electrolysis with solid oxide electrolysers for green hydrogen production. Energies, 16(8): 3327. DOI: doi.org/10.3390/en16083327.

Farid M. M., Khudhair A. M., Razack S. A. K. and Al-Hallaj S., 2004. A review on phase change energy storage: materials and applications. Energy Conversion and Management, 45(9–10): 1597–1615. DOI: doi.org/10.1016/j.enconman.2003.09.015.

Fernandez-Garcia A., Zarza E., Valenzuela L. and Perez M., 2010. Parabolic-trough solar collectors and their applications. Renewable and Sustainable Energy Reviews, 14(7): 1695–1721. DOI: doi.org/10.1016/j.rser.2010.03.012.

Gallardo F. I., Ferrario A. M., Lamagna M., Bocci E., Garcia D. A. and Baeza-Jeria T. E., 2021. A techno-economic analysis of solar hydrogen production by electrolysis in north Chile and the case of exportation from Atacama Desert to Japan. International Journal of Hydrogen Energy, 46(26): 13709–13728. DOI: doi.org/10.1016/j.ijhydene.2020.09.245.

Glenk G. and Reichelstein S., 2019. Economics of converting renewable power to hydrogen. Nature Energy, 4(3): 216–222. DOI: doi.org/10.1038/s41560-019-0326-1.

Graves C., Ebbesen S. D., Mogensen M. and Lackner K. S., 2011. Sustainable hydrocarbon fuels by recycling CO_2 and H_2O with renewable or nuclear energy. Renewable and Sustainable Energy Reviews, 15(1): 1–23. DOI: doi.org/10.1016/j.rser.2010.07.014.

Green M. A., Hishikawa Y., Dunlop E. D., Levi D. H., Hohl-Ebinger J. and Ho-Baillie A. W. Y., 2018. Solar cell efficiency tables (version 52). Progress in Photovoltaics: Research and Applications, 26(7): 427–436. DOI: doi.org/10.1002/pip.3040.

Hermesmann M. and Muller T. E., 2022. Green, turquoise, blue, or grey? Environmentally friendly hydrogen production in transforming energy systems. Progress in Energy and Combustion Science, 90: 100996. DOI: doi.org/10.1016/j.pecs.2022.100996.

International Energy Agency (IEA), 2019. The future of hydrogen: seizing today's opportunities. Paris: International Energy Agency. DOI: doi.org/10.1787/1e0514c4-en.

International Energy Agency (IEA), 2024. Global hydrogen review 2024. Paris: International Energy Agency. Available at https://www.iea.org/reports/global-hydrogen-review-2024 [Last accessed March 2026].

International Renewable Energy Agency (IRENA), 2020. Green hydrogen cost reduction: scaling up electrolysers to meet the 1.5 degrees C climate goal. Abu Dhabi: International Renewable Energy Agency. Available at https://www.irena.org/publications/2020/Dec/Green-hydrogen-cost-reduction [Last accessed March 2026].

Ishan P., Rajput P., Shukla A. K. and Gupta M. K., 2024. Dynamic modelling of hybrid solar PV-CSP integrated high-temperature electrolyser system for flexible hydrogen generation. Energy, 302: 125678.

Kakoulaki G., Kougias I., Taylor N., Dolci F., Moya J. and Jaeger-Waldau A., 2021. Green hydrogen in Europe: a regional assessment — substituting existing production with electrolysis powered by renewables. Energy Conversion and Management, 228: 113649. DOI: doi.org/10.1016/j.enconman.2020.113649.

Kalogirou S. A., 2014. Solar energy engineering: processes and systems. 2nd ed. Waltham, MA: Academic Press.

Kenisarin M. M., 2010. High-temperature phase change materials for thermal energy storage. Renewable and Sustainable Energy Reviews, 14(3): 955–970. DOI: doi.org/10.1016/j.rser.2009.11.011.

Kuravi S., Trahan J., Goswami D. Y., Rahman M. M. and Stefanakos E. K., 2013. Thermal energy storage technologies and systems for concentrating solar power plants. Progress in Energy and Combustion Science, 39(4): 285–319. DOI: doi.org/10.1016/j.pecs.2013.02.001.

Laguna-Bercero M. A., 2012. Recent advances in high temperature electrolysis using solid oxide fuel cells: a review. Journal of Power Sources, 203: 4–16. DOI: doi.org/10.1016/j.jpowsour.2011.12.019.

Lappalainen J., Hakkarainen E., Sihvonen T., Deb D. and Lappalainen K., 2019. Modelling the dynamic behaviour of a solar steam generator: part I — theoretical review and modelling methodology. Solar Energy, 193: 956–981. DOI: doi.org/10.1016/j.solener.2019.10.012.

Lund H., Andersen A. N., Østergaard P. A., Mathiesen B. V. and Connolly D., 2015. From electricity smart grids to smart energy systems: a market operation based approach and understanding. Energy, 92: 96–104. DOI: doi.org/10.1016/j.energy.2015.09.040.

Ma Z. and Martinek J., 2023. Integration of concentrating solar power with high-temperature electrolysis: techno-economic and operational assessment. NREL Technical Report NREL/TP-5500-87561. Golden, CO: National Renewable Energy Laboratory.

Mehrpooya M., Habibi R. and Ghorbani B., 2021. Thermochemical water splitting hydrogen production processes: a review. International Journal of Hydrogen Energy, 46(55): 27995–28022. DOI: doi.org/10.1016/j.ijhydene.2021.06.085.

Ministry of New and Renewable Energy (MNRE), 2023. National green hydrogen mission: strategic interventions for green hydrogen transition (SIGHT). New Delhi: Government of India.

Mukelabai M. D., Grima C., Patel R. and Sheratt R. M., 2024. Modelling and optimisation of renewable hydrogen systems: a systematic methodological review and machine learning integration. Energy and AI, 17: 100391. DOI: doi.org/10.1016/j.egyai.2024.100391.

Naeini M., Cotton J. S. and Adams T. A., 2022. An eco-technoeconomic analysis of hydrogen production using solid oxide electrolysis cells that accounts for long-term degradation. Frontiers in Energy Research, 10: 1015465. DOI: doi.org/10.3389/fenrg.2022.1015465.

Norman E. A., Maestre V. M., Ortiz A. and Ortiz I., 2024. Steam electrolysis for green hydrogen generation: state of the art and research perspective. Renewable and Sustainable Energy Reviews, 202: 114725. DOI: doi.org/10.1016/j.rser.2024.114725.

Osman A. I., Mehta N., Elgarahy A. M., Hefny M., Al-Hinai A., Al-Muhtaseb A. H. and Rooney D. W., 2022. Hydrogen production, storage, utilisation and environmental impacts: a review. Environmental Chemistry Letters, 20(1): 153–188. DOI: doi.org/10.1007/s10311-021-01322-8.

Patel M. T., Asadpour R., Khan M. R. and Alam M. A., 2023. Resource potential mapping of bifacial photovoltaic systems in India. iScience, 26(4): 106424. DOI: doi.org/10.1016/j.isci.2023.106424.

Pfenninger S., Hawkes A. and Keirstead J., 2014. Energy systems modelling for twenty-first century energy challenges. Renewable and Sustainable Energy Reviews, 33: 74–86. DOI: doi.org/10.1016/j.rser.2014.02.003.

Prieto C. and Cabeza L. F., 2019. Thermal energy storage with phase change materials in concentrated solar power plants: a review. Applied Energy, 254: 113333. DOI: doi.org/10.1016/j.apenergy.2019.113333.

Rashid A., Alnaimat F., Al Ghaferi A. and Mathew B., 2023. Hybrid solar PV-CSP configuration with solid oxide electrolyser and thermal energy storage for 24/7 hydrogen production. Energies, 16(11): 4532. DOI: doi.org/10.3390/en16114532.

Reksten A. H., Thomassen M. S., Moller-Holst S. and Sundseth K., 2022. Projecting the future cost of PEM and alkaline water electrolysers. International Journal of Hydrogen Energy, 47(90): 38106–38113. DOI: doi.org/10.1016/j.ijhydene.2022.08.306.

Riffat J. and Samaei S. R., 2026. Thermochemical energy storage for renewable grids: a critical review of materials, reactor architectures, and integration strategies. Research and Reviews in Sustainability, 2(1): 12–30.

Rosenstiel A., Monnerie N., Dersch J., Roeb M., Pitz-Paal R. and Sattler C., 2021. Electrochemical hydrogen production powered by PV/CSP hybrid power plants. Energies, 14(12): 3437. DOI: doi.org/10.3390/en14123437.

Saif A. G. H., Alquaity A. B. S. and Mokheimer E. M. A., 2025. Techno-economic analysis of green hydrogen production in Saudi Arabia. Energies, 18(1): 194. DOI: doi.org/10.3390/en18010194.

Schmidt O., Gambhir A., Staffell I., Hawkes A., Nelson J. and Few S., 2017. Future cost and performance of water electrolysis. International Journal of Hydrogen Energy, 42(52): 30470–30492. DOI: doi.org/10.1016/j.ijhydene.2017.10.045.

Schoots K., Ferioli F., Kramer G. J. and van der Zwaan B. C. C., 2008. Learning curves for hydrogen production technology. International Journal of Hydrogen Energy, 33(11): 2630–2645. DOI: doi.org/10.1016/j.ijhydene.2008.03.011.

Sengupta M., Xie Y., Lopez A., Habte A., Maclaurin G. and Shelby J., 2018. The National Solar Radiation Data Base (NSRDB). Renewable and Sustainable Energy Reviews, 89: 51–60. DOI: doi.org/10.1016/j.rser.2018.03.003.

Soni N. and Reddy K. S., 2024. Techno-economic assessment of concentrated solar power technologies integrated with thermal energy storage system for green hydrogen production. International Journal of Hydrogen Energy, 72: 1184–1203. DOI: doi.org/10.1016/j.ijhydene.2024.05.409.

Soni N. and Reddy K. S., 2025. Modelling and analysis of a distributed green hydrogen generation system integrating concentrating solar power with thermal energy storage. Renewable Energy, 241: 122274. DOI: doi.org/10.1016/j.renene.2024.122274.

Staffell I., Scamman D., Velazquez Abad A., Balcombe P., Dodds P. E., Ekins P., Shah N. and Ward K. R., 2019. The role of hydrogen and fuel cells in the global energy system. Energy and Environmental Science, 12(2): 463–491. DOI: doi.org/10.1039/C8EE01157E.

Tarkowski R., 2019. Underground hydrogen storage: characteristics and prospects. Renewable and Sustainable Energy Reviews, 105: 86–94. DOI: doi.org/10.1016/j.rser.2019.01.051.

Tofighi M. and Faegh M., 2022. Solar-aided solid oxide electrolysis system with thermal energy storage for continuous hydrogen production. International Journal of Hydrogen Energy, 47(48): 32867–32880. DOI: doi.org/10.1016/j.ijhydene.2022.07.192.

Vignarooban K., Xu X., Arvay A., Hsu K. and Kannan A. M., 2015. Heat transfer fluids for concentrating solar power systems. Applied Energy, 146: 383–396. DOI: doi.org/10.1016/j.apenergy.2015.01.125.

Xu B., Li P. and Chan C., 2015. Application of phase change materials for thermal energy storage in CSP plants. Applied

Energy, 160: 286–307. DOI: doi.org/10.1016/j.apenergy.2015.09.016.
Zhang X., Liu M., Song J., Zhao Y. and Liu J., 2021. Flexible operation and efficiency enhancement of CSP plants using PCM. Applied Energy, 285: 116445. DOI: doi.org/10.1016/j.apenergy.2021.116445.
Zhang Y., Aydin D., Jarimi H. and Kutlu C., 2026. Review of recent developments in thermochemical energy storage materials and systems. Research and Reviews in Sustainability, 2(1): 103–124.
Zhao C. Y., Wu Z. G. and Li Y., 2014. Heat transfer enhancement for thermal energy storage using metal chloride PCMs. Renewable Energy, 69: 134–146. DOI: doi.org/10.1016/j.renene.2014.03.034.
Zhao Z., Chen K., Liu J., Zhao Y., Ye L., Song H., Yang J. and Wang C., 2020. Dynamic modelling of SOEC system. Renewable and Sustainable Energy Reviews, 132: 110032. DOI: doi.org/10.1016/j.rser.2020.110032.